

---

This is an electronic reprint of the original article.  
This reprint may differ from the original in pagination and typographic detail.

Ferreira, Miguel; Bohner, Edgar; Al-Neshawy, Fahim  
**NPP containment wall mock-up for long -term NDE and monitoring**

*Published in:*  
XXIIIth Symposium on Nordic Concrete Research & Development - Proceedings

Published: 23/08/2017

*Document Version*  
Publisher's PDF, also known as Version of record

*Please cite the original version:*  
Ferreira, M., Bohner, E., & Al-Neshawy, F. (2017). NPP containment wall mock-up for long -term NDE and monitoring. In M. Tange Hasholt (Ed.), *XXIIIth Symposium on Nordic Concrete Research & Development - Proceedings* (pp. 71 - 74). (Nordic concrete research). Norsk Betongforening.

---

This material is protected by copyright and other intellectual property rights, and duplication or sale of all or part of any of the repository collections is not permitted, except that material may be duplicated by you for your research use or educational purposes in electronic or print form. You must obtain permission for any other use. Electronic or print copies may not be offered, whether for sale or otherwise to anyone who is not an authorised user.

# Nordic Concrete Research

Proceedings of the XXIII Nordic Concrete Research Symposium  
Aalborg, Denmark 2017



Nordic  
Concrete  
Federation

# **NORDIC CONCRETE RESEARCH**

**Proceedings of  
XXIII Nordic Concrete Research Symposium**

**Aalborg, Denmark**

**21-23 August, 2017**

**Edited by:  
MARIANNE TANGE HASHOLT**

**Publisher:  
NORSK BETONGFORENING  
Postboks 2312, Solli  
N-0201 Oslo  
Norway**



## Preface

Every third year the Nordic Concrete Federation organises a research symposium, where on-going and new research projects in the five Nordic countries – Denmark, Finland, Iceland, Norway and Sweden – within the broad field of concrete technology and concrete construction are presented. The research symposium held this year in the Danish city Aalborg is the 23<sup>rd</sup> symposium in this succession of research symposia.

The continuous row of research symposia is a cornerstone in the work of the Nordic Concrete Federation. A Nordic Concrete Research Symposium is more than an event, where research conducted in the Nordic countries is presented. It is a forum, where researchers meet; they have face-to-face discussions, they extend their network, new ideas arise and working relationships between Nordic colleagues emerge. This year, we have invited our concrete colleagues from the Baltic countries, hopefully this will make the event even more fruitful for all of us.

This year's Symposium is organised by the board of the Danish Concrete Association. When the planning of the Symposium started, it was with Dr. Dirch H. Bager as the driving force in the organising committee. Unfortunately, Dirch H. Bager suddenly passed away February 3<sup>rd</sup>, 2016.

Dr. Dirch H. Bager was very well-known in the Nordic concrete community. He joined the Research Committee of the Nordic Concrete Federation in year 2000, and for more than 15 years, he was a very active member. For many years, he edited the bi-annual publication "Nordic Concrete Research". In the prefaces of the proceedings of the research symposia, there was always a special thank to Dirch. H. Bager, because he assisted the national organising committees with all sorts of tasks, great and small. In 2008, Dirch H. Bager received the NCF medal for his extraordinary contribution to make the Nordic cooperation prosper.

Dirch H. Bager left a gap, which it has not been easy to fill out. However, we have done our utmost to follow in his footsteps, and we very much look forward to welcoming you in Aalborg for the XXIII Nordic Concrete Research Symposium!

Kgs. Lyngby, July 2017

Anette Berrig,  
Chairman of the Danish Concrete Association

Marianne Tange Hasholt  
Chairman of the Research Council of the Nordic Concrete Federation

## **Scientific committee**

### **(The Research Council of the Nordic Concrete Federation as per August 2017)**

Ass. professor Marianne Tange Hasholt, Technical University of Denmark (DK) - chairman

Senior consultant Gitte Normann Munch-Petersen, Danish Technological Institute (DK)

Professor Jouni Punkki, Aalto University (FI)

Professor Jukka Lahdensivu, Tampere University of Technology (FI)

Dr. Jón E. Wallevik, Innovation Center Iceland (IS)

Dr. Olafur H. Wallevik, Innovation Center Iceland (IS)

Dr. Terje F. Rønning, Heidelberg Cement (NO)

Professor Mette Rica Geiker, NTNU (NO)

Tekn. Dr. Peter Utgenannt, CBI Swedish Cement and Concrete Research Institute (SE)

Section manager Mårten Janz, ÅF (SE)

## Contents

	page
<b>Preface</b>	III
<b>Scientific committee</b>	IV
<b>Contents</b>	V
<b>A1 BINDER SYSTEMS WITH AND WITHOUT SUPPLEMENTARY CEMENTITIOUS MATERIALS (SCM)</b>	1
Martin Kaasgaard and Claus Pade: <b>Properties of concrete with a new type of cement with low carbon footprint</b>	3
Danute Vaiciukyniene, Ruben Paul Borg, Andrius Kiele and Aras Kantautas: <b>Alkali activated calcined <math>AlF_3</math> production waste – Clay blends</b>	7
Tapio Vehmas, Markku Leivo and Erika Holt: <b>Comparison of experimental and modelled pore solutions of low-pH Ordinary Portland Cement based mix designs</b>	11
Alisa Machner, Maciej Zajac, Mohsen Ben Haha, Knut. O. Kjellsen, Mette R. Geiker and Klaartje De Weerd: <b>Investigation of the products of the dolomite reaction in Portland cement pastes</b>	15
Serina Ng and Tone Østnor: <b>Ternary cement blends with Fly ash-Calcined clay-OPC: An evaluation on their early age and mechanical properties as binders</b>	19
Wilson Ricardo Leal Da Silva, Lars Nyholm Thrane, Thomas Lennart Svensson and Claus Pade: <b>Performance-based design procedure for the selection of concrete binder systems with low environmental impact</b>	23
Wolfgang Kunther, Sergio Ferreira and Jørgen Skibsted: <b>The compressive strength of C-S-H phases with two different Ca/Si ratios</b>	27

<b>A2</b>	<b>FIBRE REINFORCEMENT, TEXTILE REINFORCEMENT, ETC.</b>	31
	Natalie Williams Portal, Mathias Flansbjerg and Urs Mueller: <b>Experimental study on anchorage in textile reinforced reactive powder concrete</b>	33
	Eythór Rafn Thórhallsson, Guðmundur Úlfar Gíslason, Guðni Jónsson and Jónas Th. Snaebjörnsson: <b>Basalt fiber reinforced precast concrete panels - an alternative concept</b>	37
	Marika Eik, Anna Antonova, Jouni Punkki and Jari Puttonen: <b>Study of adhesive bond properties between the cement-paste and short steel or polypropylene fibres by X-ray nano-Computed Tomography</b>	41
	Mathias Flansbjerg and Natalie Williams Portal: <b>3D analysis of strains in fibre reinforced concrete using X-ray tomography and digital volume correlation</b>	45
	Cristian Sabau, Jaime Gonzalez-Libreros and Björn Täljsten: <b>Flexural behaviour of textile reinforced concrete (TRC) slabs</b>	49
	Johan Silfwerbrand: <b>Load tests on industrial steel fibre concrete floors</b>	53
<b>A3</b>	<b>TESTING</b>	57
	Mathias Flansbjerg and Jan Erik Lindqvist: <b>Methodology for mesomechanical study of concrete material</b>	59
	Anders Ansell, Lamis Ahmed and Alvaro Guarin: <b>Computed tomography as investigation method for steel fibre reinforced tunnel shotcrete</b>	63
	Lamis Ahmed and Anders Ansell: <b>Dynamic measurements for determination of Poisson's ratio of young concrete</b>	67
	Miguel Ferreira, Edgar Bohner and Fahim Al-Neshawy: <b>NPP containment wall mock-up for long-term NDE and monitoring</b>	71
	Oskar Linderöth and Peter Johansson: <b>Development of a laboratory method for assessing the cement content of an arbitrary sample of mortar or concrete</b>	75
	Guzel Shamsutdinova, Max A. N. Hendriks and Stefan Jacobsen: <b>Concrete-ice abrasion: Laboratory studies using a sawn concrete surface</b>	79

<b>A4 DURABILITY OF CONCRETE WITH SUPPLEMENTARY CEMENTITIOUS MATERIALS (SCM)</b>	83
Andres Belda Revert, Mette Rica Geiker, Klaartje De Weerd and Ulla Hjorth Jakobsen: <b>SEM-EDS analysis of products formed under natural and accelerated carbonation of concrete with CEM I, CEM II/B-M and CEM II/B-V</b>	85
Monica Lundgren, Arezou Babaahmadi and Urs Mueller: <b>On the porosity development in cement pastes containing slag: Influence of curing conditions and the effect of carbonation</b>	89
Arezou Babaahmadi, Monica Lundgren and Urs Mueller: <b>Durability of slag blended binder systems towards sulphate ingress</b>	93
Mette Rica Geiker, Klaartje De Weerd, Sergio Ferreira Garzón, Mads Mønster Jensen, Björn Johannesson and Alexander Michel: <b>Durability testing of low clinker binders - chloride ingress in similar strength mortars exposed to seawater</b>	97
Helén Jansson, Robin Snibb, Karl Bohlin and Ingemar Löfgren: <b>Carbonation of concrete with mineral additions</b>	101
Nadia Al-Ayish, Otto During and Katarina Malaga: <b>The influence of low chloride migration in concrete with mineral addition on minimizing climate impact of bridges</b>	105
<b>A5 CARBONATION, CHLORIDE INGRESS AND CORROSION</b>	109
Erik Nordström: <b>Evaluation after 17 years of field exposures on cracked steel fibre reinforced shotcrete</b>	111
Edgar Bohner and Miguel Ferreira: <b>Extending service life design by coupling the limit states of corrosion initiation and corrosion induced cracking</b>	115
Tobias Danner, Klaartje De Weerd and Mette Rica Geiker: <b>μ-XRF – Characterisation of chloride ingress and self-healing in cracked concrete</b>	119
Carlos G. Berrocal, Ignasi Fernandez, Ingemar Löfgren and Karin Lundgren: <b>Corrosion-induced cracking and bond behaviour of corroding reinforcement bars in SFRC</b>	123

	Arto Köliö, Jukka Lahdensivu and Matti Pentti: <b>Corrosion probability and service life in reinforced concrete facades in Nordic climate</b>	127
	Claus Vestergaard Nielsen: <b>Durability assessment and service life design for reinforced concrete exposed to chloride ingress – an easy to use design diagram</b>	131
<b>A6</b>	<b>AIR ENTRAINING AGENTS AND FROST ACTION</b>	135
	Martin Strand and Katja Fridh: <b>The air void contents effect on the salt frost scaling of uncarbonated concrete containing siliceous fly ash or slag</b>	137
	Ingemar Löfgren: <b>The influence of carbonation and age on salt frost scaling of concrete with mineral additions</b>	141
	Andrei Shpak, Marcin Turowski, Ole Petter Vimo and Stefan Jacobsen: <b>Effect of AEA-SP dosage sequence on air content and air void structure in fresh and hardened fly ash mortar</b>	145
	Fahim Al-Neshawy and Jouni Punkki: <b>Stability of air-entrainment with PCE-superplasticizers</b>	149
	Eneli Liisma: <b>Approach of an elevated criterion for frost resistance of concrete according to Estonian practice in concrete industry</b>	153
	David Wahlbom, Katja Fridh, Teddy Feng-Chong, Patrick Dangla, Vu Quoc Huy, Mette Geiker, Stefan Jacobsen and Jan Skoceck: <b>Frost salt scaling of concrete</b>	157
<b>A7</b>	<b>ALKALI-AGGREGATE REACTIONS</b>	161
	Hans Christian Brolin Thomsen, Bent Grelk, Ricardo Antonio Barbosa and Kurt Kielsgaard Hansen: <b>Alkali release from typical Danish aggregates to potential ASR reactive concrete</b>	163
	Siff Brask, Sophie Andersen, Bent Grelk and Kurt Kielsgaard Hansen: <b>New method "Texas.dot" for continuous measurement of potential expansion of ASR reactive concrete</b>	167

Børge Johannes Wigum and Jan Lindgård: <b>The RILEM approach to mitigate alkali aggregate reactions (AAR) in concrete</b>	171
Simen Sørgaard Kongshaug, Terje Kanstad, Max Hendriks, Mahdi Kioumars and Gro Markeset: <b>Challenges related to structural modelling and assessment of concrete structures affected by alkali-silica reactions</b>	175
<b>A8 SPECIAL APPLICATIONS</b>	179
Markku Leivo, Tapio Vehmas and Erika Holt: <b>Concrete mix designs for tunnel end plugs in nuclear waste repository</b>	181
Magnus Döse and Johan Silfwerbrand: <b>Reduction of radon gas in concrete – effects and evaluation of effective dose</b>	185
Pia Schönbeck, Malin Löfsjögård and Anders Ansell: <b>Requirements on concrete floor structures - a comparison of medical imaging facilities</b>	189
Madumita Sadagopan, Katarina Malaga and Agnes Nagy: <b>A study on recycling of concrete in Sweden</b>	193
Mohammad Hajmohammadian Baghban: <b>Thermal conductivity based mix design of cementitious materials</b>	197
Harald Justnes and Ola Skjølvold: <b>Characterization of cements for injection</b>	201
Ellen Dolk: <b>Concrete pavements' resistance to studded tyres</b>	205

<b>B1</b>	<b>STRUCTURAL DESIGN</b>	209
	Per Goltermann: <b>Challenging the limits for beam bending designs</b>	211
	Kent Kempengren: <b>Strut and tie method – A powerful method to use in continuity and discontinuity regions in reinforced concrete structures in the design process</b>	215
	Mohammad Hajmohammadian Baghban and Mohammadreza Ghazaei: <b>Seismic performance of reinforced concrete frame for the risk assessment process</b>	219
	Jelena Zivkovic and Jan Arve Øverli: <b>Shear capacity of lightweight aggregate concrete beams without shear reinforcement</b>	223
	Tuomas Lehtonen and Matias Hirvikoski: <b>Comparison of punching shear design according to the new Finnish national annex for Eurocode 2 and the former national method</b>	227
	Reignard Tan, Max A.N. Hendriks, Mette Geiker, Dan-Evert Brekke and Terje Kanstad: <b>Evaluation and improvement of crack width calculation method for large concrete structures</b>	231
	Rasoul Nilforoush, Martin Nilsson and Lennart Elfgren: <b>Tensile breakout capacity of cast-in-place headed anchors in concrete</b>	235
<b>B2</b>	<b>EXISTING STRUCTURES (I) CONDITION ASSESSMENT, ESTIMATION OF LOAD-CARRYING CAPACITY &amp; REPAIR</b>	239
	Louise Andersson, Johan Silfwerbrand, Anders Selander and Jan Trägårdh: <b>Preventive bridge maintenance in Sweden - introduction to a PhD-project</b>	241
	Mattias Blomfors, Kamyab Zandi, Karin Lundgren, Oskar Larsson Ivanov and Dániel Honfi: <b>Reliable engineering assessments of corroded concrete structures</b>	245
	Lennart Elfgren, Poul Linneberg, Guðmundur Valur Guðmundsson, Markku Leivo and Jochen Köhler: <b>Quality control plans for European concrete road bridges. Experiences from cooperation within COST action TU 1406</b>	249

<b>B3</b>	<b>EXISTING STRUCTURES (II) CONDITION ASSESSMENT, ESTIMATION OF LOAD-CARRYING CAPACITY &amp; REPAIR</b>	253
	Samanta Robuschi, Ignasi Fernandez Perez, Kamyab Zandi and Karin Lundgren: <b>Assessment of the load-carrying capacity of existing structures with corroded smooth reinforcement bars</b>	255
	Magdalena Paciorek, Terje Kanstad, Max Hendriks, Mahdi Kioumars and Gro Markeset: <b>The effect of reinforcement corrosion on the structural behaviour of prestressed bridges in the Norwegian coastal regions</b>	259
	Niklas Bagge, Jonny Nilimaa, Gabriel Sas, Thomas Blanksvärd, Lars Bernspång, Björn Täljsten, Anders Carolin and Lennart Elfgren: <b>Assessment of concrete bridges - Structural capacity. Experiences from full-scale testing to failure of a bridge in Kiruna</b>	263
	Niklas Bagge, Jonny Nilimaa, Gabriel Sas, Thomas Blanksvärd, Björn Täljsten, Anders Carolin, Björn Paulsson and Lennart Elfgren: <b>Assessment of concrete bridges - Prestress forces. Experiences from full-scale testing to failure of a bridge in Kiruna</b>	267
	Jiangpeng Shu, Mario Plos and Kamyab Zandi: <b>Multi-level assessment of a field tested RC bridge deck slab</b>	271
<b>B4</b>	<b>WORKSHOP ON TEACHING</b>	275
	Per Goltermann, Lisbeth Ottosen, Jacob Wittrup Schmidt and Jens Henrik Nielsen: <b>Project families: A new concept for student thesis activities</b>	277
	Gitte Normann Munch-Petersen and Lars Nyholm Thrane: <b>Green concrete workshops for students</b>	281

<b>B5</b>	<b>FINITE ELEMENT METHOD (FEM)</b>	285
	Daniel Eriksson and Tobias Gasch: <b>Comparison of mechanistic and phenomenological approaches to model drying shrinkage of concrete</b>	287
	Mohammad Hajmohammadian Baghban and Saeid Gerivani: <b>Evaluating the seismic behavior of reinforced concrete piers of bridges by using fibre plastic hinge elements</b>	291
	Håkan Hansson: <b>Analyses of concrete structures subjected to extreme loading</b>	295
	Rikard Hellgren and Richard Malm: <b>Stability assessment of concrete dams with non-linear FEA</b>	299
	Sheida Hooshmandi, Mahdi Kioumarsi, Benyamin Kioumarsi and Mohammad H. Baghban: <b>Application of response surface method (RSM) on sensitivity analysis of reinforced concrete bridge pier wall</b>	303
<b>B6</b>	<b>THERMAL CRACKING</b>	307
	Jukka Lahdensivu and Tapio Aho: <b>Evaluation of concrete tank degradation</b>	309
	Richard Malm, Pär Grahm and Matti Nord: <b>Evaluation of a full-scale test of a concrete dome plug for nuclear repository</b>	313
	Anja B. E. Klausen, Terje Kanstad and Øyvind Bjøntegaard: <b>Early age crack assessment of concrete structures: Experimental and theoretical approaches</b>	317
	Jonny Nilimaa, Anders Hösthagen and Mats Emborg: <b>Validation of the Swedish crack risk estimation models</b>	321
	Anders Hösthagen, Jan-Erik Jonasson, Mats Emborg and Martin Nilsson: <b>Thermal crack risk estimations of concrete walls – Temperature and strain measurements correlated to the equivalent restraint method</b>	325

<b>B7</b>	<b>SHRINKAGE AND CREEP</b>	329
	Tobias Gasch and Anders Ansell: <b>Influence of varying ambient conditions on time-dependent deformations in concrete using multi-field modelling</b>	331
	Andreas Sjölander and Anders Ansell: <b>Analysis of the interaction between rock and shotcrete for tunnel support</b>	335
	Faez Sayahi, Mats Emborg and Hans Hedlund: <b>Effect of water-cement ratio on plastic shrinkage cracking in self-compacting concrete</b>	339
	Martin Persson, Ulf Ohlsson, Johan Silfwerbrand and Mats Emborg: <b>Interface stresses in concrete bridge deck overlays subjected to differential shrinkage</b>	343
<b>B8</b>	<b>CONCRETE RHEOLOGY AND OTHER PROPERTIES OF FRESH CONCRETE</b>	347
	Rolands Cepuritis, Stefan Jacobsen and Jon Spangenberg: <b>The Particle-Matrix model: limitations and further improvements needed</b>	349
	Lasse Frølich: <b>Segregation in concrete – should it be measured more often and how?</b>	353
	Judy Luong, Kari Aarstad, Klaartje De Weerd and Øyvind Bjøntegaard: <b>Excavated rock materials from tunnels for sprayed concrete</b>	357
	Yahya Ghasemi and Mats Emborg: <b>A method for obtaining optimum packing of aggregates for concrete at the onset of flow</b>	361
	Øyvind Fremmergård, Mats Fjærestrand, Simen M. D. Hjelseth, Ann Karina Lassen and Mahdi Kioumars: <b>Reasons to the low use of self-consolidating concrete in Norway</b>	365
	Erika Holt, Markku Leivo, Ville Sjöblom and Johanna Hansen: <b>Development and demonstration of concrete for investigative deep borehole sealing at Olkiluoto nuclear repository site</b>	369



**Session A1:**

**BINDER SYSTEMS WITH AND WITHOUT  
SUPPLEMENTARY CEMENTITIOUS MATERIALS (SCM)**



## Properties of concrete with a new type of cement with low carbon footprint



Martin Kaasgaard  
Consultant, M.Sc.  
Danish Technological  
Institute  
Gregersensvej  
DK-2630 Taastrup  
E-mail:  
mkaa@teknologisk.dk



Claus Pade  
Team Manager, M.Sc.  
Danish Technological  
Institute  
Gregersensvej  
DK-2630 Taastrup  
E-mail:  
cpa@teknologisk.dk

### ABSTRACT

In this study, which is part of the H2020 ECO-Binder project, C32/40 concretes with three different BYF (Belite, Ye'elimite, Ferrite) cements combined with different aggregate types were produced and tested. The concretes were batched and mixed in the laboratory using an industrial scale concrete mixing station and applying procedures ensuring high batching accuracy and identical mixing sequence. The concretes were subject to a test program comprising measurement of fresh, hardening and hardened concrete properties, including consistency, setting time, heat development, strength development, E-modulus and shrinkage. The results obtained are presented and discussed in relation to properties of Portland cement based concrete. The most unique features of BYF cement concrete appear to be high early strength and low shrinkage.

**Keywords:** Sustainability, BYF cement, concrete properties, strength development, shrinkage

### 1. INTRODUCTION

BYF cements constitute a new family of binders resulting from research into the reduction of CO<sub>2</sub> emissions in the cement industry. The clinker, composed of belite, ye'elimite and ferrite, is ground with calcium sulfate to produce the cement. The raw materials are similar to ordinary Portland cement (OPC), but used in different proportions leading to a different phase composition. The cement combines the high early strength development of calcium-sulfoaluminate cements with durability properties of belite cements. The main reactive, early strength providing phase in OPC clinker is alite, whereas in BYF it is ye'elimite. The ye'elimite and belite contents can be adjusted to give different properties. Compared to OPC, CO<sub>2</sub> emissions from production are estimated to be around 30% lower due to lower calcium content (calcination), lower clinkering temperature and lower required grinding energy.

In the ECO-Binder project, concrete with BYF cement is combined with insulating materials and advanced functional surface treatment to obtain a new generation of prefabricated building envelope components, which are sustainable and cost-effective. The project furthermore addresses the need for documentation of physical, mechanical and durability properties of concrete based on BYF cement as a prerequisite for standardization. This is the subject of the current study, where three different BYF cements produced by respectively HeidelbergCement, LafargeHolcim and Vicat have been documented.

## 2. MATERIALS AND METHODS

Three different BYF cements (B, D and E) have been analysed. The composition, fineness and setting time of the cements appear from Table 1.

*Table 1 – Composition, fineness and setting time of the cements.*

	Cement B	Cement D	Cement E
Ye'elimite	40-50 %	30-40 %	20-30 %
Belite	20-30 %	30-40 %	40-50 %
Ferrite	0-5 %	10-20 %	5-10 %
Sulfates	10-20 %	5-10 %	5-10 %
Others	10-20 %	0-5 %	10-20 %
Fineness, Blaine	4500 cm <sup>2</sup> /g	5500 cm <sup>2</sup> /g	3780 cm <sup>2</sup> /g
Setting time	42 min	30 min	50 min

The cements were combined with three aggregate types to give a total of nine concretes. The aggregate types were:

- Italian limestone/quartz river sand and gravel (*NT*)
- Danish quartz dominated sea dredged sand combined with two fractions of Norwegian crushed granite – siliceous (*sil*)
- Norwegian crushed limestone in three fractions – calcareous (*cal*)

Before mixing the concretes on the industrial scale mixing station, initial small-scale trial mixing was carried out. The purpose was to define the appropriate water/cement ratio for each cement to obtain a C32/40 strength class concrete. The required water/cement ratios were found to be 0.48, 0.50 and 0.43 respectively for cement B, D and E. Furthermore, the small-scale mixing served to determine the superplasticizer (MasterGleniumSKY 631) dosage needed to obtain an initial slump of 230 mm for each concrete.

Subsequently, 250 litre of concrete was mixed using the mixing station and samples taken and specimens cast for the following tests:

- Consistency (DS/EN 12350-2)
- Setting time (DS 423.17)
- Heat development (NT Build 488)
- Compressive strength development (DS/EN 12390-3) – 0.5, 1, 2, 7, 28 and 91 days
- E-modulus development (DS 423.25) – 7, 28 and 91 days
- Shrinkage (DS 434.6)

## 3. RESULTS AND DISCUSSION

The properties measured for the nine different concretes are presented in Table 2.

Table 2 – Properties measured for the nine different concretes.

		B-NT	B-sil	B-cal	D-NT	D-sil	D-cal	E-NT	E-sil	E-cal
Setting time	[h:min]	04:10	05:10	04:20	05:40	09:20	06:10	02:30	02:30	02:50
Heat dev. parameters	Q [kJ/kg]	280,5	261,8	276,8	272,3	296,7	274,9	223,7	217,0	229,3
	$\tau$ [hours]	6,03	7,28	6,61	9,84	11,67	10,13	6,84	6,56	7,20
	$\alpha$	2,79	3,93	2,79	3,73	5,01	4,10	1,49	1,67	1,24
Compressive strength [MPa]	0.5 d	18,9	18,9	21,0	0,0	0,0	0,0	15,4	17,3	16,3
	1 d	22,5	24,3	21,7	23,8	31,9	28,6	25,3	27,4	26,6
	2 d	22,5	23,7	21,6	26,5	35,6	30,2	30,4	31,9	31,1
	7 d	26,7	28,8	24,7	31,9	45,0	36,5	37,1	39,0	38,0
	28 d	35,3	33,9	32,1	39,5	51,5	41,9	43,4	47,1	43,2
	91 d	40,2	39,9	35,5	42,2	50,4	41,5	47,5	50,9	46,6
Elastic modulus [GPa]	7 d	26,7	32,3	26,2	25,8	36,0	28,4	30,6	35,8	30,2
	28 d	30,0	34,7	29,0	28,6	36,9	30,0	32,6	39,7	32,5
	91 d	29,6	36,9	30,2	29,9	38,6	29,1	33,7	39,9	33,8
Shrinkage [%]	14 d	0,16	0,11	0,13	0,16	0,11	0,11	0,06	0,05	0,04
	28 d	0,20	0,14	0,16	0,22	0,13	0,14	0,10	0,05	0,06
	56 d	0,21	0,15	0,18	0,26	0,15	0,17	0,12	0,08	0,08
	91 d	0,23	0,16	0,19	0,28	0,18	0,19	0,12	0,08	0,09

When comparing the setting time there are clear differences between concretes with the three cements. Cement E concrete has the shortest setting time and cement D concrete the longest (more than twice as long). For comparison, concretes ( $w/c = 0.53$ ) of similar strength with respectively a Danish CEM II/A-LL 52.5 R and a German CEM II/A-LL 42.5 N had setting times of 5 hours and 40 minutes and 7 hours, i.e. at the same level as for cement D concrete, longer than for cement B concrete and more than twice as long as for cement E concrete.

The heat development “initiation” ( $\tau$ ) is the same for cement B and E concrete (6-7 hours), and 3 hours later for cement D concrete. The total heat development (Q) and rate ( $\alpha$ ) is lower for cement E concrete. For comparison, a concrete ( $w/c = 0.40$ ) with a Danish CEM I 52.5 N and 25% (of binder) fly ash had a Q of 295.3 kJ/kg,  $\tau$  of 15.47 hours and  $\alpha$  of 1.09, i.e. the heat development of BYF cement concrete is earlier and faster, but the total heat development lower. Regarding strength development, it is seen from Figure 1 that the very early strength development is quite different for the three cements.

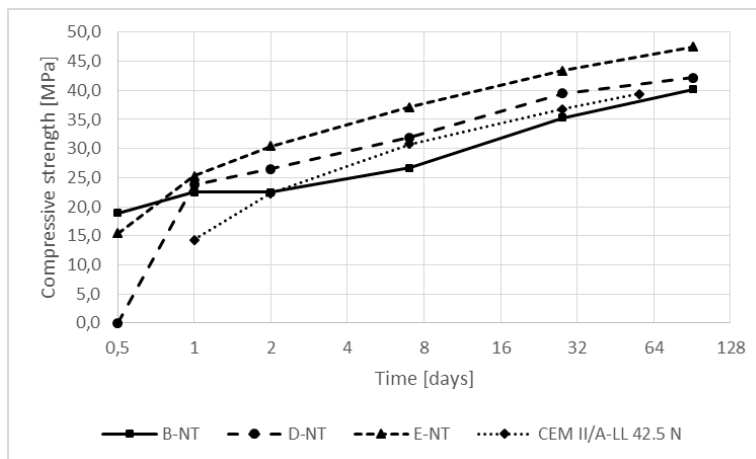


Figure 1 – Compressive strength development of the BYF cement concretes with Italian aggregate and a CEM II/A-LL 42.5 N concrete for comparison.

Cement B concrete had the highest 0.5-day strength, cement E concrete a bit lower, whereas cement D concrete had no 0.5-day strength at all. After 1 day, the concretes had rather similar strength. For cement B concrete there was very little strength increase from 0.5 to 2 days. From 2 to 91 days, the strength increase is rather similar for the different concretes. For cement E and particularly cement D, the strength of concrete with siliceous aggregate is higher than with the Italian and calcareous aggregates (see Table 2).

The E-modulus (see Table 2) is higher for the concretes with cement E, when comparing concretes with the same aggregate type. When comparing concretes with the same cement, the E-modulus is similar for concretes with the Italian and calcareous aggregates and somewhat higher for concrete with the siliceous aggregate.

Finally, the shrinkage of concrete was found to be somewhat different for the three BYF cements as seen from Figure 2.

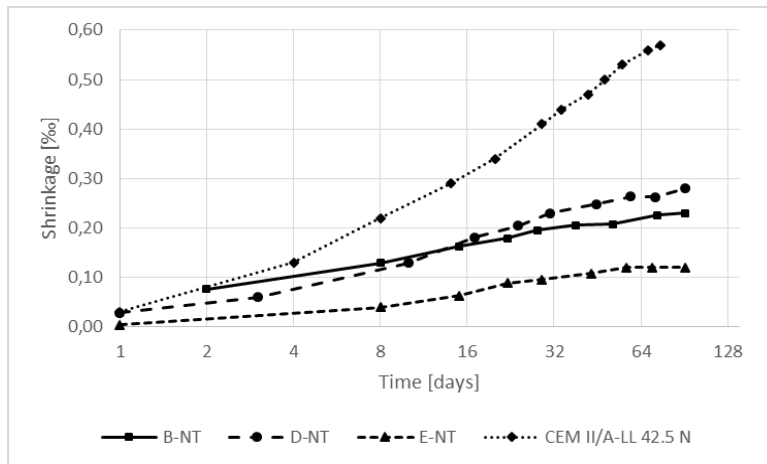


Figure 2 – Shrinkage of the BYF cement concretes with Italian aggregate and a CEM II/A-LL 42.5 N concrete for comparison.

Cement E concrete has clearly the lowest shrinkage, while cement B and D concretes are more comparable. The shrinkage of BYF cement concrete is significantly lower than for the CEM II/A-LL 42.5 N concrete.

#### 4. CONCLUSIONS

Concrete of strength class C32/40 with three different BYF cements combined with three different aggregate types was mixed and tested. The early strength was found to be high, above 15 MPa at 0.5 days for two of the cements and above 21 MPa at 1 day for all three cements. Setting time is relatively short (between 2.5 and 6 hours). Compared to OPC concrete, the total heat development is relatively low, but with a high initial rate. The shrinkage is significantly lower than for OPC concrete. Based on its properties being comparable to those of OPC concrete and the low projected carbon footprint, BYF cement concrete seems a promising candidate for future sustainable application of concrete.

#### 5. ACKNOWLEDGEMENTS

The authors gratefully acknowledge the partners in the ECO-Binder project and the European Commission for funding the project under Horizon 2020 grant agreement no 637138.

## Alkali activated calcined $\text{AlF}_3$ production waste – Clay blends



Danutė Vaičiukynienė  
 Professor. dr.  
 Kaunas University of Technology  
 Faculty of Architecture and civil engineering  
 Studentų g. 48-401, 51367 Kaunas, Lithuania  
 e-mail: danute.palubinskaite@ktu.lt



Ruben Paul Borg,  
 Dr. Spec.  
 University of Malta, Faculty for the Built Environment  
 Msida MSD 2080, Malta  
 e-mail: ruben.p.borg@um.edu.mt



Andrius Kiele  
 PhD student  
 Kaunas University of Technology, Faculty of Architecture and civil  
 engineering  
 Studentų g. 48-401, 51367 Kaunas, Lithuania  
 e-mail: andrius.kiele@ktu.edu



Aras Kantautas  
 Assoc. Professor  
 Kaunas University of Technology, Faculty of Chemical Technology  
 Radvilėnų pl. 19-152, 51367 Kaunas, Lithuania  
 e-mail: aras.kantautas@ktu.lt

### ABSTRACT

In today's world, alkali activated materials have great potential for use in the construction industry. The aim of this research was to study the influence of  $\text{AlF}_3$  production waste from a fertilizer production plant, on the properties of alkali activated clay. The  $\text{AlF}_3$  production waste which is rich in alumina and silica contributed with better mechanical behavior for all cases investigated in the research. This demonstrated the effective potential use of this waste material. It was noted that the dosage of  $\text{Na}_2\text{O}$ ,  $\text{Al}_2\text{O}_3$  and  $\text{SiO}_2$  are significant factors which influence the binding mechanism and properties of alkali-activated clay samples.

**Key words:** alkali activated material, reuse and recycling, clay,  $\text{AlF}_3$  production waste.

## 1. INTRODUCTION

Alkali activation is an important and rapidly developing field of activity in the global research and development community. Commercial-scale deployment of alkali-activated cements and concretes is now proceeding rapidly in many countries. Alkali-activated materials have received a lot of attention lately because they have the potential to partly replace ordinary Portland cement as a construction material. Studies have shown that alkali-activated materials have mechanical properties as good as, or sometimes better than, ordinary Portland cement materials. Alkali activated material has to consist of a certain amount of silicate and aluminate phases which can be dissolved by the alkaline medium. In this process, stable polymeric networks of aluminosilicates will be formed. It is important to suggest alternative low cost primary materials and one of these could potentially be clay [1].

Aluminosilicate sources could include some types of calcine clays. Alkali activated products are synthesized by activation of kaolinitic clay with a sodium hydroxide solution. Alkali activated geopolymers are synthesized. The inorganic polymers have excellent resistance to saline water and sulfate attack [2]. The investigation [3] focuses on the suitability of illite/smectite clay to form a geopolymer after thermal and alkaline activation. Therefore, clay containing mainly illite was thermally activated between 550 and 950 °C. The performance of the geopolymer binder in terms of strength as well as the phase composition was studied. El Hafid et al. [4] reported that heated kaolinitic-illitic raw clay was etched with NaOH aqueous solution (4–14 M) and cured at different temperatures (30–85 °C) and different periods of time (up to 30 h). Chabazite, natrolite and sodium carbonate formed in the cured alkali-activated heated clay. The neo-formed zeolites differed from the predictable ones. The experimental factors and properties of the cured samples were correlated. Reig et al. [5] investigated the properties and microstructure of alkali-activated cement pastes and mortars produced using red clay brick waste. The work shows that the type and concentration of alkali activator can be optimized to produce mortar samples with compressive strengths up to 50 MPa after curing for 7 days at 65 °C.

In this research the influence of  $AlF_3$  production waste on the properties of alkali activated clay was studied. Alkaline activation supports the use of waste materials (with reactive  $SiO_2$  and  $Al_2O_3$ ) that are not suitable in other industries. The material used in this research, namely  $AlF_3$  production waste from fertilizers plant, is an unsuitable material for use in Portland cement based materials due to the harmful fluoride compounds.

## 2. MATERIALS AND METHODS

In this study, clay rich in CaO from Malta (a source of Blue Clay deposit in the Maltese Islands) was used as a raw material for alkali activated material. XRFA elemental analysis was used to determine the chemical composition of the clay. Elemental composition was recalculated to oxides.

The XRD analysis of clay shows peaks of quartz, calcite and some of clay minerals such as illite, muscovite and kaolinite (Fig. 1, a). Along with the clay, by-product silica ( $AlF_3$  production waste) was used as a Si and Al source. High amounts of amorphous  $SiO_2$  and  $Al_2O_3$  makes this waste a good raw material for alkali activated binding material. The X-ray diffraction curve (Fig. 1, b) presents amorphous  $SiO_2 \cdot nH_2O$  (rise from 10 up to 30°) and crystalline  $AlF_3 \cdot 3.5 H_2O$  (diffraction angles  $2\theta = 16.16^{\circ}, 10.3^{\circ}, 23.02^{\circ}, 26.98^{\circ}, 29.36^{\circ}, 36.72^{\circ}, 51.28^{\circ}$  and  $52.92^{\circ}$ ). Alkali activator reagent NaOH (Delta Chem, Czech Republic) was used. The XRF analysis of dried silica gel showed that it contained the following: 60.15 %  $SiO_2$ , 35.52 %  $AlF_3$ , 4.43 %  $Al_2O_3$ . Very high fluoride concentrations were obtained through the amorphous silica XRF analysis. It is believed that fully un-reacted  $H_2SiF_6$  in the silica investigated should be left in addition to these compounds. The presence of  $H_2SiF_6$  in heterogeneous systems is problematic.

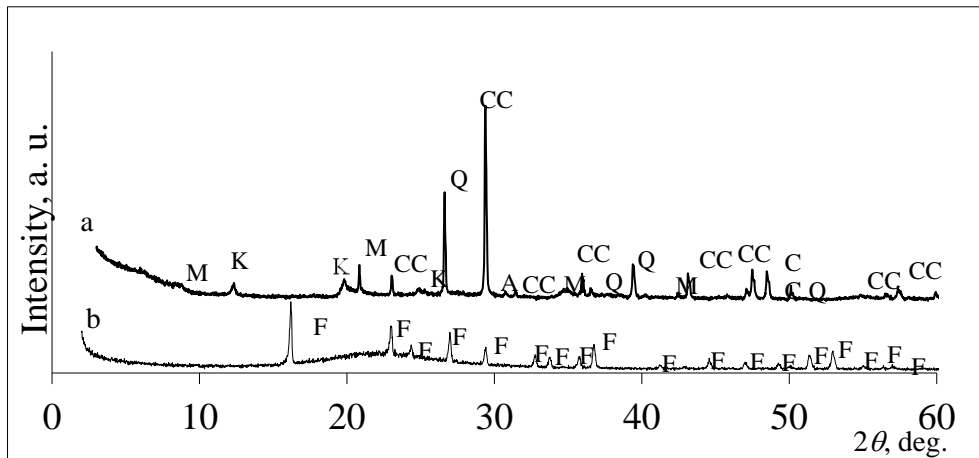


Figure 1 - X-ray diffraction pattern of the raw clay (a) and  $\text{AlF}_3$  production waste (b). Notes: Q is quartz  $\text{SiO}_2$  (78-1253), I is illite ( $\text{K}, \text{H}_3\text{O}$ ) $\text{Al}_2\text{Si}_3\text{AlO}_{10}(\text{OH})_2$  (26-911), M is muscovite  $\text{KAl}_3\text{Si}_3\text{O}_{10}(\text{OH})_2$  (75-948), CC is calcite  $\text{CaCO}_3$  (72-1214), K is kaolinite  $\text{Al}_2\text{Si}_2\text{O}_5(\text{OH})_4$  (1-527), A is ankerite  $\text{Ca}(\text{Fe,Mg})(\text{CO}_3)_2$  (41-586), F is rosenbergite  $\text{AlF}_3 \cdot 3.5 \text{H}_2\text{O}$  ( ).

The mixtures based on clay and  $\text{AlF}_3$  production waste were activated with NaOH solution. The  $\text{AlF}_3$  production waste was blended with clay to provide the necessary alumina and silica content. The amount of NaOH was determined on the basis of the  $\text{SiO}_2/\text{Na}_2\text{O}$  required for a certain mix. In the experimental investigation, 4 different mixtures with different  $\text{SiO}_2/\text{Na}_2\text{O}$  ratios have been studied (Table 1).

Table 1 - The quantities of primary materials for alkali activation.

Mix No.	Clay, %	$\text{AlF}_3$ production waste, %	Clay + $\text{AlF}_3$ production waste, g	NaOH, g	$\text{H}_2\text{O}$ , g	$\text{SiO}_2/\text{Na}_2\text{O}$ mol	W/S*
1	100	0	80	18.4	45	1.71	0.46
2	90	10	80	18.4	45	1.89	0.46
3	75	25	80	18.4	45	2.15	0.46
4	50	50	80	18.4	45	2.6	0.46

\*Water and solid materials ratio.

The XRD analysis for the raw materials were performed on the D8 Advance diffractometer (Bruker AXS, Karlsruhe, Germany) operating at the tube voltage of 40 kV and tube current of 40 mA. The X-ray beam was filtered with Ni 0.02 mm filter to select the  $\text{CuK}\alpha$  wavelength. Diffraction patterns were recorded in a Bragg-Brentano geometry using a fast counting detector BrukerLynxEye based on silicon strip technology. The specimens were scanned over the range  $2\theta = 3\text{--}60^\circ$  at a scanning speed of 6 min $^{-1}$  using a coupled two theta/theta scan type".

The XRFA analysis of Clay and  $\text{AlF}_3$  production waste were performed on the fluorescence spectrometer S8 Tiger (Bruker AXS, Karlsruhe, Germany) operating at the counter gas Helium 2 bar.

Paste samples were cast in 20×20×20 mm moulds and left for 1 hour in ambient laboratory conditions. After a 1-hour period the moulds were put into sealed bags to prevent drying and cured at an elevated temperatures of 60 °C for 24 hours. The samples were then cured at room temperature for 27 days. The compressive strength of samples was tested using a hydraulic press ToniTechnik 2020 after 7 and 28 days.

### 3. RESULTS AND DISCUSSION

Since most of these raw materials contain  $\text{AlF}_3$  production waste and clay minerals have a high loss on ignition, they were heated at  $600^\circ\text{C}$  to improve their activity. X-ray diffraction (XRD) analysis was carried out to determine the different minerals and the degree of dehydroxylation in each mixture.

The microstructure of the cured products was investigated through X-ray diffraction, Fourier transform infrared spectroscopy, and scanning electron microscopy. The effects of the  $\text{AlF}_3$  production waste on the mechanical strength and density of the cured samples were evaluated.

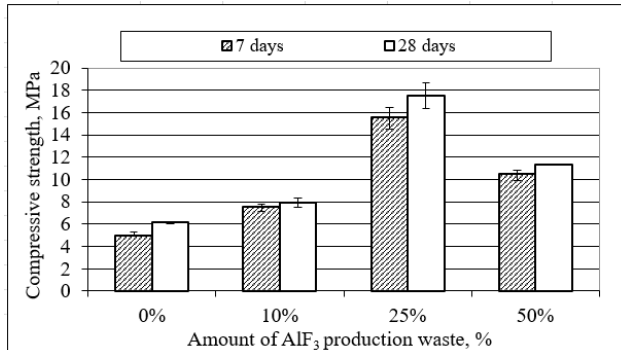


Figure 2 - The dependence of alkali activated samples compressive strength on the amount of  $\text{AlF}_3$  production waste after 7 and 28 days of hydration.

The compressive strength development of alkali activated clay pastes with different amounts of  $\text{AlF}_3$  production waste and different  $\text{Al}_2\text{O}_3$ ,  $\text{Na}_2\text{O}$  and  $\text{Si}_2\text{O}$  constant at 28 days curing is shown in Fig. 2. The highest compressive strengths (17.50 MPa) were observed in alkali activated clay samples based on 25 % of  $\text{AlF}_3$  production waste.

### 4. CONCLUSION

This study presents the use of  $\text{AlF}_3$  production waste as the sources alumina and silica and in all investigated cases this waste contributed in the better mechanical behavior. This demonstrates a new potential added value reuse application for this important waste material. The dosage of  $\text{Na}_2\text{O}$ ,  $\text{Al}_2\text{O}_3$  and  $\text{SiO}_2$  are significant factors influencing the binding mechanism and properties of alkali-activated clay samples.

### RERERENCES

1. Provis, J. L., Palomo, A., & Shi, C. (2015). Advances in understanding alkali-activated materials. *Cement and Concrete Research*, 78, 110-125.
2. Slaty, F., Khoury, H., Rahier, H., & Wastiels, J. (2015). Durability of alkali activated cement produced from kaolinitic clay. *Applied Clay Science*, 104, 229-237.
3. Buchwald, A., Hohmann, M., Posern, K., & Brendler, E. (2009). The suitability of thermally activated illite/smectite clay as raw material for geopolymer binders. *Applied Clay Science*, 46(3), 300-304.
4. El Hafid, K., & Hajjaji, M. (2015). Effects of the experimental factors on the microstructure and the properties of cured alkali-activated heated clay. *Applied Clay Science*, 116, 202-210.
5. Reig, L., Tashima, M. M., Borrachero, M. V., Monzó, J., Cheeseman, C. R., & Payá, J. (2013). Properties and microstructure of alkali-activated red clay brick waste. *Construction and Building Materials*, 43, 98-106.

## Comparison of experimental and modelled pore solutions of low-pH Ordinary Portland Cement based mix designs



Tapio Vehmas  
M.Sc., Research Scientist  
VTT Technical Research Centre of Finland Ltd.  
Kemistintie 3 Espoo, FI-02044 VTT  
e-mail: tapio.vehmas@vtt.fi



Markku Leivo  
D.Sc., Principal Scientist  
VTT Technical Research Centre of Finland Ltd.  
Kemistintie 3 Espoo, FI-02044 VTT  
e-mail: markku.leivo@vtt.fi



Erika Holt  
D.Sc., Principal Scientist, Programme Manager  
VTT Technical Research Centre of Finland Ltd.  
Kemistintie 3 Espoo, FI-02044 VTT  
e-mail: erika.holt@vtt.fi

### ABSTRACT

Posiva Oy is constructing one of the world's first long-term nuclear waste repositories in Finland. Cementitious materials will be in direct contact with backfill and closure materials. It is assumed that cementitious leachates will interact with backfill and closure materials but not to extent that compromises the long-term safety of the barrier system. In this study, existing modelling tools were compared to experimental samples. Applicability to model the low-pH cementitious materials pore solution compositions was evaluated. Accurate modelling will enable long-term evaluation of the cementitious leachates effect to the backfill and closure materials.

**Key words:** Cement, Modelling, Nuclear.

## 1. INTRODUCTION

Posiva Oy is constructing one of the world's first long-term nuclear waste repositories in Finland. The safety of the nuclear waste repository is ensured with a combination of natural and engineered barriers. Final nuclear waste disposal will take place in a deep underground repository in Olkiluoto bedrock at a depth of 400–450 meters. The natural barrier consists of the surrounding Olkiluoto bedrock and its inherent isolating properties. The engineered barrier system consists of water- and gas-tight sealed copper canisters with a cast iron insert and bentonite-based buffer and backfill.[1]

Cementitious materials will be in direct contact with backfill and closure materials. It is assumed that cementitious leachates will interact with backfill and closure materials but not to extent that compromises the long-term safety of the barrier system. To meet the designed performance requirements during the lifecycle of the repository, the properties of the engineered barrier system should not alter due the presence of cementitious materials.[3]

Extremely long lifetime of the repository makes it difficult to predict the evolution of the low-pH cementitious materials. Modelling is a useful tool to predict to long-term behaviour of the materials, but on the other hand, the modelling greatly depends on the used parameters.

The scope of the current study was to compare existing modelling tools to experimental samples and evaluate applicability of modelling on the long-term behaviour of the cementitious materials.

## 2 MATERIALS AND METHODS

Batch samples of Ordinary Portland Cement (OPC) and colloidal silica was prepared in C/S – ratios: 0.2, 0.4, 0.6, 0.8, 1.0, 1.2, 1.4, 1.6, 1.8, 2.0, 2.6 and 3.14. Water/binder –ratio of the samples were 1. The used OPC was Anlåggninscement from Cementa (elemental oxide composition: CaO 64.70%, SiO<sub>2</sub> 18.10%, Fe<sub>2</sub>O<sub>3</sub> 5.17%, SO<sub>3</sub> 4.02%, Al<sub>2</sub>O<sub>3</sub> 3.61%, MgO 0.76%, K<sub>2</sub>O 0.64%, TiO<sub>2</sub> 0.28%, MnO 0.28%, Na<sub>2</sub>O 0.08%) and the used colloidal silica was Levasil 100/45 from AkzoNobel (Ammonium, sodium stabilized colloidal silica, average particle size 30nm, pH 10). The samples were stored in sealed vials for over 200 days to reach chemical equilibrium. After the storing, the pH of the pore solution was measured in ion exchanged water with the method described in the reference [3]. Ion exchanged water was de-aired prior the measurement with ELE water de-airing equipment. Liquid phase, presenting the pore solution was further centrifuged and decanted. Ion concentrations of the liquid phase were determined with high resolution ICP-MS (Element 2™ ThermoScientific).

Identical compositions of the batch samples were modelled with thermodynamic modelling. Gibbs energy minimization simulation was performed with GEMS-Selektor and CEMDATA14 database. Chemical composition of the Anlåggninscement was taken from the literature.[4]

## 3 RESULTS AND DISCUSSION

Comparison of the measured and modelled pore solution concentrations is presented in the Figure 1.

Most of the measured ion concentrations were higher than predicted by the modelling. Largest difference between the modelled and measured results was observed with iron. Modelling indicated that the solubility of iron was limited due the precipitation of iron hydroxide (goethite), a ferrous mineral with low solubility. It is likely that the storing period of the

experimental samples was too short to induce precipitation of ferrous hydroxide. Therefore the measured iron concentrations were significantly higher than the modelled concentrations. In the modelling, magnesium concentrations were limited by the precipitation of brucite (magnesium hydroxide). It is also likely that brucite was not fully precipitated in the measured samples.

Measured alkali concentrations deviated from the modelled. Modelled sodium concentrations decreased as C/S –ratio lowered. In the measured samples, concentrations increased. Modelled potassium concentrations were higher than the measured values. The difference in modelled and measured potassium concentrations can be explained with calcium-silicate-hydrate alkali absorption. Potassium was effectively bound to calcium-silicate-hydrate structure in low C/S-ratios. Absorption effects are not accounted in thermodynamic modelling. Also the sodium concentrations were controlled by a process that was not accounted in the modelling.

Thermodynamic modelling of calcium-silicate-hydrates has proven to be a difficult task. Calcium-silicate-hydrates are a solid solution which composition alters according C/S –ratio. The used model accounts calcium-silicate-hydrates as solid solution but the model is greatly influenced by the selection of the calcium-silicate-hydrate end-members. Measured silicon concentrations were higher than the modelled. The difference can arise from slow kinetics of calcium-silicate-hydrate transformations or insufficient thermodynamic parameters of calcium-silicate-hydrate solid solution.

Measured and modelled pH values had good correspondence in high C/S- ratios. In low C/S –ratio samples, the modelled and measured values deviated. Measured pH values were higher than modelled. In low C/S –ratios, uncertainties related to alkali absorption and calcium-silicate-hydrate phases induced differences in the modelled and measured values.

#### **4 CONCLUSIONS**

Thermodynamic modelling proved to be a powerful tool to estimate solution and solid compositions of hydrated low-pH OPC mixtures. The differences between the modelled and the measured results potentially originated from three sources: slow kinetics of the chemical processes, absorption processes and insufficient parametrisation of the solid phases.

The modelling accuracy could be increased by excluding the mineral phases that are known to have extremely slow kinetics at the time span of the experimental samples. Adding an absorption process to the modelling increases the accuracy of the measured and modelled alkali concentrations. Improvements in thermodynamic parametrisation of calcium-silicate-hydrate could also increase to modelling accuracy.

#### **5 ACKNOWLEDGEMENTS**

The research leading to these results has received funding from The European Union's European Atomic Energy Community's (Euratom) Horizon 2020 programme (NFRP-2014/2015) under grant agreement 662147–Cebama.

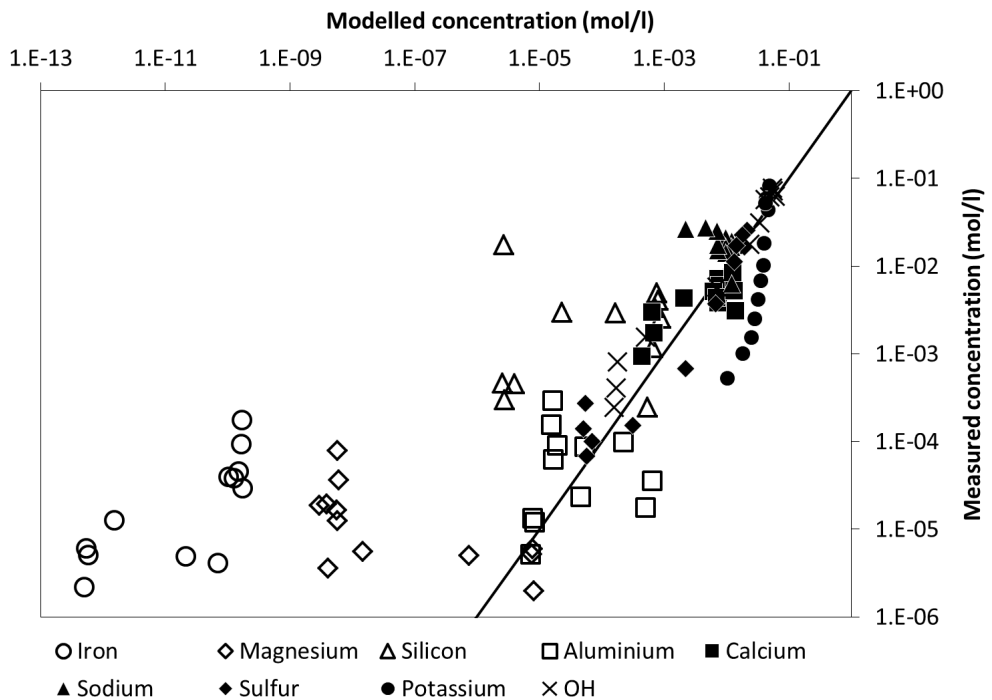


Figure 1 – Comparison of measured and modelled concentrations. Solid black line presents the theoretical full correlation.

## REFERENCES

- [1] Palomäki, J., Ristimäki, L. (edit.): “Facility Description 2012: Summary Report of the Encapsulation Plant and Disposal Facility Designs”, Posiva Oy, Working Report 2012-66, 148 pp. (2013)
- [2] Koskinen, K.: “Effects of Cementitious Leachates on the EBS”, Posiva Oy, Working Report 2013-4, 63 pp. (2014)
- [3] M. Alonso, J. Garcia Calvo, C. Walker, M. Naito, S. Pettersson, I. Puigdomenech, M. Cunado, M. Vuorio, H. Weber, H. Ueda, K. Fujisaki: “Development of an accurate pH measurement methodology for the pore fluids of low pH cementitious materials,” Svensk Kärnbränslehantering AB, August (2012)
- [4] Lagerblad, B., Trägårdh, J.: “Conceptual model for concrete long time degradation in a deep nuclear waste repository, Swedish Cement and Concrete Research Institute, technical report 95-21, 104pp, (1994)

## Investigation of the products of the dolomite reaction in Portland cement pastes



Alisa Machner  
Industrial PhD student  
Norcem AS  
NTNU Department of Structural  
Engineering  
NO – 7034 Trondheim  
alisa.machner@ntnu.no

Maciej Zajac  
Mohsen Ben Haha  
Heidelberg Technology Center  
DE – 69181 Leimen  
maciej.zajac@htc-gmbh.com  
mohsen.ben.haha@htc-gmbh.com

Knut O. Kjellsen  
R&D Manager  
Norcem AS  
FoU  
NO – 3991 Brevik  
knut.kjellsen@norcem.no

Mette R. Geiker, professor  
Klaartje De Weerd, professor  
NTNU Department of Structural  
Engineering  
NO – 7034 Trondheim  
klaartje.d.weerd@ntnu.no  
mette.geiker@ntnu.no

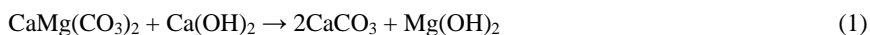
### ABSTRACT

The formation of potentially deleterious reaction products from the reaction of dolomite fines in Portland cement pastes was investigated. It was shown that the reaction of dolomite fines did not follow the commonly accepted dedolomitization reaction. Instead, similar hydration phases as reported for the Portland cement containing limestone are observed, with the exception that also hydrotalcite is formed. It was shown with SEM-EDS and XRD that hydrotalcite is the only magnesium containing hydration product of the dolomite reaction, as no brucite or M-S-H were detected. In the next step of this study this reaction will be investigated in Al-rich systems.

**Keywords:** Supplementary cementitious materials (SCM)

### 1. INTRODUCTION

Due to the scarceness of high-quality limestone as required for CEM II Portland-limestone cements, other carbonate sources, like dolomite ( $\text{CaMg}(\text{CO}_3)_2$ ), are in the focus as alternative mineral replacement for cement clinker. However, dolomite is assumed to undergo the so-called dedolomitization reaction in high-pH environments. In this reaction, dolomite reacts with calcium hydroxide (portlandite) to form calcium carbonate (calcite) and magnesium hydroxide (brucite) [1-3], as shown in equation 1.



There is still an ongoing discussion whether this reaction is harmful to concrete made with dolomitic aggregates. It was recently shown, that in cementitious systems, where other ions are present (Al, Si), the reaction of dolomite results in products similar to those of hydrating Portland-limestone cement with the exception of additional hydrotalcite [4]. The aim of this study was to investigate the influence of replacement of Portland cement clinker by dolomite on the phase assemblage. This was done with focus on whether other magnesium-containing and potentially harmful phases are formed during the reaction of dolomite i.e. brucite (expansive) or

M-S-H (low cementing properties). In a next step of this study the influence of additional aluminium by the addition of metakaolin on the dolomite reaction will be investigated.

## 2. EXPERIMENTAL

The cement pastes investigated in this study were prepared by replacing 40 %wt of a Portland cement clinker by natural dolomite. Precipitated gypsum was added, when mixing, in order to achieve a sulphate content of 2.5 %wt per gram of binder. The cement clinker was ground in a laboratory ball mill until a Blaine surface of approx. 400 m<sup>2</sup>/kg was achieved. The dolomite was used as received (Blaine surface: 340 m<sup>2</sup>/kg). The chemical compositions of the major elements of the materials used are given in Table 1. The paste samples were prepared with a w/b ratio of 0.45 and were stored under sealed conditions at a relative humidity of 100% at 38 °C or 60 °C for 360 days.

*Table 1 – Chemical composition of the clinker and dolomite used.*

	SiO <sub>2</sub>	Al <sub>2</sub> O <sub>3</sub>	Fe <sub>2</sub> O <sub>3</sub>	CaO	MgO	K <sub>2</sub> O	Na <sub>2</sub> O	SO <sub>3</sub>	LOI
<b>Clinker</b>	20.6	5.6	3.12	63.26	2.66	1.23	0.51	1.37	-
<b>Dolomite</b>	0.52	0.01	0.04	31.52	20.14	0.00	0.00	0.00	46.79

In order to investigate the phase assemblage and microstructure of the samples with scanning electron microscopy (SEM), a 3 mm slice was cut off the cured cement paste and immersed in isopropanol for min. 1 week. Polished and carbon coated sections of the paste samples were prepared for SEM analysis. Elemental mapping and spot analyses were carried out using a Hitachi S-3400N microscope equipped with an energy dispersive spectrometer (EDS) from Oxford. Prior to X-ray diffraction (XRD) analyses, the hydration of the cement pastes was stopped by double solvent exchange using isopropanol and petroleum ether. For the XRD analyses a D8 Focus diffractometer from Bruker was used for the measurements with a Bragg-Brentano  $\theta - \theta$  geometry and Cu-K $\alpha$  radiation (approx. 1.54 Å).

## 3. RESULTS AND DISCUSSION

Figure 1 shows the BSE images and the elemental maps of magnesium, aluminium, oxygen, calcium and silicon for the investigated sample cured at 38 °C and 60 °C. The large uniform grains (length up to 70  $\mu$ m) in both images contain magnesium and calcium and are poor in silicon and aluminium. These particles are unreacted dolomite grains. For the sample cured at 60 °C (Figure 1 – upper row) a darker reaction rim can be observed within the original grain boundaries of the dolomite grains. These rims appear to be enriched in magnesium compared to the original dolomite grains. Additionally they contain high amounts of aluminium but are poor in silicon and calcium. High oxygen levels were measured in these rims, indicating that the products formed in them are hydrates. The original grain boundaries of the dolomite grains are still visible because a bright thin layer of C-S-H phase has precipitated around them at early ages. This layer then persisted even after the dolomite started to react at later ages. The dark thick reaction rims within the former dolomite grain boundaries indicate a high reaction degree of the dolomite at 60 °C, which results in complete reaction of the smaller dolomite particles. The sample cured at 38 °C shows almost no reaction of the dolomite (Figure 2 – lower row). Only around small cracks in the dolomite particles and directly at the surface, aluminium and oxygen are slightly increased. This is in-line with the findings of Zajac et al. [4], who reported a notably higher reaction degree for dolomite in a composite cement when cured at 60 °C compared to 38 °C. Also other authors reported an increased dissolution rate of dolomite at elevated curing temperatures [2,3]. From the elemental map of magnesium it can be seen, that magnesium is present only inside the former dolomite grain boundaries. This is probably due to

the low mobility of magnesium in high pH environment. The results of the SEM-EDS point analyses of the reaction rims are plotted in Figure 2 as the Mg/Si over the Al/Si ratio. The data points for the sample cured at 38 °C coincide with the y-axis. This is probably due to the limited rim thickness, which results in the measurement of the unreacted dolomite rather than an actual reaction product. In the case of the sample cured at 60 °C, the data points describe a linear line. This indicates that the reaction product has a fixed Mg/Al ratio and does not contain silicon. It can therefore be concluded, that no M-S-H has formed during the reaction of dolomite. The reaction product can be identified as hydrotalcite ( $Mg_{4+x}Al_2(CO_3)_y(OH)_{16} \cdot 4(H_2O)$ ) [5]. The Mg/Al ratio of the hydrotalcite formed was 3.2 in this study. Zajac et al [4] measured a lower Mg/Al ratio of approx. 2 in their samples, probably due to the lower dolomite addition they used in their mixes as they used a similar clinker.

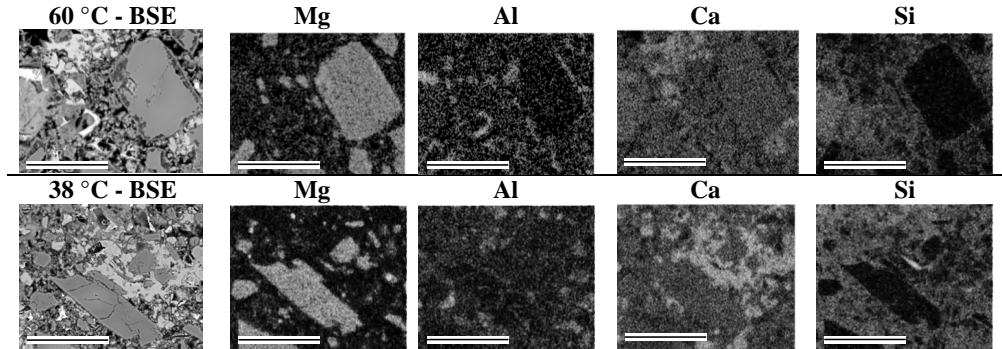


Figure 1 – BSE image and elemental maps of Mg, Al, O, Ca and Si of the sample 60C40D cured at 60 °C (upper row) and 38 °C (lower row) for 360 days. The scales (white bars) represent a length of 50 μm.

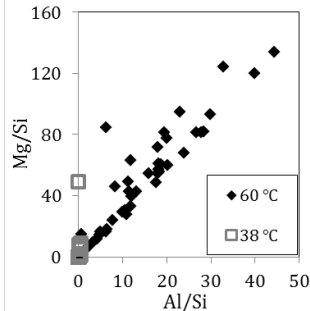


Figure 2 – Mg/Si over Al/Si ratio of the reaction rim in the samples cured at 60 °C or 38 °C.

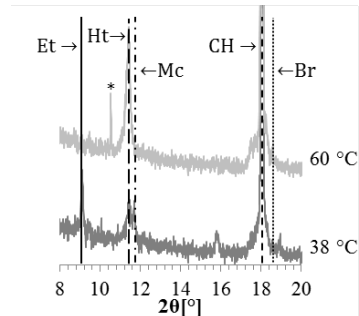


Figure 3 – XRD plots of the samples cured at 60 °C or 38 °C for 360 days. (\* indicates a peak of unknown origin)

Figure 3 shows the XRD plots for the samples cured at 38 °C and 60 °C in the range of 8 to 20 °2θ. The main reflections of ettringite (Et) (9.1 °2θ), hydrotalcite (Ht) (11.4 °2θ), monocarbonate (Mc) (11.7 °2θ), portlandite (CH) (18.1 °2θ) and brucite (Br) (18.6 °2θ) are indicated. The sample cured at 38 °C, shows a clear ettringite peak and small peaks of hydrotalcite and monocarbonate. The reaction of dolomite delivers CO<sub>2</sub> to the system, which can stabilize ettringite by the formation of monocarbonate at 38 °C. This is in agreement with the findings of Zajac et al. [4]. At 60 °C, the stable phases differ significantly from those at

38 °C. The ettringite peak is not observed as this phase is not stable at 60 °C [6]. Moreover, monocarbonate is not detected. The main diffraction peak observed is hydrotalcite, which shows a notably higher and sharper peak at 60 °C compared to the sample cured at 38 °C. This is in good agreement with the observations made by SEM-EDS, which showed a notably higher reaction degree of dolomite at 60 °C compared to 38 °C. In both samples no clear brucite peaks could be observed by XRD. Hydrotalcite is therefore assumed to be the only magnesium-containing reaction product of the dolomite reaction. The proposed reaction based on our observations of dolomite in a cementitious system is given in equation 2.



The dolomite will react with portlandite and alumina in the pore solution to form hydrotalcite and provides carbonate ions to the system which might partially react further to calcite or carbonate AFm. No potentially harmful phases such as brucite or M-S-H were observed.

#### 4. CONCLUSION

It has been shown that the reaction of dolomite fines, when used as replacement for Portland cement clinker, results in the formation of hydrotalcite, especially at 60 °C. Additionally, at 38 °C the stabilization of ettringite due to the formation of monocarbonate can be observed. Contrary to the commonly assumed reaction of dolomite in high-pH environments no brucite was detected. Hydrotalcite was the only magnesium containing product of the dolomite reaction. The reaction of dolomite fines in cementitious systems is therefore not assumed to form any deleterious hydration products. In a next step of this study we will investigate the influence of additional aluminium by the addition of metakaolin on the dolomite reaction.

#### 5. ACKNOWLEDGEMENTS

We acknowledge the industrial Ph.D. programme (project-nr: 241637) of the Norwegian Research Council and the Heidelberg Technology Center for their financial support.

#### REFERENCES

1. E. Garcia, P. Alfonso, M. Labrador, S. Galí, Dedolomitization in different alkaline media: Application to Portland cement paste, *Cem Concr Res* 33 (2003) 1443–1448.
2. S. Galí, C. Ayora, P. Alfonso, E. Tauler, M. Labrador, Kinetics of dolomite-portlandite reaction - Application to Portland cement concrete, *Cem Concr Res* 31 (2001) 933–939.
3. X. Zhang, F.P. Glasser, K.L. Scrivener, Reaction kinetics of dolomite and portlandite, *Cem Concr Res* 66 (2014) 11–18.
4. M. Zajac, S.K. Bremseth, M. Whitehead, M. Ben Haha, Effect of  $\text{CaMg}(\text{CO}_3)_2$  on hydrate assemblages and mechanical properties of hydrated cement pastes at 40 °C and 60 °C., *Cem Concr Res* 65 (2014) 21–29.
5. M. Ben Haha, B. Lothenbach, G. Le Saout, F. Winnefeld, Influence of slag chemistry on the hydration of alkali-activated blast-furnace slag — Part I: Effect of  $\text{MgO}$ , *Cem Concr Res* 41 (2011) 955–963.
6. B. Lothenbach, F. Winnefeld, C. Alder, E. Wieland, P. Lunk, Effect of temperature on the pore solution, microstructure and hydration products of Portland cement pastes, *Cem Concr Res* 37 (2007) 483–491.

## **Ternary cement blends with Fly ash-Calcined clay-OPC: An evaluation on their early age and mechanical properties as binders**



Dr. Serina Ng  
Research Scientist  
Richard Birkelandsvei 3  
7465 Trondheim, Norway  
E-mail: serina.ng@sintef.no



Tone Østnor  
Research Engineer  
Richard Birkelandsvei 3  
7465 Trondheim, Norway  
E-mail: tone.ostnor@sintef.no

### **ABSTRACT**

The synergetic effect of SCMs, fly ash (F) and calcined clay (C) in ternary mixes at 20% replacement was evaluated. It was found that due to the complementary water demand of F and C, pastes made of ternary blends of FC-OPC showed similar or better rheology than OPC pastes. This was coupled with an increase in heat evolved during early age of hydration and a comparable 28 days compressive strength. The results indicate that ternary mix of FC-OPC can be future green cements, where C can be utilized even in the transition stage with existing SCM, such as F.

**Key words:** Ternary blended cements, Rheology, Hydration, Compressive strength, Calcined clay, Fly ash, Cement, Supplementary cementing materials, SCM

### **1. INTRODUCTION**

Cement production contributes to ~6% CO<sub>2</sub> emission annually worldwide [1]. To reduce this, greener and more environmentally friendly binders are sought after. Using supplementary cementing materials (SCMs) is one of the main drivers as it results in a direct reduction in CO<sub>2</sub> emission, making them a popular choice in the cement industry for materials development. Calcined clays is one such SCM. It has shown very favourable performance as an SCM to produce favourable or even enhanced mechanical properties and better durability [2,3]. However, implementation of changes requires a transition period, where introduction of new SCMs are most successful when they can be coupled and employed with the existing materials. Additionally, limitations such as decreased workability with calcined clay need to be solved before they can be of significant commercial values. Technically, we have shown that calcined

clay and fly ash possessed contrasting rheological properties when blended as binary cements [4,5]. Additionally, the strength developed for F and C binary cements appeared to be complementary as well.

The purpose of this investigation is thus to highlight the possibility of creating a ternary cement blend based on fly ash (most common commercial SCM) and calcined clay (new promising SCM). The early age rheological behaviours, heat of hydration and 28 days compressive strength will be highlighted in this article.

## 2. MATERIALS AND EXPERIMENTAL

An OPC and F supplied by Norcem AS (Brevik, Norway), and a smectite rich (~50%) calcined clay (C) from Saint-Gobain Weber (Oslo, Norway) were employed. Detailed chemical compositions of the materials can be found in previous investigations [4]. The specific Blaine surfaces of OPC and F are 382 m<sup>2</sup>/kg and 357 m<sup>2</sup>/kg, while that as measured by BET for C is 15.1 m<sup>2</sup>/g. All materials were utilised as per obtained. Dry powder were manually blended before wetting to produce the binder mixes (Table 1).

*Table 1 - Formulation of dry mixes for investigation*

Mix [wt.%]	C0F20	C5F15	C10F10	C15F5	C20F0	C100	F100	CF0 (OPC)
C	0	5	10	15	20	100	0	0
F	20	15	10	5	0	0	100	0
OPC	80	80	80	80	80	0	0	100

All cement pastes were prepared at a low w/b of 0.36. Dry powder was added to water and mixed under high shear for 1min, let stand for 5min and a final high shear mixing of 1min to avoid false setting. Rheological measurements were performed with a Physica MCR 300 rheometer (Anton Paar, Graz/Austria) equipped with parallel plate geometry. The Bingham viscosity ( $\mu_2$ ) and dynamic yield point ( $\tau_d$ ) were measured. Calorimetric investigation was conducted using an isothermal TAM Air calorimeter (TA Instrument, New Castle/USA) up to 24h. 28 days compressive strength was measured according to EN197-1. More details on the experimental procedures can be found in previous investigations [4].

## 3. RESULTS AND DISCUSSION

**Workability of pastes:** The rheology of reference samples OPC, C and F were first measured. OPC displayed an initial  $\tau_d$  of 269 Pa and corresponding  $\mu_2$  of 0.32 Pa·s. F sample demonstrated an initial  $\tau_d$  of 26 Pa and corresponding  $\mu_2$  of 0.19 Pa·s. The thixotropy of pure C paste was too high for any flow measurements to be registered at the employed w/c of 0.36.

When cement blends containing C-F-OPC with 20% replacement were prepared, the dynamic yield stress of the cement blends varied according to the amount of F and C added. Replacement by 20% F only resulted in a binary paste with  $\tau_d = 147$  Pa, which increased linearly ( $R^2 = 0.9859$ ) as C replaces F by weight percentage to a C20F0 paste possessing  $\tau_d = 374$  Pa (Fig. 1). This indicated that the impact of C to F ratio on the structural skeleton of the cement matrix is additive, governed by the inherent dynamic yield stress exerted by each individual SCM.

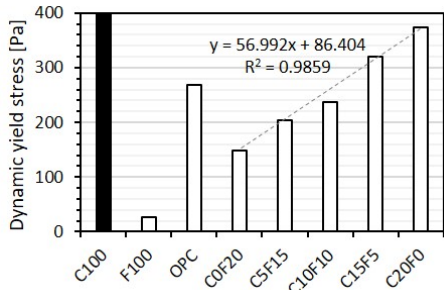


Fig 1 - Dynamic yield stress of cement blends ( $w/b = 0.36$ )

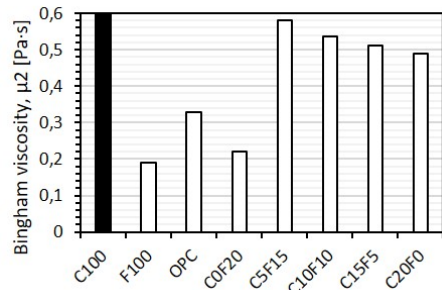


Fig 2 - Bingham viscosity of cement blends ( $w/b = 0.36$ )

On the other hand, such a trend was absent when Bingham viscosity was measured as shown in Fig 2. COF20 displayed a  $\mu_2$  of 0.22 Pa·s, showing high influence of F on the viscosity of the cement blend, possibly a result of the spherical nature of F particles that can 'slip' between particles and decrease the resistance to deformation. Upon replacement with C, a surge in  $\mu_2$  was observed to hit a maximum  $\mu_2$  of 0.58 Pa·s for C5F15, which decreased to 0.49 Pa·s for C20F0. No explanation is possible at the moment, but it indicated that potential interactions between C and F may be present. Additionally, the results demonstrated that C played a greater role in affecting the viscosity of the ternary blends than F.

**Heat of hydration:** Both F (3 J/g) and C (6 J/g) showed negligible cumulative amount of heat released by 24h, whereas OPC registered a cumulative heat evolved of 121 J/g as shown in Fig 3. When binary cement blends were measured, the heat evolved was ~15% and 10% lower than that for OPC when F and C were employed respectively, due to a decrease in initial reactivity in the presence of SCM. However, the heat evolved increased when ternary blends were measured, reaching a maximum of 120 J/g for C15F5 (118 J/g for C10F10), comparable to that for OPC. The results confirm that synergetic interaction between C and F occurred, shading light on the variation in Bingham viscosity.

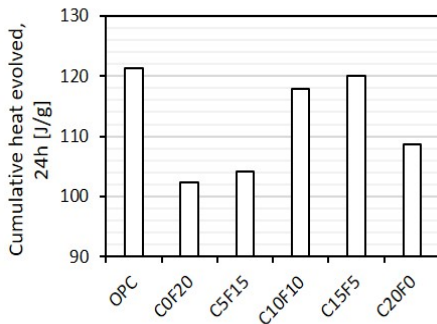


Fig 3 - Cumulative heat evolved at 24h ( $w/b = 0.36$ )

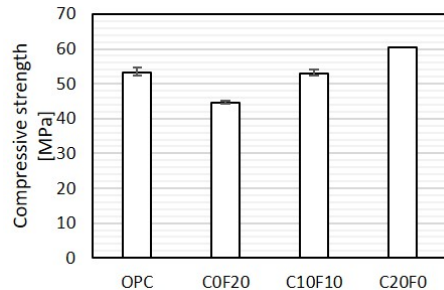


Fig 4 - Compressive strengths at 28 days ( $w/b = 0.36$ )

**Compressive strength analysis:** The compressive strengths of OPC, COF20, C20F0 and C10F10 at 28 days were measured (Fig 4). At 28 days, the compressive strength of OPC mortar was 53.2 MPa, whilst that for the binary mixes were 60.4 MPa (C20F0) and 44.7 MPa (COF20)

respectively. The differences in strengths can be attributed to the pozzolanic nature of C, and low reactivity of F. When an equal proportion of F and C (C10F10) were employed to produce the ternary blended cement, the compressive strength was 53.0 MPa, within standard deviation from that for OPC.

#### **4. CONCLUSION**

The rheological properties, heat of hydration and 28 days compressive strength of ternary cement blends made from calcined clay, fly ash and ordinary Portland cement were investigated. It has been found that calcined clay-fly ash-OPC ternary blends possess properties, both early age workability and strength comparable to OPC, making them potential candidates as future cements.

This opens up the possibility of a new source of green abundant SCM based on clay that can be employed on a larger scale than current applications, while supporting adaptation of technology when transiting from old to new SCMs.

#### **5. REFERENCES**

- [1] Cement Industry Energy and CO<sub>2</sub> Performance (2011) Getting the numbers right, World Business Council for Sustainable Development, The cement sustainability initiative.
- [2] Østnor T, Justnes H (2014) Durability of Mortar with Calcined Marl as Supplementary Cementing Material, *Advances in Cement Research*, 26, pp. 344–352.
- [3] Justnes H, Østnor T, Ng S (2016) Applicability of Nordic Clays as SCM, International RILEM Conference on Materials, Systems and Structures in Civil Engineering Conference segment on Concrete with Supplementary Cementitious materials 22–24 August, Technical University of Denmark, Lyngby, Denmark
- [4] Ng S, Justnes H (2015) Influence of plasticizers on the rheology and early heat of hydration of blended cements with high content of calcined marl, *Cement and Concrete Composites*, 60, pp. 123–134.
- [5] Ng S, Justnes H (2016) Influence of plasticizers on the rheology and early heat of hydration of blended cements with high content of fly ash, *Cement and Concrete Composites*, 65, pp. 41–54.

## Performance-based design procedure for the selection of concrete binder systems with low environmental impact



Wilson Ricardo Leal da Silva  
M.Sc., Ph.D., Civil Engineer  
Danish Technological Institute  
Gregersensvej 4, DK-2630 Taastrup  
e-mail: wrls@teknologisk.dk



Lars Nyholm Thrane  
M.Sc., Ph.D., Civil Engineer  
Danish Technological Institute  
Gregersensvej 4, DK-2630 Taastrup  
e-mail: lnth@teknologisk.dk



Thomas Lennart Svensson  
M.Sc., Civil Engineer  
Danish Technological Institute  
Gregersensvej 4, DK-2630 Taastrup  
e-mail: thsv@teknologisk.dk



Claus Pade  
M.Sc., Chemical Engineer  
Danish Technological Institute  
Gregersensvej 4, DK-2630 Taastrup  
e-mail: cpa@teknologisk.dk

### ABSTRACT

Within the framework of today's prescriptive norms and standards, the use of SCMs often results in concrete mix designs with relatively low water to binder ratio, leading to concretes with high viscosity, which is a hindrance to a widespread use of green concrete. To overcome this issue, we propose a performance-based procedure for the selection of binder systems. The method relies on a parameter study that enables the identification of alternative low-environmental impact binder systems for further concrete development. This paper presents an example of this procedure.

**Keywords:** Cement, Performance-based design, Supplementary Cementitious Materials (SCM)

### 1. INTRODUCTION

The Innovation Consortium "Green Transition of Cement and Concrete Production" is a project supported by the Danish Innovation Fund. The project aims to create the foundation for a green transition of cement and concrete production in Denmark. Estimates suggest that by 2050 the amount of concrete produced globally will be about twice that of today [1]. Thus, the demand for environmental friendly concrete structures is increasing and even a small reduction in CO<sub>2</sub> emissions can make a significant difference. In this context, several research work has been done on SCMs to partially replace cement [2]. Within present prescriptive norms, however, the

use of SCMs usually results in mix designs with low water to binder ratio. This translates into highly viscous mixtures, thus hindering the widespread implementation of green concrete technologies [3,4]. Therefore, a transition from prescriptive material specifications to a performance-based design procedure is investigated in this project. The aim of the performance-based design procedure is to propose binder systems with a low environmental impact as a starting point for further concrete development. Here, an example is presented for the selection of a binder system composed of cement and fly ash. Further studies focus on the use of calcined clay and limestone filler.

## 2 PERFORMANCE-BASED OPTIMISATION OF BINDER COMPOSITIONS

The suggested framework of a performance-based design procedure for the selection of concrete binder systems with low-environmental impact consists of four steps:

- 1) Determine the target application and a reference concrete mix design. Relevant properties are selected and target criteria are defined based on the performance of the reference mixture.
- 2) Select SCMs and define an experimental test programme at mortar level.
- 3) Evaluate and compare the obtained results with the reference mixture. An optimisation procedure is carried out targeting both technical performance and environmental impact.
- 4) Propose alternative low-environmental impact binder system based on the target criteria from Step 1. These binder systems are used as a starting point for further concrete development and documentation including other relevant concrete properties.

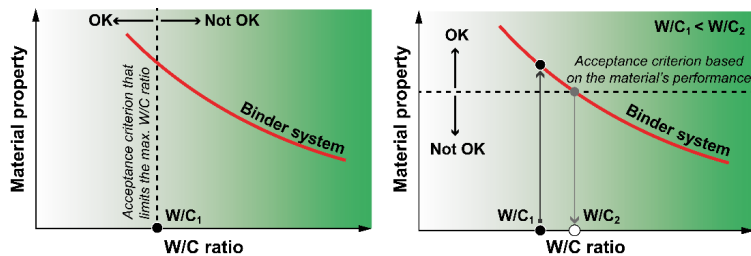


Figure 1 - Design method based on a prescriptive (left) and a performance-based design (right).

Fig.1 illustrates the principles of a traditional prescriptive mix design procedure versus a performance-based design procedure. It shows a certain material property, e.g. the compressive strength, as a function of the W/C ratio. In accordance with a prescriptive design, a maximum W/C ratio is usually specified for a given exposure class; e.g. the DS2426 standard [5] limits the W/C ratio to 0.40, 0.45 and 0.55 for Danish exposure classes E, A and M. In a performance-based approach, the W/C is variable, while the performance is fixed, i.e. a limit acceptance criterion set on the performance. As a target criterion, we propose to measure the performance of the reference mixture. The example (Fig.1) shows that the binder system over-performs at a prescribed water to cement ratio (W/C<sub>1</sub>). Ideally, the application of performance-based design allows mix designs with higher W/C and a lower environmental impact, without compromising performance (W/C<sub>2</sub>).

### 2.2 EXPERIMENTAL PROGRAM

A parameter study was implemented to optimise the binder composition based on the use of FA as SCM. The aim was to propose a binder composition with equivalent or improved performance over a reference mix design for civil engineering applications. The selected binder compositions were used as a starting point for the concrete development, which was then used in the first demonstration bridge for the Danish Road Directorate. The reference concrete, E40,

was provided by Unicon A/S. The mix design is currently used for civil engineering applications, and it is in full compliance with the existing standards and rules specified by the Danish Road Directorate, i.e. cement type, maximum w/c ratio, and minimum cement content. For the target properties, we selected: 1)  $\mu$  (Pa.s) - plastic viscosity, 2)  $f_{c,28d}$  (MPa) - compressive strength at 28 days, and 3)  $J$  ( $\times 10^{-12}$  m<sup>2</sup>/s) - chloride penetration resistance at 91 days, well-knowing that this is a simplification of very complex issue. Table 1 shows the mass composition (per m<sup>3</sup> of concrete) of the investigated mortars. Notice that the paste volume was fixed at 56% to enable comparison of results. The superplasticiser content was adjusted for each mix to obtain mortars with similar yield stress, which corresponds to similar slumps in concrete. The 4C-mini-Rheometer® was used to measure the plastic viscosity.

*Table 1 Mix composition (FA is included with a factor of 0.5 for W/C ratio, whereas for W/C ltd. ratio, FA is included with a factor of 0.5 up to a content of 33% of the cement content [5]).*

ID	W/C	W/C ltd.	W/B	FA/C	Kg/m <sup>3</sup>				kg/ton
					C	FA	W	S	CO <sub>2</sub> -equiv
R	0.37	0.37	0.35	0.15	359	54	143	580	332.5
1	0.40	0.40	0.35	0.33	305	101	142	580	254.6
2	0.40	0.51	0.30	1.00	209	209	125	580	175.5
3	0.60	0.60	0.53	0.33	243	80	170	580	203.2
4	0.60	0.77	0.45	1.00	171	171	154	580	143.9

To select a candidate FA-based binder system, limit values for  $\mu$ ,  $f_{c,28d}$  and  $J$  were chosen based on the mortar results from the reference mixture. This reference was produced with a CEM I 42.5 N (EA), whereas mixtures 1 to 4 (Table 1) were produced with CEM I 52.5 N (LA). The reference had a  $\mu = 8.5$  Pa.s and  $J = 4.9 \times 10^{-12}$  m<sup>2</sup>/s at 91 days, and  $f_{c,28d} = 78.0$  MPa. Notice that in Table 2, the limit value ( $f_{ck,28d}$ ) was set at 71.0 MPa. A design review of the bridge showed that it is possible to reduce the concrete strength class to C35. The experimental results for the mixtures 1 to 4 are shown in Figure 2, and the analysis of results is described as follows.

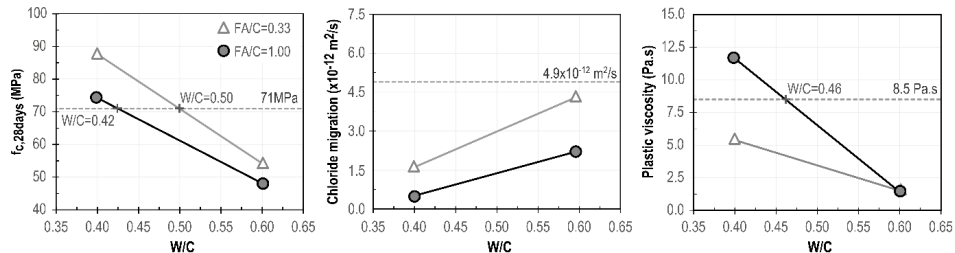


*Figure 2 - Experimental results: a)  $f_{c,28d}$  (MPa) b)  $J$  ( $\times 10^{-12}$  m<sup>2</sup>/s) and c)  $\mu$  (Pa.s).*

First, the W/C that fulfils the strength criterion was computed by interpolation of results. The accepted W/C interval is 0.42 to 0.50 as indicated in Fig.1 (left). From a sustainability perspective, the mix composition with the highest FA content, i.e. FA/C=1.0 and W/C=0.42, represents the best solution. Within the W/C interval 0.42 to 0.50, the chloride migration criterion is also fulfilled. However, at FA/C=1.0 and W/C=0.42 the plastic viscosity criterion is not fulfilled. To find the optimal solution, Table 2 displays the mix design options, between W/C=[0.42-0.50], which fulfils  $f_{c,28d} = 71.0$  MPa. The interpolation shows that the all criteria are fulfilled at a W/C=0.45 and FA/C=0.77, which represent the optimal solution from both a technical and environmental impact point of view.

Table 2. Mix design interpolations W/C=0.42 to 0.50 for  $f_{c,28d}=71.0\text{MPa}$ .

Mix ID	Ref.	2&4	← Interpolation for $f_{c,28d} = 71\text{MPa}$ →				1&3
CEM I 42.5 N	359.0	-	-	-	-	-	-
CEM I 52.5 N	-	202.4	206.6	<b>221.0</b>	238.2	259.2	269.2
FA	54.0	202.4	197.0	<b>171.1</b>	141.8	107.8	89.1
W	143.0	129.0	131.2	<b>137.9</b>	145.3	153.4	156.7
S (0-4mm)	580.0	580.0	580.0	<b>580.0</b>	580.0	580.0	580.0
W/C	0.37	0.42	0.43	<b>0.45</b>	0.47	0.49	0.50
FA/C	0.15	1.00	0.95	<b>0.77</b>	0.60	0.42	0.33
$f_{c,28d}$ (MPa)	71.0	71.0	71.0	<b>71.0</b>	71.0	71.0	71.0
$J$ ( $\times 10^{-12}\text{m}^2/\text{s}$ )	4.9	0.7	0.8	<b>1.4</b>	2.0	2.6	2.9
$\mu$ (Pa.s)	8.5	10.4	9.7	<b>7.5</b>	5.6	4.1	3.5
kg-CO <sub>2</sub> /m <sup>3</sup>	332.5	170.1	173.5	<b>185.3</b>	199.5	216.7	224.9
↓CO <sub>2</sub>	-	-48.9%	-47.8%	<b>-44.3%</b>	-40.0%	-34.8%	-32.4%

The optimal binder system is found to be at a replacement ratio of FA/C=0.77, for W/C=0.45. Such system conveys a reduction of 44.3% in CO<sub>2</sub> when compared to the reference mixture.

### 3. CONCLUSION

A performance-based design procedure for selecting binder systems with low-environmental impact was presented. With a focus on civil engineering applications, the procedure was used to propose an alternative FA-based binder system. The resulting W/C ratio of the binder systems is as high as 0.54 when calculated according to DS2426. If the proposed binder system were to fulfil  $W/C \leq 0.40$ , the concrete would be less environmentally friendly and the plastic viscosity would be much higher than that of the reference mixture with poor production and execution properties, most like making it impossible to use in practice.

### 4. ACKNOWLEDGEMENTS

This work is part of the project "Green transition of cement and concrete production". The financial support from the Danish Innovation Fond (InnovationsFonden) and the contribution from project partners is acknowledged.

### REFERENCES

- [1] Wray, P., Scrivener, K. "Straight talk with Karen Scrivener on cements, CO2 and sustainable development". American Ceramic Society Bulletin, vol. 91, p. 47-50 (2012)
- [2] Glavind, M., and Munch-Petersen, C. Green Concrete: A life cycle approach. In: Challenges of Concrete Construction, Proc. of Int. Congress, pp. 642–50, Scotland, 2002.
- [3] Schneider M., Romer M., Tschudin M., Bolio H. Sustainable cement production at present and future, Cem. and Conc. Res. 41(7):642-650, 2011.
- [4] Lothenbach B., Scrivener K., Hooton R. D. Supplementary cementitious materials. Cem. and Conc. Res. 41(12):1244-1256, 2010.
- [5] DS2426 - EN 206-1:2011: Concrete – Materials – Rules for application of EN206-1 in Denmark, The Danish Standards Association (2011).

## The compressive strength of C-S-H phases with two different Ca/Si ratios



Wolfgang Kunther  
Ph.D.  
Aarhus University, Department of Chemistry and iNANO  
Langelandsgade 140, 8000 Aarhus C  
Denmark  
e-mail: wkunther@googlemail.com



Sergio Ferreiro  
Ph.D.  
Aalborg Portland A/S, Cementir Holding  
DK-9100 Aalborg  
Denmark  
e-mail: sergio.f.garzon@aalborgportland.com



Jørgen Skibsted  
PhD, associate professor  
Aarhus University, Department of Chemistry and iNANO  
Langelandsgade 140, 8000 Aarhus C  
Denmark  
e-mail: jskib@chem.au.dk

### ABSTRACT

Model C-S-H phases have been synthesized with two different Ca/Si ratios to investigate the relation between the chemical composition of the main binding phase in concrete and its mechanical properties. The data shows that the compressive strength of the C-S-H phases is higher for the low Ca/Si ratio sample for all hydration times. Several characterization methods have been employed to study the materials across length scales from atomic environments (NMR) to the millimeter scale of SEM. These measurements are compared with the chemical compositions of the C-S-H phases and the compressive strengths of hydrated paste samples.

**Key words:** Mix Design, Supplementary Cementitious Materials (SCM), Sustainability.

### 1. INTRODUCTION

The recent focus on the development of new cementitious building materials with lower carbon footprint during cement production has shown that it is challenging to design alternative binder materials with equal material performance for the same price. The contribution to CO<sub>2</sub> emission from cement production can in this light also be seen as a consequence of the success story of this building material. One of the main approaches to reduce the clinker content is the partial replacement of the Portland clinkers with SCM's in particular when they originate from other industrial processes as by-products (e.g. fly ash and slags) or have a low economical value such as heat-treated impure clays. Changes in cement composition as the result of the introduction of SCM's affect also the phase assemblages and mechanical performance of the hydrated material.

For Portland cement binders with variable fractions of limestone and alumino-silicate rich SCM's for a constant combined replacement level, it has been shown that better mechanical performances are observed in the presence of higher quantities of calcium-aluminate hydrate phases such as the monocarbonate AFm phase and ettringite which are easily detected by XRD [1,2]. For high replacement levels, the principal binding component in hydrated cements, the calcium-silicate-hydrate (C-S-H) phase, is also affected by changes in binder composition. The C-S-H phase formed in hydrated Portland cements has usually a Ca/Si ratio of 1.5 – 1.8, whereas the ratio is significantly lower for Portland cement – SCM blends. To study the influence of compositional changes of the C-S-H phase on the mechanical performance, we have synthesized monolithic C-S-H phases with different Ca/Si ratios, analyzed them by several characterization techniques and tested their mechanical properties with conventional machinery. This direct synthesis approach has the advantage that similar porosities are obtained and that C-S-H phases with different Ca/Si ratios can be obtained without leaching of the samples.

## 2 MATERIALS & METHODS

Synthetic C-S-H phases were prepared for Ca/Si ratios of 0.83 and 1.5. The two Ca/Si ratios match the ratios for tobermorite ( $C_5S_6H_9$ ) and jennite ( $C_9S_6H_{11}$ ), which are often considered as C-S-H analog phases [3]. C-S-H pastes from stoichiometric mixtures of  $Ca(OH)_2$ , silica (Fluka silica gel 60, particle size 40-63  $\mu m$ , Sigma Aldrich) and deionized water were prepared using a fixed water/solid ratio of 1.1 by volume without consideration of the superplasticizer (SP). The amount of SP was adjusted to 20 wt.% of the mass of silica to ensure a reasonable workability, in particular for the low Ca/Si ratio mix. The resulting w/b ratios (incl. water from SP) were 0.70 and 0.64 for the Ca/Si ratio of 0.83 and 1.5 respectively. The samples were casted into mini-Rilem molds ( $19 \times 19 \times 144 \text{ mm}^3$ ), demolded after one day, and their compressive strengths were determined after hydration for 7, 14, 28 and 91 days, where earlier times were excluded to avoid effects from a possible retardation of the hydration caused by the unusual SP quantity. The samples were analyzed by  $^{29}Si$  MAS NMR, thermogravimetric analyses (TGA), powder X-ray diffraction (XRD) as well as the electron microscopy techniques BSE-SEM and electron dispersive X-ray spectroscopy (EDX).

## 3 RESULTS & DISCUSSION

### 3.1 Mechanical Properties

Figure 1 shows the changes in compressive strength during hydration of the two C-S-H pastes.

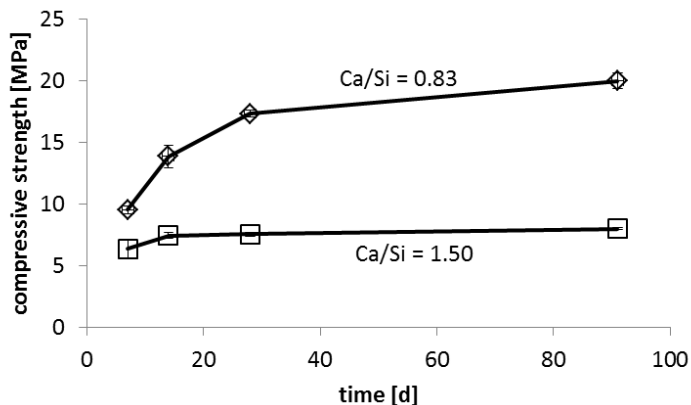


Figure 1 – Strength development of the two C-S-H model phases.

The compressive strength is at all times higher for the low Ca/Si ratio C-S-H phase and the final strength is approximately double of the value for the high Ca/Si ratio C-S-H. The strengths are in general not very high but comparable to those for other model binders. The standard deviations of the four individual measurements are low as displayed for each of the strength values.

### 3.2 Microstructure and characterization data

Figure 2 displays BSE micrographs of both C-S-H samples, which show that the mix design has an influence on the binder, despite the high reactivity of the initial silica particles, which has been confirmed by  $^{29}\text{Si}$  NMR and EDX analysis. The original silica particles do not dissolve instantaneously and thereby they provide different density distributions in the microstructure as they remain as brighter and thus denser particles in their original shape [4]. The denser parts can be viewed as “inner C-S-H” type microstructures and the differences in density distribution may explain initial strength differences. However, this seems not to be the decisive factor, as the strengths increase during hydration while the location of the denser parts are unaltered and persist during the whole testing period.

The  $^{29}\text{Si}$  NMR spectra of the samples reveal a complete reaction for the silica within the first week of hydration whereas the SEM-EDX analysis shows that after 3 months of hydration almost all inner C-S-H domains display Ca/Si ratios similar, but marginally lower, to those of the outer C-S-H regions. The characterization of the samples by XRD and TGA shows the typical patterns for pure C-S-H phases of the chosen Ca/Si ratios, while small quantities of portlandite ( $\text{Ca}(\text{OH})_2$ ) are present in the high Ca/Si-ratio binder.

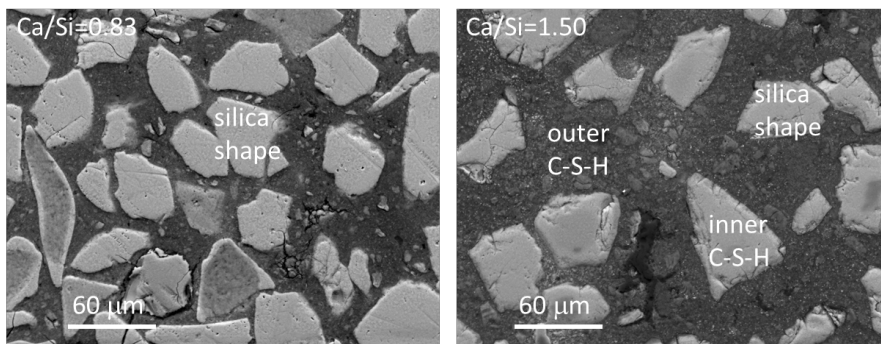


Figure 2 – Microstructures of the two C-S-H model phases after 91 days of hydration.

## 4 DISCUSSION

The experimental data shows that the model C-S-H binder produces a complex microstructure that replicates cementitious binders in most aspects. Macroscale specimens of C-S-H phases have been produced for the first time in the absence of other hydrate phases or unreacted clinker. The presence of unreacted clinker may also affect the strength of cementitious materials [5]. The absence of other phases simplifies the interpretation of the present results which solely relies on properties of the C-S-H phase.

Contrary to the presented work, Monte Carlo simulations of the electro-kinetic potential of C-S-H surfaces predict overcharging of C-S-H phases in the presence of calcium for high pH environments [6], and thereby a stronger cohesion is expected for higher Ca/Si ratios. However, these effects may be compensated by significantly larger surface areas that have been calculated for these binders (Table 1) based on the mix design and molar specific surface areas reported by Hass and Nonat [7].

*Table 1 – Calculated specific surface areas per gram C-S-H.*

Ca [-]	Si [-]	H/Si taken from [8]	specific surface area [m <sup>2</sup> /g]
0.83	1.00	1.25	270
1.50	1.00	1.7	131

## 5 CONCLUIONS

The reported data suggests strongly that the composition of the main binding phase of cementitious materials has a strong influence on the mechanical properties of cementitious building materials. This relation between C-S-H composition and compressive strength has not been considered so far (more details can be found in a related publication [9]). Furthermore, the observations may have an important impact on increasing the SCM replacement levels in Portland cement – SCM binders, in particular for silicate-rich SCM's since a certain range of lower Ca/Si ratio may improve the mechanical performance of these materials if sufficient reactivity of the SCMs is secured.

## ACKNOWLEDGEMENTS

We thank the Danish Strategic Research Council for financial support to the LowE-CEM project (No. 11-116724) and the Danish Council for Independent Research (Technology and Production) for the support of W. Kunther (No. DFF – 4184-00114). We thank the Electron Microscopy Center at Empa - Swiss Federal Laboratories for Materials Science and Technology in Dübendorf, Switzerland, for the use of their FEI ESEM XL30 electron microscope.

## REFERENCES

- [1] De Weerd, K., Ben Haha, M., Le Saout, G., Kjellsen, K. O., Justnes, H. and Lothenbach, B.: "Hydration mechanisms of ternary Portland cements containing limestone powder and fly ash" *Cement and Concrete Research*, 41, 279-291 (2011)
- [2] Steenberg, M., Herfort, D., Poulsen, S. L., Skibsted, J. and Damtoft, J. S.: "Composite cement based on Portland cement clinker, limestone and calcined clay", *Proceedings of the XIII ICCI International Congress on the Chemistry of Cement*, A. Palomo, A. Zaragoza, J.C. López Agüi (Eds.), Madrid, Spain (2011).
- [3] Richardson, I.: "Model structures for C-(A)-S-H(I)" *Acta Crystallographica Section B*, 70, 903-923 (2014)
- [4] Famy, C., Scrivener, K. L., Crumbie, A. K.: "What causes differences of C-S-H gel grey levels in backscattered electron images?" *Cement and Concrete Research*, 32, 1465-1471 (2002)
- [5] Feldman, R.F., Beaudoin, J.J.: "Microstructure and strength of hydrated cement", *Cement and Concrete Research*, 6, 389-400 (1976)
- [6] Labbez, C., Nonat, A., Pochard, I., Jönsson, B.: "Experimental and theoretical evidence of overcharging of calcium silicate hydrate" *Journal of Colloid and Interface Science*, 309, 303-307 (2007)
- [7] Haas, J., Nonat, A.: "From C-S-H to C-A-S-H: Experimental study and thermodynamic modelling" *Cement and Concrete Research*, 68, 124-138 (2015)
- [8] Lothenbach, B., Nonat, A.: "Calcium silicate hydrates: Solid and liquid phase composition" *Cement and Concrete Research*, 78, 57-70 (2015).
- [9] Kunther, W., Ferreira, S., Skibsted, J.: "Influence of the Ca/Si ratio on the compressive strength of cementitious calcium-silicate-hydrate binders" (submitted, May 2017).

**Session A2:**

**FIBRE REINFORCEMENT, TEXTILE REINFORCEMENT, ETC.**



## Experimental study on anchorage in textile reinforced reactive powder concrete



Natalie Williams Portal  
M.Sc., Ph.D., researcher  
RISE Research Institutes of Sweden, Mechanics Research  
Box 857 SE-501 15 Borås, Sweden  
E-mail: Natalie.williamsportal@ri.se



Mathias Flansbjerg  
M.Sc., Ph.D., Adj. Prof., researcher  
RISE Research Institutes of Sweden, Mechanics Research  
Box 857 SE-501 15 Borås, Sweden  
E-mail: Mathias.flansbjerg@ri.se



Urs Mueller  
M.Sc., Ph.D., senior researcher  
RISE Research Institutes of Sweden, CBI Swedish Cement and  
Concrete Research Institute  
Box 857 SE-501 15 Borås, Sweden  
E-mail: Urs.mueller@ri.se

### ABSTRACT

The EC funded project SESBE (Smart Elements for Sustainable Building Envelopes) focused on utilizing new types of cementitious materials for reducing the mass and thickness of façade elements while maintaining and increasing their thermal performance. This paper presents a method enabling the quantification and verification of the required anchorage length for a given textile reinforced reactive powder concrete (RPC), which was used for sandwich elements. Pull-out tests were conducted to quantify the required anchorage length, while uniaxial tensile tests were performed to quantify the ultimate strength and verify the suitability of the anchorage length in thin RPC panels at a composite level. The combination of these two experimental methods was deemed useful to determine the overlapping length required for larger scale façade applications.

**Key words:** Reactive powder concrete, textile reinforcement, anchorage, testing.

### 1 INTRODUCTION

Within the scope of SESBE [1], an RPC formulation with higher amounts of supplementary cementitious materials (SCMs) was developed and combined with carbon textile reinforcement for use in prefabricated concrete façades. RPC is a variant of ultra-high performance concrete (UHPC) which has a maximum aggregate size of 2 mm or smaller. It is characterized as having a compressive strength above 120 MPa and a very low amount of capillary pores. The volume

proportions of the RPC mix compared to common standard concrete and UHPC mixes are exemplified in Figure 1. The complexity of the RPC mix is such that it consists of six to eight different components; thus, potentially rendering this mix sensitive to proportioning errors. Additional details pertaining to the development of the RPC mix applied in this study can be found in [2].

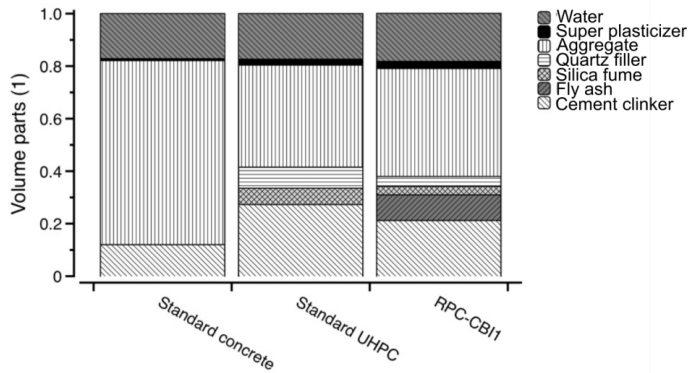


Figure 1 – Volume proportions of the reactive powder concrete mix compared to a standard concrete and UHPC. The illustrated fly ash content of mix RPC-CBII includes also the fly ash from the cement.

The inherent high strength of RPC however causes it to be extremely brittle leading to virtually no fracture energy. To mitigate this brittle behaviour for use in façade elements, textile reinforcement has been incorporated into the matrix to allow for a ductile post-cracking behaviour marked by closely spaced fine cracks. The textile reinforcement applied is an epoxy impregnated carbon textile grid (Solidian GRID Q85/85-CCE-21). Epoxy coating has been found to significantly increase the bond between the carbon textile and matrix. The mean breaking strength of the textile grid, as per the producer, is 3300 MPa (longitudinal direction).

## 2 PULL-OUT TESTS

To gain an understanding of the bond behaviour between the given textile reinforcement and RPC matrix as well as to determine a suitable anchorage length (overlapping length), unsymmetrical single sided pull-out tests were conducted, see Figure 2 (left). The embedment length,  $L_e$ , is defined by means of cutting away a part of the yarn within the panel. In this case, the variation of the embedment length was selected based on the centre-to-centre grid spacing of 21 mm. Three specimens were tested for each embedment length variation studied: 1) 2G,  $L_e = 42$  mm, 2) 3G,  $L_e = 63$  mm and 3) 4G,  $L_e = 84$  mm. The load was introduced to the free end of the roving by gripping the end anchorage (100 mm aluminium tube filled with epoxy) in the conventional hydraulic grip of the testing machine. The anchorage length of the specimen was clamped between two stiff steel plates of clamping devices attached to the testing machine. The tests were performed in an electro mechanical testing machine and the load was controlled by a displacement rate of 1 mm/min. A video extensometer technique was used to measure the active end-slip of the reinforcement relative to the concrete end.

From the pull-out tests, a distinct increase in the maximum load was observed as the embedment length increased as per Figure 2 (right). The embedment length corresponding to four grid spacings, i.e. 4G ( $L_e = 84$  mm), was found to be a suitable anchorage length since textile rupture was generally achieved.

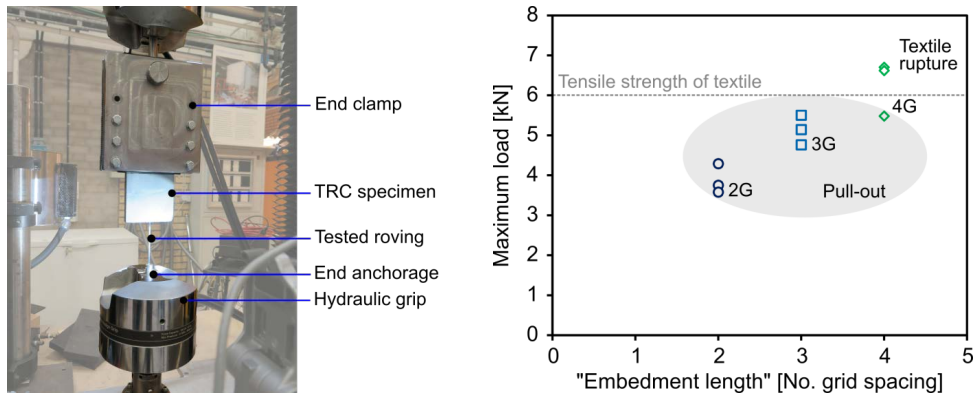


Figure 2 – Pull-out test setup (left) and failure mechanisms observed with respect to maximum load and embedment length (right).

### 3 UNIAXIAL TENSILE TESTS

The tensile behaviour of thin textile reinforced RPC panels was characterized using uniaxial tensile tests in accordance with the recommendation of RILEM TC 232-TDT [3] along with Digital Image Correlation (DIC) measurements. Rectangular panel specimens (700 x 100 x 25 mm) reinforced by two layers of textile reinforcement were tested with and without a centrally placed overlap splice in the reinforcement grids as per Figure 3 (left). The overlap was prescribed according to the most suitable anchorage length determined by the pull-out tests (4G). Three specimens were tested for each variation, denoted as RPC-(1-3) for reference samples and RPCO-(1-3) for overlap samples. A panel fastened to an alignment frame was placed in the testing machine where the ends of the clamping devices were thereafter hinged connected to the testing machine, see Figure 3 (right). These tests were carried out using the same testing machine as applied for the pull-out tests, and controlled by the cross-head displacement.

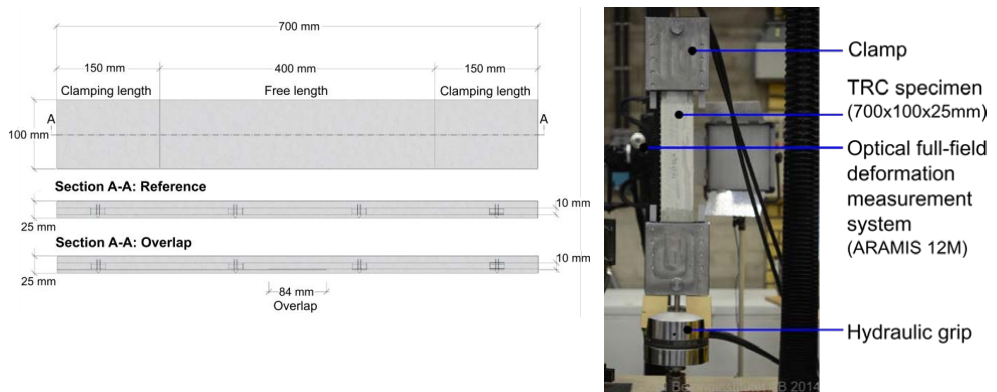


Figure 3 – Specimen configuration (left) and uniaxial tensile test setup (right).

The load versus global displacement relationship along with DIC measurements obtained from the uniaxial tensile tests is typified in Figure 4 for two specimens, RPC-1 (reference) and RPCO-1 (overlap). From this figure, it is possible to follow the formation of individual cracks along with related deformations at different load stages. Both specimens achieved comparable

ultimate strength values and multiple cracking across the free zone of the specimens. Since cracks propagated within the overlap region for RPCO-1, this is an indication that the prescribed overlap of 4G ( $L_e = 84$  mm) is suitable when introduced in the composite.

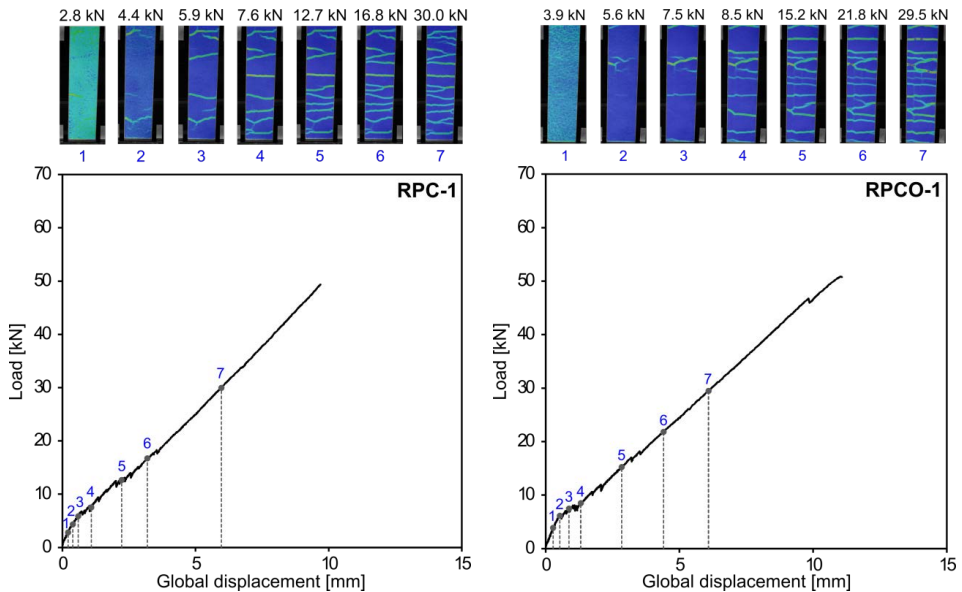


Figure 4 – Tensile load versus global displacement with corresponding major strain overlays at different loading stages. RPC-1 reference panel (left) and RPCO-1 overlap panel (right).

#### 4 CONCLUDING REMARKS

Combining pull-out and uniaxial tensile tests has been presented in this work as a method to both quantify and verify the anchorage length required for textile reinforced RPC. An anchorage length amounting to four grid spaces (equivalent to 84 mm) was found to be suitable for the given composite to achieve adequate load transfer across a reinforcement overlap splice. Ultimately, the quantified overlapping length can be further implemented on a larger scale such as in precast concrete façade elements.

#### ACKNOWLEDGEMENTS

The SESBE project was supported by the European Commission within the Framework Programme 7 under the Grand Agreement no. 608950. The authors would like to thank the European Commission for funding the project and making this work possible.

#### REFERENCES

- [1] SESBE project, [Cited 9<sup>th</sup> February 2017], Available from: <http://www.sesbe.eu/>
- [2] Mueller, U., Williams Portal, N., Chozas V., Flansbjerg, M., Larazza, I., da Silva, N., Malaga, K.: “Reactive powder concrete for façade elements – A sustainable approach”, *Journal of Façade Design and Engineering*, vol. 4, pp. 53-66 (2016)
- [3] RILEM TC 232-TDT (Wolfgang Brameshuber): “Recommendation of RILEM TC 232-TDT: test methods and design of textile reinforced concrete – Uniaxial tensile test: test method to determine the load bearing behavior of tensile specimens made of textile reinforced concrete”, vol. 49 (12), pp. 4923-4927 (2016)

## Basalt fiber reinforced precast concrete panels - an alternative concept



Eythór Rafn Thórhallsson  
Associate professor  
Reykjavik University  
Menntavegi 1, 101 Reykjavik  
Iceland  
E-mail: eythor@ru.is



Guðmundur Úlfar Gíslason, BSc  
Graduate student  
Reykjavik University  
Menntavegi 1, 101 Reykjavik  
Iceland  
E-mail: guðmundurug12@ru.is



Guðni Jónsson, MSc  
Civil Engineer  
Efla Consulting Engineers  
Höfðabakki 9, 110 Reykjavik  
Iceland  
E-mail: gudni.jonsson@efla.is



Jónas Th. Snaebjörnsson, PhD  
Professor  
Reykjavik University  
Menntavegi 1, 101 Reykjavik  
Iceland  
E-mail: jonasthor@ru.is

### ABSTRACT

The project focuses on the feasibility of strengthening the exterior face of precast wall elements by using basalt fiber mat reinforcement instead of traditional steel bars. Structural testing and numerical calculations revealed that the concrete mixture as well as the cross sections performed well and even better than predicted. For that reason, it seems clear that considerable savings and even improved durability can be achieved by using basalt fibers in precast units and thereby allowing for a reduced thickness of the weather coating from 70mm down to 20mm, as corrosion protection is not needed. In addition, it is an environmentally favourable solution as material is reduced and the use of steel avoided.

**Key words:** Concrete, Mix Design, Frost Action, Basalt Fibers, Precast Units, Testing, Cost.

### 1 INTRODUCTION

The exterior walls are the most heavily exposed parts of buildings during their lifetime. This project investigates the feasibility of using basalt fiber mats instead of steel bars as a reinforcement of the exterior layer of precast walls to transmit tension forces and control micro cracking. Basalt fibers have shown many advantages for use in concrete structures and are corrosion free [1]. Therefore, the thickness of the exterior layer can be reduced, as a large portion of the traditional thickness of a concrete wall mainly serves as a corrosion protection for the reinforcement. As a consequence the weight of the precast unit is reduced, which should result in various savings, for instance in transportation costs and easier handling at the work place.

### 2 MATERIALS

The dry materials used in the concrete mixture came from the concrete plant, BM Valla, Reykjavik (Anleggsement CEM I from Norcem AS and local aggregate with maximum aggregate size 8 mm). It was decided to mix the concrete without any air entrainment. This was done in order to increase the strength of the concrete. The downside is that concrete without any air-cells is generally sensitive to frost effects. The air-cells protect the concrete when the temperature goes below 0°C and the water contained within the concrete starts to freeze and increase its volume. Without air-cells, created by air entrainment, there is an increased risk of micro cracking. Therefore, to make the concrete more frost resistant the water/cement ratio was lowered to 0,31. The workability was then achieved by adding a sufficient amount of water reducing admixture (MasterGlenium SKY 615, from BASF).

The concrete was taken directly from the mixer to the panel formwork. It was placed in two layers with the basalt-fiber mat right in the middle of the cross-section (between the two concrete layers). The formwork was then placed on a vibration-table to obtain bonding between the placement layers and a smooth surface of the concrete panel. After the vibration-work the panel forms were placed on a table and covered with a plastic wrap to prevent evaporation. The concrete was in the formwork for about 12 hours, or until it was considered safe to remove it from the formwork. The panels were then placed in tubs with 20°C hot water for 28 days to be fully cured for the strength testing. The panels were all 0.6 m wide and 1.0 m long, but their thickness was 20mm, 35mm and 50mm. Total of 9 panels were concreted, three of each thickness. In addition, three 100x200mm cylinders were concreted for compressive strength testing and a single 150x300mm cylinder was concreted for a frost resistance test.

The basalt fiber mat used in this investigation was procured by Reykjavik University from the Belgian manufacturer Basaltex, i.e.: “*Basalt Geogrid 200-11x12mm*”, (see Fig. 1a). The name refers to the weight/m<sup>2</sup>, which is 200g and the mesh size, which is 11x12mm. This type of mat was initially intended for road construction, primarily to increase the lifetime and reduce the effect of cracking due to congestion and temperature changes. The Basalt fiber mat is orthotropic in behaviour and has for example double the tensile strength in one direction. The maximum tension strength of the basalt mat is listed as 429 MPa.



Figure 1. a) The basalt mat used. b) The finished panels (0.6m wide, 1.0m long). c) Three point bending test setup.

### 3 STRUCTURAL AND MATERIAL TESTING

#### 3.1 Material testing

Three concrete cylinder samples with diameter 100x200mm made were tested in a standard compression test according to EN 12390-3 to verify their strength. The average compressive strength of the samples was 55.23 MPa, with a standard deviation of 1.57 MPa. The concrete compression strength was therefore found to be slightly less than the mixture design target strength of at least 60 MPa. The reason is probably that part of the cement was not reacted due to the low water/cement ratio, but acted as filler material in the mixture. As the cement is considerably weaker than the alternate filler material, the compressive strength was overestimated.

The concrete was tested for frost-resistance test according to the Swedish standard SS 13 72 44. The 150x300mm cylinder, was cut down into 50 mm thick sections, each 150 mm in diameter. The samples were placed in a freeze-thaw cabinet. The experiment is conducted by measuring the scaling of cylindrical concrete sections at regular intervals (1-2 weeks) over a 56-day period. The scaling was always well below the most conservative reference values. After 56 days the scaling of the samples tested was only 0,16kg/m<sup>2</sup> whereas the strict reference limit is 0.5 kg/m<sup>2</sup>. Which indicates that the concrete mixture has good frost resistance.

### 3.2 Structural testing

After fully curing in a water bath in 28 days, the panels were tested in three point bending test, to evaluate their bending strength. The panels were placed in a hydraulic jack rig (see Fig. 1c), and loaded gradually across their width until they broke. The centre deflection along with the force applied were continuously recorded. Three panel samples were tested for each thickness (20mm, 35mm and 50mm) i.e. 9 panels in all. The strength of the panels was estimated using reinforced concrete formulae in EN 1992-1-1. The calculated capacity was then compared with the experimental results. The moment of the cross section just before fractures developed was estimated. After the loading reaches that point, then only the basalt fiber net carried the tension and the mechanics of the cross section changes. The estimated maximum moment before cracking occurred,  $M_{cr}$ , was compared with the experimental results, as shown in Table 1. As seen, the values for  $M_{cr}$  from the testing were considerably higher than the values calculated in accordance with EN 1992-1-1. This could indicate that the panels have a higher tensile strength than anticipated. On the other hand, when the moment capacity after cracking,  $M_{Rd}$ , is investigated the difference between theory and experiment was only of the order of 10%, as shown in Table 1.

Table 1 – Comparison between estimated and experimental moment capacity.

Thickness (mm)	Parameter	Estimated value (kNm)	Experiment (kNm)	Ratio Experiment/Estimated
20 mm	Moment before cracking ( $M_{cr}$ )	0.169	0.348	2.06
	Moment after cracking ( $M_{Rd}$ )	0.259	0.290	1.12
35 mm	Moment before cracking ( $M_{cr}$ )	0.517	0.866	1.68
	Moment after cracking ( $M_{Rd}$ )	0.462	0.533	1.15
50 mm	Moment before cracking ( $M_{cr}$ )	1.055	1.74	1.65
	Moment after cracking ( $M_{Rd}$ )	0.664	0.689	1.04

## 4 MATERIAL SAVING ANALYSIS

The objective was to compare the material saving of using a traditional precast unit reinforced with steel bars versus using a modified unit with a thin exterior layer reinforced with basalt mat. A sketch showing the new option is given in Figure 2. The tentative connection bar shown in Fig. 2 between the inner and out layer of the modified unit, could for instance be a basalt fiber bar.

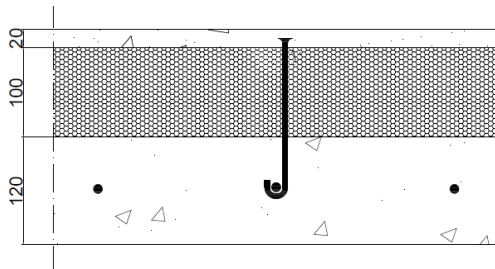


Figure 2 - A sketch of precast concrete wall unit with a 20 mm thick outer layer instead of traditional 70 cm outer layer.

The required amount of cement and the units overall weight was calculated (see Table 2). The calculations were based on a modified precast-unit with a 20mm thick exterior-layer and a

traditional one with 70mm thick exterior layer. Both units had a 130 cm thick reinforced inner layer. As seen in Table 2, the savings in amount of cement can be up to 52% if the 20mm panels are used instead of the traditional one. This would reflect in the carbon footprint of the unit. Moreover, the unit will be much lighter, making it less costly to transport, and easier to handle. The weight gain between the two options is 71% for the exterior layer only and 26% for the sandwich panel unit in total. This difference is mainly caused by the corrosion protection of 30mm required for the traditionally reinforced precast-unit.

*Table 2 - Cost comparison between traditional precast wall unit and a modified one.*

Type of exterior layer	Mass per cement volume (kg/m <sup>3</sup> )	Mass of exterior layer		Mass of the wall unit	
		Cement (kg/m <sup>2</sup> )	Total mass (kg/m <sup>2</sup> )	Cement (kg/m <sup>2</sup> )	Total mass (kg/m <sup>2</sup> )
20mm thick with basalt mat	560	11.2	51	50.8	356
70mm thick with steel bars	330	23.1	178	62.7	483
Saving of using 20mm panels instead of 70mm:		52%	71%	19%	26%

## 5 FINAL REMARKS

The objective of the investigation described herein was to test the feasibility to modify traditional precast concrete wall units by using non-corrosive reinforcement in their exterior layer. Thereby allowing the exterior layer to be considerably thinner than practically possible while using traditional steel reinforcement bars. The options tested were concrete plates of varying thickness reinforced with a commercially available basalt mat.

It was found that all the sections tested, exceeded the predicted moment capacity. Also, the concrete mixture used, performed well in the frost-resistance test, as the scaling measured was far below the limit values.

The use of a thinner exterior layer in precast concrete wall units creates unquestionable savings in material cost, transportation cost and carbon footprint.

Overall, it can be concluded that the concept tested, i.e. a thin panel tension reinforced with a basalt mat has shown great potential and it should be worthwhile to pursue this idea further. The next step could be to construct an actual complete precast wall unit using this approach and test it in comparison with the traditional wall units.

## ACKNOWLEDGEMENTS

Special thanks are due to Efla Consulting Engineers ([www.efla-engineers.com](http://www.efla-engineers.com)) for the access to their research laboratory. Einingaverksmiðjan hf ([www.ev.is](http://www.ev.is)) provided part of the materials used for the experimental work, which is gratefully acknowledged. Thanks are also due to Stefán Björnsson (BSc), a former student at Reykjavik University for his contribution to the work presented here.

## REFERENCES

- [1] Thorhallsson, Eythor Rafn, Jónas Thór Snæbjörnsson (2016): Basalt Fibers as New Material for Reinforcement and Confinement of Concrete. *Solid State Phenomena*; 249:79-84., DOI:10.4028/www.scientific.net/SSP.249.79

## Study of adhesive bond properties between the cement-paste and short steel or polypropylene fibres by X-ray nano-Computer Tomography



Marika Eik  
M.Sc., Ph.D., Postdoctoral researcher  
Aalto University School of Engineering  
Rakentajanaukio 4 A, 02150 ESPOO  
e-mail: marika.eik@aalto.fi



Anna Antonova  
M.Sc., Doctoral student  
Aalto University School of Engineering  
Rakentajanaukio 4 A, 02150 ESPOO  
e-mail: anna.antonova@aalto.fi



Jouni Punkki  
Professor of Practice  
Aalto University School of Engineering  
Rakentajanaukio 4 A, 02150 ESPOO  
e-mail: jouni.punkki@aalto.fi



Jari Puttonen  
M.Sc., Lic.Sc., D.Sc., Professor  
Aalto University School of Engineering  
Rakentajanaukio 4 A, 02150 ESPOO  
e-mail: jari.puttonen@aalto.fi

### ABSTRACT

The overall performance and efficiency of fibre reinforced cement composites depend on the adhesive bond strength/properties between fibre and cement-matrix, which is mainly influenced by the characteristics of inter-facial transition zone, (ITZ).

Within the present research the morphology of ITZ was studied by using the X-ray nano-Computer Tomography provided by the European Synchrotron Radiation Facility. This scanning approach enables to study more accurately the three-dimensional nature and properties of adhesion between the cement-matrix and fibre.

**Key words:** Cement, Fibres, Interfacial Transition Zone, X-ray nano-Computer Tomography, Adhesion.

## 1. INTRODUCTION

Fibre reinforced concrete, (FRC), is becoming more and more popular in construction industry due to its refined mechanical properties as compared to conventionally reinforced concrete, [1,2,5]. Fibres are added to fresh concrete mass during the mixing stage. The diameter of fibres can vary between  $0.2\ \mu\text{m}$  –  $1.0\ \text{mm}$  as well as the geometrical shape of fibres can be straight, undulated, crimped, with hooked-ends and etc., [1,4]. The volume fraction of fibres added to  $1.0\ \text{m}^3$  of concrete using the conventional practice of concreting with modern super-plasticizers is usually less or equal to 2%, [1].

Concrete demonstrates good resistance to compression, while even minor tensile stress causes its extensive cracking and brittle failure, [4]. The addition of fibres enables to improve the mechanical properties of concrete from brittle to more ductile, which results in refined tensile strength and more ductile post-cracking behaviour, [1,2]. A considerable advantage of FRC is a short construction time necessary for building a structural element or a member compared to the same structure made of conventionally reinforced concrete, since the reinforcement placing phase is usually avoided, which, in turn, allows to decrease the labour costs, [6]. The structures or structural elements of complex geometrical shapes or thin-walled structures can also be easily implemented using FRC, [6].

FRC is a multi-phase and multi-scale material meaning that multiple phases constituting the material cover the scales from nano- (crystals of Calcium-Silicate-Hydrate, (C-S-H), portlandite  $\text{Ca}(\text{OH})_2$ , (CH)), micro- (internal micro-cracks, voids), meso- (orientation of fibres) up to macro scale (volume fraction of fibres, geometry and size of fibres, average strength of concrete). The presence of such a wide range of scales complicates both the empirical investigation methods and the modelling approaches. Load-bearing capacity and crack resistance of FRC to a great extent depend on the adhesive strength (stiction) presented at fibre-concrete interface, [2]. However, the nature of adhesion of concrete to fibres is unclear and require further and more deep study, [3,5]. Thereby, the physio-chemical properties of adhesion and its influence on de-bonding of fibres are the major interest and importance.

## 2. SCIENTIFIC BACKGROUND

The bond between fibre and concrete is assumed being created by adhesion, friction and mechanical anchorage in case the fibres have deformed shape, [1]. A particular contribution and value of each bonding component to load-bearing capacity and crack resistance of FRC are still ambiguous. The present research project is focused on the study of adhesive properties present at short steel and polypropylene fibre-concrete interface on nano-scale using X-ray computer tomography. The adhesive bond is mostly influenced by the Interfacial Transition Zone, (ITZ), which is forming between fibres or reinforcement bars, aggregates and cement-paste, Figure 1. The expected thickness of the ITZ layer varies between  $40 - 70\ \mu\text{m}$ , [3].

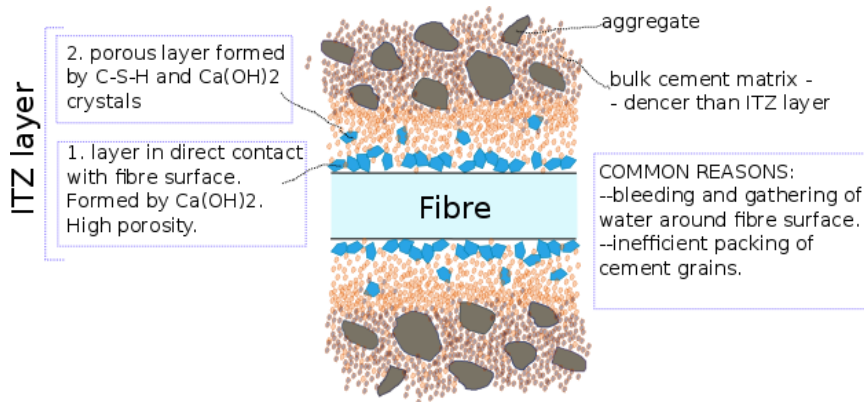


Figure 1 - Interfacial Transition Zone, (ITZ), at fibre-concrete interface.

Essentially, the ITZ layer is more pronounced around the inclusions with rather large diameter, [1,3]. It is assumed, that the ITZ layer has heterogeneous and porous micro-structure, [1,2,3], Figure 1, which either facilitates the de-bonding of fibre or can initiate de-bonding away from fibre surface. Thereby, the ITZ controls how strongly the constituents of the composite are joined together into a single unit, which enables the individual components perform together.

The micro-structure of the ITZ, such as porosity, thickness, continuity/discontinuity due to adjoining/touching aggregates specifies the adhesive strength presented at fibre-concrete interface. The investigation of physio-chemical interaction between fibre and concrete utilising X-ray nano-computed tomography, (nano-CT), enables most accurately assess the nature of adhesion and its characteristics.

### 3. MATERIALS AND METHODS

Within the present research it is decided to turn to European Synchrotron Radiation Facility, (ESRF), which is the world's most intense X-ray source and a centre of excellence for fundamental and innovation-driven research in condensed and living matter science. ESRF is specialising in micro-analysis, 3D material characterisation based on advanced imaging techniques including synchrotron technology.

By using the facilities of the ESRF it is possible to scan the samples represented on Figure 2 with a pixel size under 100 nm and without the blinking effect – artefact – caused by steel fibre.

For present study were prepared 7 cement-samples with aligned fibres inside: 3 cylinder-samples with polypropylene fibre with  $\varnothing=1\text{mm}$ ; 4 cylinder-samples with short steel fibre with  $\varnothing=0.2\text{mm}$ , Figure 2.

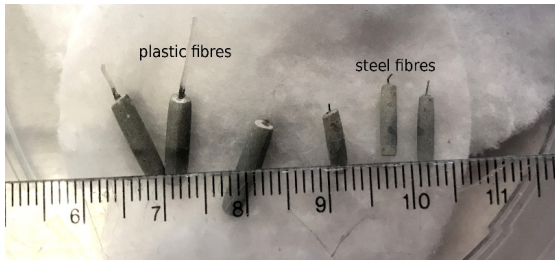


Figure 2 - Cylinder-samples made of cement-paste with aligned fibre. Left: The diameter of samples is approximately 3.0 mm, the diameter of polypropylene fibres is 1.0 mm. Right: The diameter of samples is approximately 2.0 mm, the diameter of short steel fibres is 0.2 mm.

#### 4. RESULTS EXPECTED

FRC is widely used in construction industry especially in industrial floors (steel fibres), but not in load-bearing structural elements. The reason for this situation is the lack of proper technological and design standards supported by high-level research. The quantitative and qualitative evaluation of the adhesive characteristics between fibre and concrete using the advanced methods such as high resolution nano-CT scanning will strengthen the reliability of using FRC in load bearing structures such as tunnels, bridges, residential buildings. The study approach proposed has not yet been applied in civil engineering for examining the bond properties between fibre/reinforcement bar and concrete. Thus, the expected outcomes are relevant not only for FRC, but also for conventionally reinforced concrete. The chemical composition of cement-paste is complicated (different calcium silicate compounds, calcium hydroxide, etc.) and the actual structure of the ITZ – zone (crystals and pores) around steel fibres, bars or aggregates – is poorly known. The outcomes of the study will also deepen the basic understanding of the reinforced concrete as a construction material by high resolution and quality nano-CT investigations.

#### REFERENCES

- [1] A. Bentur and S. Mindess: “Fibre Reinforced Cementitious Composites”, Taylor & Francis, 2nd edition (2007)
- [2] Siaw Foon Lee and Stefan Jacobsen: “Study of interfacial microstructure, fracture energy, compressive energy and debonding load of steel fiber-reinforced mortar”, *Materials and Structures* no. 44(8), pp. 1451–1465 (2011)
- [3] Xiao Hui Wang, Stefan Jacobsen, Jian Ying He, Zhi Liang Zhang, Siaw Foon Lee, and Hilde Lea Lein: “Application of nanoindentation testing to study of the interfacial transition zone in steel fiber reinforced mortar”, *Cement and Concrete Research* no. 39(8), pp. 701 – 715 (2009)
- [4] Andrzej M. Brandt: “Fibre reinforced cement-based (FRC) composites after over 40 years of development in building and civil engineering”, *Composite Structures* no. 86, pp. 3 – 9 (2008)
- [5] Tayfun Uygunoglu: “Investigation of microstructure and flexural behavior of steel-fiber reinforced concrete”, *Materials and Structures* no. 41(8), pp. 1441–1449 (2008)
- [6] David Fall, Karin Lundgren, Rasmus Rempling, Kent Gylltoft: “Reinforcing tailor-made concrete structures: Alternatives and challenges”, *Engineering Structures* vol. 44, pp. 372–378 (2012)

## 3D analysis of strains in fibre reinforced concrete using X-ray tomography and digital volume correlation



Mathias Flansbjerg  
M.Sc., Ph.D., Adj. Prof., researcher  
RISE Research Institutes of Sweden, Mechanics Research  
Box 857 SE-501 15 Borås, Sweden  
E-mail: Mathias.flansbjerg@ri.se



Natalie Williams Portal  
M.Sc., Ph.D., researcher  
RISE Research Institutes of Sweden, Mechanics Research  
Box 857 SE-501 15 Borås, Sweden  
E-mail: Natalie.williamsportal@ri.se

### ABSTRACT

In fibre reinforced concrete (FRC), understanding the underlying interaction mechanisms between discrete fibres and the surrounding concrete matrix can lead to the optimization of the fibre-matrix combination. This paper presents the initial development of a method enabling the analysis of this given interaction on a meso-mechanical level. The method is such that volume images are initially captured using X-ray Computed Tomography (XCT) on small-scale FRC specimens under loading which are thereafter analysed to measure full 3D strain and deformation via Digital Volume Correlation (DVC). It is anticipated that the method developed in this project can be a useful tool for the development of new innovative and high performance FRC.

**Key words:** Fibres, pull-out behaviour, X-ray Computed Tomography, Digital Volume Correlation.

### 1 INTRODUCTION

This paper presents findings from an ongoing project, funded by ÅForsk Foundation, dealing with the study of the interaction between short discrete fibres and concrete in fibre reinforced concrete (FRC) by means of meso-mechanical analysis. This project includes the development of a method which makes it possible to conduct X-ray Computed Tomography (XCT) on small-scale pull-out tests of specimens under load, followed by detailed analysis based on Digital Volume Correlation (DVC). XCT is a non-destructive 3D imaging technique, while DVC is a technique applied to measure full 3D strains and deformations in materials. The latter technique uses tomographic reconstruction algorithms to calculate full 3D strains and displacements from volume images. Through coupling XCT and DVC, the internal strains within the concrete structure can be studied, thus allowing for an increasing understanding of how the loads are taken and distributed in the structure under mechanical loading. In essence, the goal is to be able to visualize and understand the mechanical interaction between the fibres and the concrete matrix in FRC.

Fibre pull-out is typically aimed at being the dominating failure mechanism in FRC to avoid brittle failure, which is why it is deemed relevant to investigate the pull-out behaviour in this study. Moreover, the so-called bridging effect at a crack opening in FRC is governed by the fibre-matrix bond properties of each fibre crossing the crack [1]. Pull-out tests are typically applied to: a) characterize the behaviour of FRC leading to the optimization of fibre-matrix combination and/or b) estimate average tensile stresses in the vicinity of a crack opening [2]. Upon loading of FRC, a part of the load is transferred from the cementitious matrix to the fibres before any macro-cracks are initiated. During the initial load transfer, the bond at the fibre-matrix interface is characterized by superior elastic shear bond, also signifying that there is no relative displacement between the matrix and fibre. The stress transfer within the loaded composite can be broken down into two main types of bond, namely elastic shear bond (adhesion) and frictional shear bond [3]. The transition from elastic to frictional shear bond essentially takes place when the increasing tensile stress in the matrix exceeds the elastic shear bond limit; which, in turn, leads to relative displacement between the matrix and fibre causing the initiation of interface debonding. The frictional shear bond plays the role of resisting the displacement along the interface parallel to the fibre length while allowing relative slip. First cracking usually occurs when the ultimate strain of the matrix is exceeded due to its low tensile strain capacity compared to that of the fibres. Furthermore, it is relevant to note that the fibre geometry, in terms of deformed surface (twisted, crimped) or end-hooks, can introduce a form of additional mechanical anchorage in the composite. It is to say that the load transfer between the matrix and fibres becomes non-linear and localised at the given points of mechanical interlock/anchorage [3].

## 2 METHOD DEVELOPMENT FOR PULL-OUT AND TOMOGRAPHY

It is generally a challenge to perform simultaneous XCT imaging and accurate load application to samples on a laboratory scale [4]. In view of that, the method developed for pull-out testing was firstly tailored towards the geometric constraints of the tomography equipment and mechanical loading configuration. A single-sided pull-out test was developed within the project based on the knowledge gathered from other studies e.g. [1] to simulate a stress-state present at a crack opening. This method makes it possible to characterize the pull-out behaviour of individual fibres when pulled-out of the concrete matrix in terms of a load versus displacement relationship. A cylindrical concrete specimen ( $h=50$  mm,  $\varnothing=45$  mm) containing a singular steel fibre partly cast perpendicular and centric to the concrete surface (Figure 1, left) was specifically prepared to accommodate the preliminary test setup (Figure 1, centre, right) configured with the possibility to apply a pull-out load while being placed in a tomograph. The fibre is fitted with an end anchorage detail which is thereafter fixed to the test rig whereby the pull-out load is applied to the protruding end of the fibre.

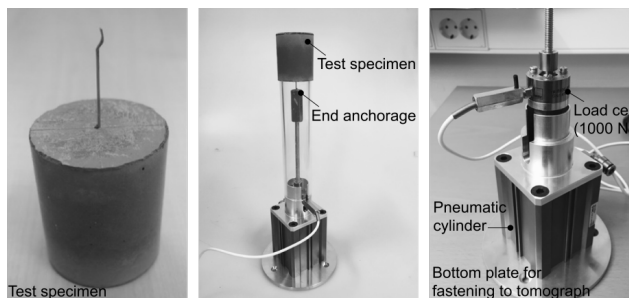


Figure 1 – Photo of concrete cylinder with cast steel fibre (left) and loading device for pull-out test to be applied in a tomograph (centre, right).

Preliminary XCT images were taken on unloaded test specimens containing a centrally cast steel fibre. It is worth noting that it is critical to achieve a sufficient natural speckle pattern on the inside of the specimen in order to further ensure the quality of the DVC analysis. Accordingly, the concrete matrix selected had a range of aggregate sizes and shapes allowing for a suitable natural scatter which was captured as a grey-scale distribution. Figure 2 illustrates both section (XY, YZ and XZ) and volumetric views of a test specimen obtained using XCT. It can be further stated that the location of the fibre-matrix interface can also be clearly visualized.

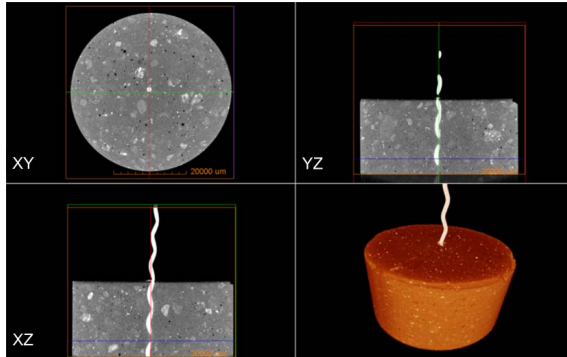


Figure 2 – Example volume images of an unloaded test specimen taken using XCT (Scale: 2000  $\mu\text{m}$ ).

### 3 PRELIMINARY TEST RESULTS

The scope of the experimental study consists of firstly executing single-sided pull-out tests on concrete cylinders with centrally cast fibres as previously described in the method development. Six types of steel fibres possessing differing mechanical anchorage details and tensile strength were investigated (Figure 3, left). Small-scale pull-out tests (Figure 3, right) were performed to characterize the load versus displacement relationship for the respective fibre types. The purpose of these tests is to primarily determine load levels which could be of interest to apply during XCT imaging followed by DVC analysis to visualize and understand the mechanical interaction between the fibres and the high performance concrete ( $d_{\text{max}} = 4 \text{ mm}$ ).

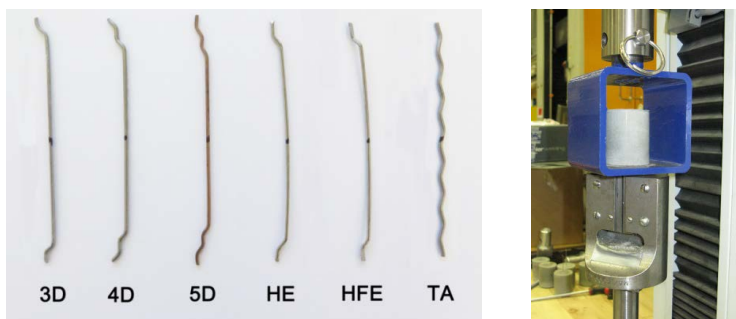


Figure 3 – Photo of investigated steel fibres (left) and pull-out test setup (right).

The selection of load levels to be applied for XCT imaging is based on the analysed load versus displacement relationships for each respective fibre type. Selected results from the performed small-scale pull-out tests are shown in Figure 4 for fibre types 3D, 4D and 5D. These presented

results have minimal scatter in terms of peak load, but do however differ in regard to failure mode being marked by either pull-out or fibre rupture. Possible explanations for differing failure modes could be: slight variations related to fibre embedment depths and inclination, fibre defects and variations in the end anchorage. Load levels prior to the peak load are relevant to be able to capture the initial debonding of the fibre and transition from mechanical adhesion to frictional bond. At load levels approaching the peak load, the plastic deformation of the fibre can likely be observed. In the case of pull-out failure, it could also be relevant to capture the extent of plastic deformation and pull-out of the fibre within the post-peak region.

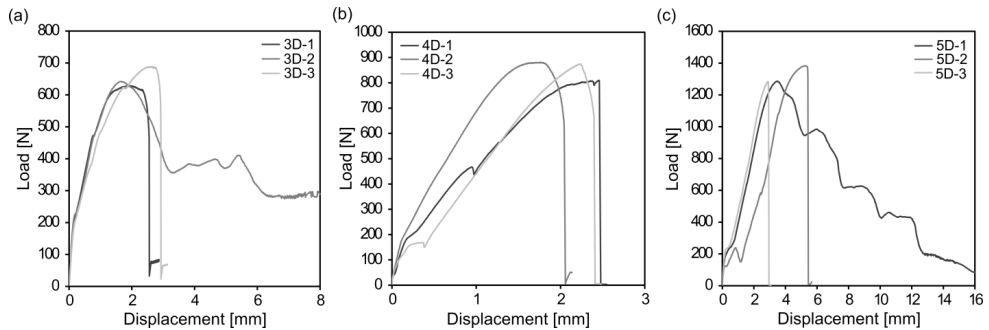


Figure 4 – Load versus displacement results: (a) 3D, (b) 4D and (c) 5D.

#### 4 CONCLUDING REMARKS

The initial development of a method to analyse the interaction between discrete fibres and the concrete matrix in FRC was presented. A loading device for simultaneous pull-out testing and tomographic imaging was developed for a small-scale cylindrical concrete specimen containing an individual fibre. Preliminary XCT volume images on an unloaded test specimen were observed to have sufficient resolution to be able to clearly visualize the fibre-matrix interface. From the presented pull-out test results, suitable load levels to be applied during XCT imaging followed by DVC analysis were identified. Subsequent steps in this project include the XCT imaging of loaded specimens coupled with DVC analysis.

#### REFERENCES

- [1] Breitenbücher, R., Meschke, G., Song, F., and Zhan, Y.: “Experimental, analytical and numerical analysis of the pullout behaviour of steel fibres considering different fibre types, inclinations and concrete strengths”, *Structural Concrete*, 15(2), pp. 126-135 (2014)
- [2] Døssland, Å.L.: “Fibre reinforcement in load carrying concrete structures”, Ph.D. Thesis, Faculty of Engineering Science and Technology – Department of Structural Engineering, Norwegian University of Science and Technology, p. 244 (2008)
- [3] Bartos, P.: “Review paper: bond in fibre reinforced cements and concretes”, *International Journal of Cement composites and Lightweight concrete*, 3(3), pp. 159-177 (1981)
- [4] Bay, B.: “Methods and applications of digital volume correlation”, *The Journal of Strain Analysis for Engineering Design*, 43(8), pp. 745-760 (2008)

## Flexural behavior of textile reinforced concrete (TRC) slabs



Cristian Sabau  
M.Sc., Ph.D. student , Marie Curie fellow  
Luleå University of Technolgy  
Laboratorievägen 12, 971 87 Luleå, Sweden  
e-mail: cristian.sabau@ltu.se



Jaime Gonzalez-Libreros  
M.Sc., Ph.D. student, Marie Curie fellow  
University of Padua  
Via Marzolo 9, 35121, Padua, Italy  
e-mail: jaime.gonzalez@dicea.unipd.it



Björn Täljsten  
Full Professor, Ph.D.  
Luleå University of Technolgy  
Laboratorievägen 12, 971 87 Luleå, Sweden  
e-mail: björn.täljsten@ltu.se

### ABSTRACT

Textile reinforced concrete (TRC) allows casting thin structural elements as the textile reinforcement does not impose any requirements on the concrete cover since there is no risk for corrosion. This paper presents the experimental results of an experimental campaign aimed to investigate the flexural behavior of textile reinforced concrete (TRC) slabs intended for cladding of buildings. In addition, the inclusion of short polyvinyl-alcohol fibers in the concrete mix, in order to improve the tension capacity of the concrete, is also investigated. Results show that the flexural capacity of the slabs was improved by the textile reinforcement. Specimens with an increased amount of short fibers showed a larger ultimate load and lower mid-span deflections at peak load.

**Key words:** Textile reinforced concrete, Fibers, Reinforcement, Bending, Slabs, Mix design.

### 1. INTRODUCTION

In recent years, new techniques for reinforcement of concrete structures have been developed. Among them, the use of textile reinforcement for replacing the traditional steel reinforcement has caught the attention of researchers worldwide. In comparison with conventional steel reinforcement, less concrete cover is needed for textile reinforced concrete (TRC) elements, as there is no need of protecting the reinforcement against corrosion. Therefore, the use of TRC allows casting thinner elements. However, TRC is still a relatively new composite material and it

is required to investigate further its behavior in terms of material properties and applications [1, 2].

To increase the strength of TRC members, the concrete can be mixed with randomly distributed short fibers. The addition of the fibers allows obtaining a more adequate cracking pattern in which several small cracks are observed instead of one or two main cracks. The fibers vary in length as short fibers help bridging the smallest cracks and longer one help bridging larger cracks. [3]

In this paper, the results of an experimental campaign aimed to investigate the effect of including short fibers in textile reinforced concrete slabs tested in bending are presented. Besides the amount of short fibers included, the influence of the textile reinforcement inside the concrete element was also analyzed.

## 2 EXPERIMENTAL CAMPAIGN

A total of 6 slabs were casted and tested. The slabs had a width  $b=300$  mm, height  $h=30$  mm, and total length of 880 mm. All specimen were cast using a ready-mix concrete with a maximum aggregate size of 3 mm. A superplasticizer was used to increase workability of the concrete. The average concrete compressive strength, determined as the average of three cylinders with dimensions  $\phi 50 \times 100$  mm in accordance with EN 12390-2 (2009) was 42 MPa. The reinforcement consisted in unbalanced bidirectional carbon fiber mesh with synthetic, filament yarns with carbon in warp direction and AR-glass in weft direction. The mesh size of the reinforcement is 20 mm in both warp and weft direction. The tensile strength of the reinforcement ( $f_{tu}$ ) and the modulus of elasticity ( $E_f$ ) of the textile were 4300 MPa and 240 GPa, as reported by the manufacturer, and the equivalent thickness of the carbon fibers was ( $t$ ) 44 mm<sup>2</sup>/m. Short monofilament polyvinyl-alcohol (PVA) fibers were used. PVA fibers had 40  $\mu$ m diameter, 8 mm length, 40GPa modulus of elasticity and 1560 MPa tensile strength as reported by the manufacturer [4].



Figure 1 – a) Experimental set up (dimensions in mm); b) slab test.

They were tested using a four-point bending scheme with a span length  $l=750$  mm, as shown in Figure 1. The test was carried out under displacement control. The initial displacement rate was set to 0.5 mm/min until the first crack was detected, then the speed was increased to 0.016 mm/s. The displacement rate was changed to 0.08 mm/s after 10 mm deflection. The test was stopped when the load dropped under 50% of maximum load ( $P_{max}$ ). A dial displacement indicator was located below the slab to measure vertical displacements ( $\Delta$ ) at mid-span.

The slabs were designated according to the convention: S%-a-#, where S% corresponds to the percentage of PVA fibers included in the concrete (S0.5= 0.5%, S1.0= 1.0%), a denotes if the slab was textile reinforced or not (RB for textile reinforced elements, NN for unreinforced elements), and Y is the specimen number. The designation of the 9 beams tested is shown in Table 1.

Table 1 – Summary of test results.

Slab	PVA (%)	$P_{max}$ (kN)	$P_{max-a}$ (kN)	$\Delta_u$ (mm)	$\Delta_{u-a}$ (mm)
S0.5-NN-1	0.5	0.56	-	1.4	-
S0.5-RB-1*	0.5	2.82	2.56	69	58
S0.5-RB-2*	0.5	2.29	-	48	-
S1.0-NN-1	1.0	1.27	-	1.3	-
S1.0-RB-1	1.0	4.02	3.43	23	-
S1.0-RB-2*	1.0	2.84	-	27	25

\*Test stopped when applied load  $P$  was approximately half of maximum load  $P_{max}$ .

### 3 RESULTS AND DISCUSSION

The applied load  $P$  versus mid-span displacement  $\Delta$  curves for the unreinforced and reinforced slabs are shown in Figure 2. Table 1 summarizes values of maximum load  $P_{max}$ , and the maximum displacement at mid-span  $\Delta_u$ , of each slab. Average values of maximum load ( $P_{max-a}$ ) and maximum displacement ( $\Delta_{u-a}$ ) for specimens of series S0.5.RB and S1.0-RB are also included in Table 1.

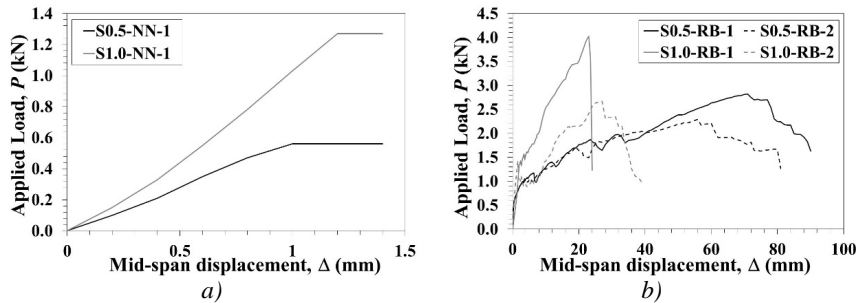


Figure 2. Applied load  $P$  vs. mid-span displacement  $\Delta$  curves for: a) Unreinforced specimens; b) Reinforced specimens

As shown in Figure 2 and Table 1, the use of textiles and PVA fibers improved the performance of the slabs in terms of maximum load and ultimate displacement. Higher values of  $P_{max}$  were attained for slabs with 1.0% of PVA fibers, with an average value of 3.53 kN. However, when the capacity increase is evaluated with respect to the unreinforced specimen, ( $P_{max-a}/P_{max}$ ), similar values are obtained for specimens with 0.5% and 1.0% of PVA fibers (2.55 and 2.70 respectively).

Increase in values of  $\Delta_u$  relative to the corresponding unreinforced specimen were also achieved. For this case, higher displacements were witnessed in specimens with 0.5% of PVA fibers. In fact, values of  $\Delta_{u-a}$  for these specimens were approximately twice as high as the ones recorded for slabs with 1.0% of PVA fibers and 40 times than for the unreinforced specimens. However, it is worth noting that for reinforced specimens, with exception of slab S1.0-RB-1, the test was stopped when  $P$  was approximately equal to  $P_{max}$  and therefore, higher values of  $\Delta_{max}$  could have been achieved if the test had been run until failure.

Before the occurrence of the first crack, the slabs present a linear elastic behavior according to the concrete stiffness. After cracking, there is a load redistribution from the mortar to the fibers. This allows the specimen to keep carrying load while cracks propagate. After  $P_{max}$ , the behavior depends on the amount of PVA fibers. For S1.0-RB specimens, there is not a noteworthy increase

in mid-span displacements after peak load. In fact, for slab S1.0-RB-1, failure occurred immediately after  $P_{max}$ . For S0.5-RB specimens, Figure 2b shows that the slabs can deform significantly after  $P_{max}$  is achieved, although lower values of  $P_{max}$  were achieved.

For the case of unreinforced slabs with PVA addition, [3] showed that maximum flexural strength capacities were obtained with PVA fiber content of 1.5%. However, the results in this paper showed that although higher contents of PVA fiber generate an increase in the capacity of the TRC slabs, the same behavior is not observed for mid-span displacements. In fact, higher values of  $\Delta$  were witnessed for specimens with lower content of PVA fibers. Based on the results presented in this paper, the authors postulate that for the case of TRC slabs, it is expected that values of PVA content higher than 1.0% will influence negatively the ductility of the specimens. However, more test are needed in order to validate this affirmation.

A brittle failure mode, characterized by concrete crushing, was observed for unreinforced specimens. A similar behavior was observed for specimen S1.0-RB-1. For the remaining reinforced specimens, a more ductile behavior was witnessed, although concrete crushing was also noted. In addition, some ruptured fibers were visible after testing but all yarns were kept together in one piece.

#### 4 CONCLUSIONS

In this paper, the results of an experimental campaign aimed to study the flexural behaviour of TRC slabs with PVA fibers addition were presented. The main conclusions that can be drawn from this study can be summarized as follows:

- The increase in the flexural capacity of the slabs depends on the amount of PVA fibers added; higher values of maximum load were seen for slabs with a higher PVA fiber addition (1.0%).
- Larger ultimate displacements were obtained in slabs with 0.5% of PVA fibers.
- The failure mode of the slabs was modified depending on the amount of PVA fibers and the presence of the textile reinforcement. With the exception of S1.0-RB-1 specimen, TRC slabs behaved in a more ductile manner as the specimens were able to deform after the maximum load was achieved.

#### REFERENCES

- [1] Brameshuber W. Report 36: Textile Reinforced Concrete - State-of-the-Art Report of RILEM TC 201-TRC: RILEM Publ.; 2006.
- [2] Portal NW. Sustainability and Flexural Behaviour of Textile Reinforced Concrete. Gothenburg, Sweden 2013: Chalmers University of Technology; 2013.
- [3] Kamal M, Khan SW, Khan S, Alam M. Experimental investigation of the mechanical properties of ECC. International Journal of Advanced Structures and Geotechnical Engineering. 2016;5(2):40-5.
- [4] Kuraray. REC 15x8 PVA Datasheet. 2017.

## Load tests on industrial steel fibre concrete floors



Johan Silfwerbrand  
 Dr., professor  
 KTH Royal Institute of Technology  
 Dept. of Civil & Architectural Engineering  
 Brinellvägen 23  
 SE-100 44 Stockholm  
 E-mail: [jsilfwer@kth.se](mailto:jsilfwer@kth.se)

### ABSTRACT

Steel fibre concrete (SFC) is a versatile alternative for industrial floors. Despite the development of guidelines and standards, there is no common Swedish view on how to design and construct SFC floors. Instead there are two competing methods resulting in significantly different results. The method based on Swedish guidelines leads to rather thick floors with high safety against failure due to load. The continental design method leads to much thinner slabs. The safety against failure is less but might still be sufficient in some cases. A method to avoid the endless debate between advocates of the two methods is to perform load tests on real industrial SFC floors.

**Key words:** Fibres. Industrial concrete floors. Load-carrying capacity. Structural Design. Testing.

### 1. INTRODUCTION

Steel fibre concrete (SFC) is a versatile alternative for industrial floors, but unfortunately, there is no common view on how to design and construct SFC floors, at least not in Sweden. Several initiatives have been taken resulting in the development of guidelines and standards [1-3]. In Sweden, there are two competing alternatives, one is based on Swedish traditions and safety concepts [1-2] and one is based on continental or Belgian concepts. At the Stockholm fib symposium in 2012, a unique Swedish-Belgian paper was published [4]. It compared the design of a pile-supported fibre concrete slab. The comparison showed that the calculated load-carrying capacity was considerably higher for the Belgian design than the Swedish design.

In a couple of Swedish cases, unanticipated and rather severe cracking on the industrial SFC floor has raised the question if the floor has been too weak to carry the loads. In these cases, the continental method has been used for the design. Recalculations showed that the load-carrying capacity was not sufficient according to the Swedish design method. Advocates of the continental design method are, however, referring to a long and broad experience with success stories from well-performing SFC floors in several countries. The reason for the success might not necessarily be that the continental design method is correct. The load-carrying capacity of a slab-on-grade is complex and beneficial factors such as arch effects, membrane effects, and stress redistributions in slabs are usually neglected. For the pile-supported slab, we usually neglect the contribution from the subbase or subgrade between the pile heads. All these contributions may together be sufficient for compensating the shortcomings in the load-carrying capacity of a small part of the SFC slab itself.

As an alternative to endless discussions on whether the continental method is right or wrong, the author of this paper proposed load tests on the floor to investigate its strength and stiffness. "Design by testing" is an old, well-known, and adequate method if used correctly [5].

## 2. DESIGNING LOAD TESTS ON INDUSTRIAL CONCRETE FLOORS

### 2.1 Aim

The aim of the load tests was to verify that the pile-supported SFC slab, that is part of the industrial floor in an investigated industrial building, is able to carry the design values of the actual loads without severe cracking or deformations. Preferably, both (i) the failure load and (ii) the long-term deformations under service load would be determined, but this is rarely possible. The load causing failure is difficult to obtain due to practical difficulties to create sufficient load magnitude (loads limited to gravity loads). Long-term deformation measurements require access to an experimental area of the floor during several months which usually is impossible for the owner of the building. Consequently, the aims have to be reduced to measuring performance (cracking and deflections) under a high load and measuring deflections under a lower load during one or two weeks.

### 2.2 Loading

Pile-supported slabs are designed for two failure modes (Figure 1). Both failure modes are developed for a uniform load  $q$  on the entire slab. This was the background for selecting a load pattern consisting of a centrally placed, uniformly loaded square slightly smaller than the area between four adjacent pile heads (Figure 2). This location of the loaded area will also lead to maximum deflection.

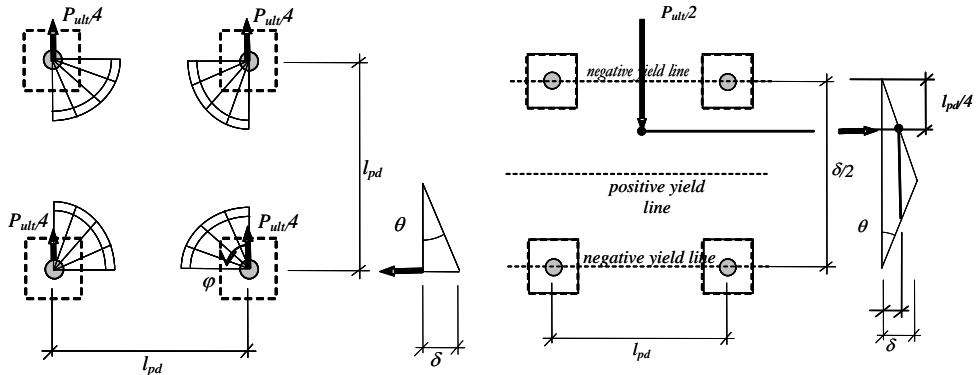


Figure 1 – Two different flexural failure modes for pile-supported slabs [3].

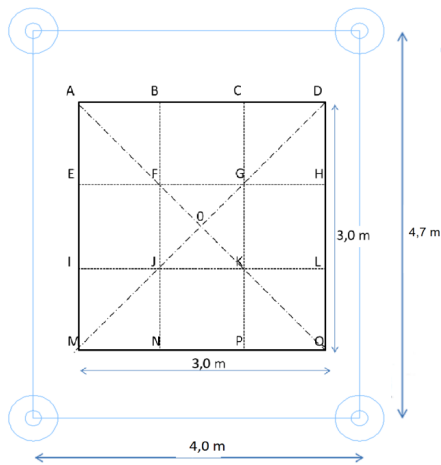


Figure 2 – Loaded area (left) and loads consisting of pallets of concrete pavers (right).

### 2.3 Measurements

The measurements consisted of deflection measurements in points A-Q (Figure 2) before, during, and after loading as well as crack pattern surveys.

### 2.4 Evaluation criteria

The evaluation criteria were based on (i) calculations of anticipated deflections of a well-performing slab of sufficient strength and stiffness and (ii) adaption of frequently used performance requirements to the specific loading case.

Table 1 – Evaluation criteria

No	Parameter	Unit	Requirement
1	Centre deflection under load (point O)	mm	< 7.0
2	Deflection under load (points A-D, E, H, I, L, M-Q)	mm	< 6.0
3	Remaining deflection (points O, A-Q)	mm	< 3.0
4	Maximum crack width	mm	< 1.0
5	Total crack length (crack width > 0.2 mm)	m	< 4.0

## 3. EXAMPLE

A load tests was performed on an industrial concrete floor close to Göteborg, Sweden. The floor consisted of a 230 mm thick pile-supported SFC slab. The concrete compressive strength was measured to 56 MPa and the fibre content to 48 kg/m<sup>3</sup>. The spacing between the piles in two perpendicular directions was 4.0 and 4.7 m, respectively. The floor was designed to carry a distributed load  $q = 40$  kN/m<sup>2</sup>.

The author had proposed a total load  $Q$  consisting of 36 sand bags, each weighing 1100 kg, totalling 39.6 metric tons or 388 kN distributed on a centrally placed area  $A = 3.0 \times 3.0 = 9.0$  m<sup>2</sup> resulting in a distributed load  $q = 43$  kN/m<sup>2</sup>. The solution with sand bags was, however, not possible. Instead, pallets of concrete pavers were used (Figure 2). Due to safety reasons, the total

load was limited to  $Q = 12.64$  metric tons distributed on an area  $3.0 \times 3.3 = 9.9 \text{ m}^2$  resulting in a distributed load  $q = 12.5 \text{ kN/m}^2$ .

The midspan deflection was measured to 2.7 mm directly after loading and increased to 3.3 mm during the week of sustained loading. After removing the load, a remaining deflection of 0.4 mm was measured. No new cracks were observed during the load tests.

Since the load was only 31 % of the design load, it is difficult to draw any conclusions regarding the relationship between the performance and the requirements. If the slab would remain uncracked at  $q = 40 \text{ kN/m}^2$ , the measured values may be considered acceptable. If, on the other hand, the slab would crack at such a load, both deflections and cracking would most likely exceed the requirements.

#### 4. CONCLUDING REMARKS

Despite the development of standards and handbooks, there is still no consensus among engineers on how to design SFC slabs for industrial floors. An alternative to computation methods is design by testing. This paper summarizes a Swedish proposal for load tests on industrial floors. The problem is to test the floor with a load of sufficient high magnitude. Neither sand bags, nor pallets of concrete pavers can be stacked to a sufficient height without jeopardizing the safety of the laboratory staff. A massive concrete block has to have a height of 1.67 m to provide a distributed load  $q = 40 \text{ kN/m}$ . All solutions with smaller elements or loose materials will lead to more intervening space and, thus, even higher stacks. One solution would be casting large cubes of concrete containing iron ore as aggregate.

If we are able to solve the loading, design by testing can be used as a tool to determine whether a certain design method is appropriate or not. The load test has to be combined with measurement on slab thickness, concrete strength, and fibre content to determine average values and scatter. We must also determine if the subbase or subgrade underneath the slab is carrying part of the load or if the piles are carrying the entire load. This may be done through coring.

#### REFERENCES

- [1] Swedish Concrete Association: "Steel Fibre Reinforced Concrete – Recommendations for Design, Construction, and Testing". ("Stålfiberbetong – rekommendationer för konstruktion, utförande och provning"). Concrete Report No. 4, 2<sup>nd</sup> Edn., Stockholm, Sweden (1997). (In Swedish).
- [2] Swedish Concrete Association: "Industrial Floors – Recommendations for Design, Material Selection, Construction, Management, and Maintenance". ("Industrigolv – rekommendationer för projektering, materialval, produktion, drift och underhåll"). Concrete Report No. 13, Stockholm, Sweden (2008). (In Swedish).
- [3] SS 812310:2014: "Fibre Concrete – Design of Fibre Concrete Structures". Swedish Standards Institute, Stockholm (2014), 38 pp.
- [4] Destrée, X., & Silfwerbrand, J.: "Steel Fibre Reinforced Concrete in Free Suspended Slabs: Case Study of the Swedbank Arena in Stockholm". Proceedings, fib Symposium on "Concrete Structures for Sustainable Community", Stockholm, Sweden, June 11-14, 2012, pp. 97-100.
- [5] SS-EN 1992-1-1:2005: "Eurocode 2: Design of concrete structures — Part 1-1: General rules and rules for buildings". Swedish Standards Institute, Stockholm, 2005.

**Session A3:**

**TESTING**



## Methodology for mesomechanical study of concrete material



Mathias Flansbjer  
M.Sc., Ph.D., Adj. Prof., researcher  
RISE Research Institutes of Sweden, Mechanics  
Research  
Box 857 SE-501 15 Borås, Sweden  
E-mail: mathias.flansbjer@ri.se



Jan Erik Lindqvist  
Ph.D., Senior researcher  
RISE Research Institutes of Sweden, CBI  
Ideon, SE-223 70 Lund, Sweden  
E-mail: janerik.lindqvist@ri.se

### ABSTRACT

This project focuses on detailed studies of how the cracking process in concrete is influenced by the concrete micro- and mesostructure. The aim is to increase knowledge of how critical parameters affect the cracking process and how this is related to the material's macroscopic properties. A methodology based on the combination of different experimental methods and measuring techniques at different scale levels has been developed. Crack propagation during tensile loading of small-scale specimens in a tensile stage was monitored by means of Digital Image Correlation (DIC) and Acoustic Emission (AE). After the test, crack patterns were studied using fluorescence microscopy.

**Key words:** Concrete, Cracking, Testing, Digital Image Correlation, Acoustic Emission, Microscopic Analysis

### 1. INTRODUCTION

Many of the characteristics of concrete mechanical behaviour observed at the macro scale can be explained by the heterogeneous structure of concrete at the micro and meso scales. Conventional strength tests on the macroscopic scale are essentially intended to characterize and compare different qualities of concrete in a standardized way, but give limited information at the micro and meso scale since they do not reflect the heterogeneous nature of the materials in a relevant way. Therefore, the combination of different experimental methods and measuring techniques at different scales is essential to enable deep investigation and understanding of the cracking process from micro to macro scale. Within this project we study how the cracking process in concrete is influenced by the concrete micro- and mesostructure, with special focus on the influence of aggregate shape. The project includes the development of a methodology that enables detailed analysis at the micro and meso scales, based on DIC, AE and microscopy. Here, a brief description of the methodology is given; a more comprehensive report of the project can be found in [1].

## 2. EXPERIMENTAL SETUP

### 2.1 Materials and specimens

The test series includes two different concrete recipes, here referred to as N038 and C038. The concretes had a w/c of about 0.38 and the coarse aggregate (8-16 mm) were of felsic rock material. The difference was related to the fine aggregate ( $< 8$  mm), which were of Natural (N038) or Crushed (C038) felsic rock material. The crushed aggregate used contained a higher amount of elongated and flaky particles compared to the more rounded natural aggregate. The cube compressive strengths  $f_{c,cube}$  at 28 days were determined to 91.5 MPa and 80.9 MPa for N038 and C038, respectively. The same materials, cast at the same time, were used in an earlier project concerning micro and meso scale material properties affecting the shear strength capacity [2].

Specimens with section dimensions  $60 \times 60 \text{ mm}^2$  were cut from larger concrete blocks. Two 10 mm deep and 5 mm wide notches were cut with a stationary diamond cutting blade. To make the meso structure of the concrete more prominent in the DIC images, the surface of the specimens was polished in a grinding machine before testing. The specimens with Natural and with Crushed fine aggregates are referred to as N038-# and C038-#, respectively.

### 2.3 Direct tensile test setup

The direct tensile test setup consists of different subsystems as illustrated in Figure 1; the tensile stage with control system, the data acquisition system, the AE system and the DIC system. The specimen is glued to the two loading platens of machine.

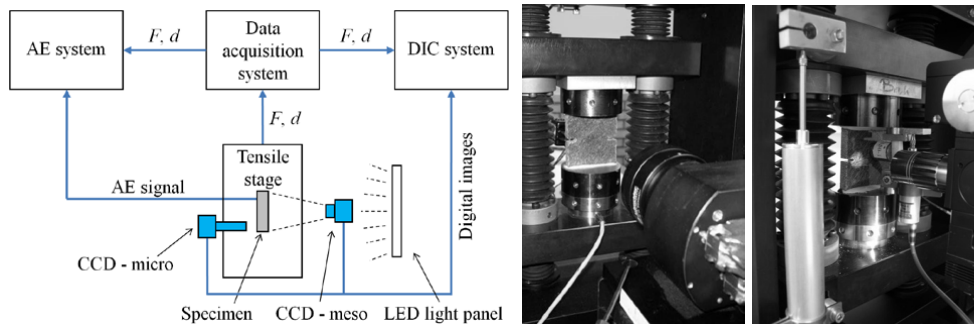


Figure 1 – Illustration of the tensile stage test system (left). Photo of test setup with camera configuration at meso scale (middle) and at micro scale (right).

The force  $F$  is recorded by a load cell with a maximum capacity of 10 kN and the relative displacement  $d$  between the two cross beams is measured with a LVDT with a measuring range of  $\pm 5.0$  mm. In these tests, the loading was controlled at a displacement rate of 0.06 mm/min.

The setup enables 2D DIC measurements on two different scale levels: one meso scale covering the entire specimen surface ( $65 \times 65 \text{ mm}^2$ ) and one micro scale focusing on one of the notches ( $8 \times 8 \text{ mm}^2$ ), see Figure 1. The system setup employed resulted in a spatial resolution of approximately  $0.63 \times 0.63$  mm and  $0.19 \times 0.19$  mm, and a coordinate measurement accuracy of approximately  $1.3 \mu\text{m}$  and  $0.16 \mu\text{m}$ , for the meso and the micro scale, respectively. The images were captured with a frequency of 5 Hz. The AE activity was recorded by one AE sensor with a resonance frequency of 150 kHz. A pre-amplification of 40 dB and a threshold level of 40 dB were used. The force and the displacement were also recorded in the DIC and the AE system.

### 3. EXPERIMENTAL RESULTS

In general no major differences were found in stress-displacement relationships or crack formation during testing between the specimens with natural (N038) or crushed aggregates (C038). Tensile test results are exemplified for one specimen (C038-5) in Figure 2.

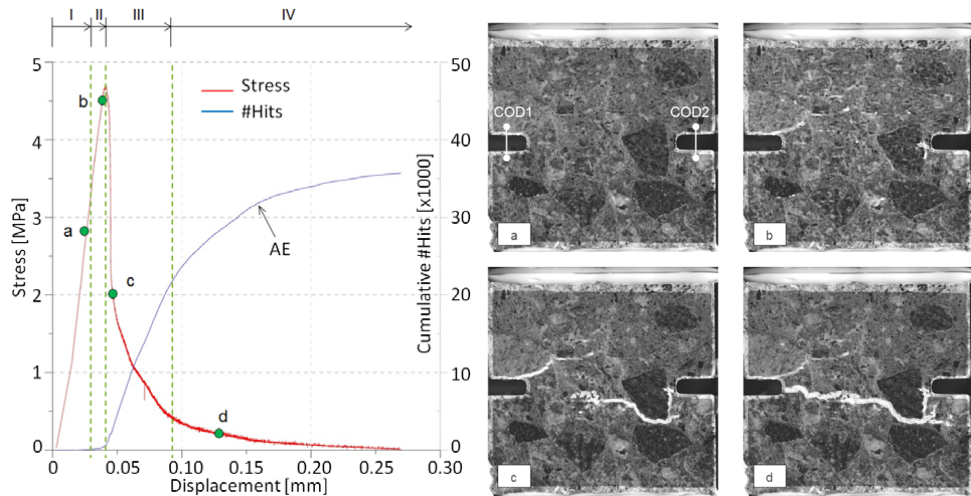


Figure 2 – Stress and cumulative AE Hits versus time (left) and example of crack formations in the different phases of the cracking process (right) for specimen C038-5.

The cracking process observed by DIC and AE during the tests may to some extent be related to different phases in the stress-displacement relationship. These findings correspond well with the four stages in the tensile fracture process defined in [3]; (I) elastic stage, (II) micro cracking, (III) macro cracking and (IV) bridging.

During the initial elastic pre-peak part (I) of the stress-displacement curve, the number of AE hits is small and probably related to the opening of existing micro-cracks in both the cement matrix and the aggregate particles. These cracks cannot really be identified by DIC. When new cracks starts to develop in phase II, mainly in the ITZ, the number of hits starts to increase, and increases further when cracks start to propagate into the cement paste matrix from the ITZ or the two notches. Close to peak stress, the crack intensity and as a result also the AE activity, increases. This corresponds well with a small non-linear section in the stress-displacement curve that occurs just before peak stress is reached, when different micro-cracks connect to each other. The hit-rate reaches the highest value during the initial part of the post-peak behaviour related to the creation of one localized macro-crack in phase III. During the last phase (IV) of the post-peak behaviour related to gradual opening of the macro-crack, the AE activity is mainly caused by the bridging effect of the aggregate particles. While the crack opens, the hit rate decreases, and eventually becomes zero as the crack is completely open. The transitions between the different phases are generally vague, and the phases overlap.

After testing, the specimens were analysed using thin section technique in fluorescence microscopy combined with image analysis. The thin sections covered the entire fracture area from notch to notch, see Figure 3. The combination of DIC measurements during testing and fluorescence microscopy after testing makes it possible to characterize and quantify the fracture down to micrometre scale and relate it to the cracking process during loading.

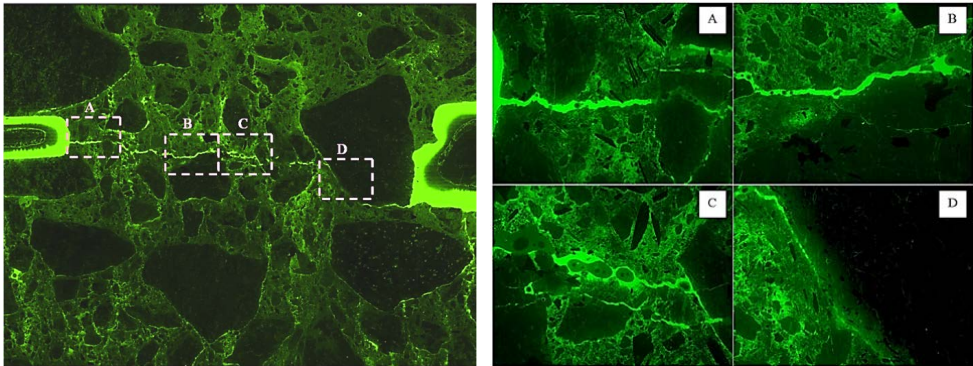


Figure 3 – Fluorescence image of C038-5 after testing, at meso (left) and micro scale (right).

The fluorescence image shown in the Figure 3 cover the area seen in the DIC images presented in Figure 2 (left). The approximate positions of the individual sub-images are indicated in Figure 3 (left). Sub-image (A) shows the area adjacent to the left notch. Sub-image (C) shows an area where the main fracture temporarily stopped during the test as can be seen in the DIC image (c) in Figure 2 (left). It can be seen that the microstructure is considerably damaged by the fracturing process in this region. Sub-image (D) shows the main fracture that was forced to go around the larger aggregate close to the right notch. It can be noted that the crack running diagonally from the left notch along the ITZ in Figure 2 (b) to (d) has to a large extent closed after the test, as can be seen in Figure 3 (left).

A comparison with results obtained from tests in shear in a previous study using the same concrete [2] show that the fracture process in tension are, as shown in the present project, less dependent on the shape of the aggregate particles than in shear. There are however differences in detail of the fracture pattern between samples with rounded natural aggregate and those with elongated crushed aggregate, also in tension. The analysis of fractures in tension show that there are more secondary fractures branching out from the primary fracture in samples with crushed aggregate. It can be seen that propagating secondary cracks often stop or are deflected at aggregate particles. It is suggested that this is more frequent in the samples with crushed aggregate. As the secondary fractures have partly grown in shear, flaky particles may act through interlocking. These meso and micro scale differences provide potential explanations of the differences in mechanical behavior and are a suitable area for continued research.

#### 4. CONCLUDING REMARKS

The present project shows that the applied combination of methods has a potential for increasing the understanding of fracture process on micro and meso scale and how it relates to the loading. The analysis show that in tension are there no major difference in fracture behaviour between concrete with crushed compared to natural sand in the aggregate finer than 8 mm. This differs from the behaviour in shear where there shape of the aggregate has a clear influence.

#### REFERENCES

- [1] Flansbjer M. and Lindqvist J. E.: *Meso mechanical study of concrete material*. SP-AR 2013:06, SP Technical Research Institute of Sweden, 2013.
- [2] Flansbjer M., Lindqvist J.E. and Silfwerbrand J.: Quantitative fracture characteristics in shear load. *fib Symposium*, Prague 8-10 June 2011. pp 567-570.
- [3] van Mier J.G.M.: *Concrete Fracture, a Multiscale Approach*, CRC Press, 2012.

## Computed tomography as investigation method for steel fibre reinforced tunnel shotcrete



Anders Ansell  
Ph.D., Professor  
KTH Royal Institute of Technology  
Division of Concrete Structures  
SE-100 44 STOCKHOLM, Sweden  
e-mail: anders.ansell@byv.kth.se



Lamis Ahmed  
Ph.D., Assistant Professor  
KTH Royal Institute of Technology  
Division of Concrete Structures  
SE-100 44 STOCKHOLM, Sweden  
e-mail: lamis.ahmed@byv.kth.se



Alvaro Guarin  
Ph.D., Researcher  
KTH Royal Institute of Technology  
Division of Building Materials  
SE-100 44 STOCKHOLM, Sweden  
e-mail: alvaro.guarin@byv.kth.se

### ABSTRACT

A laboratory study has been conducted to examine how computed tomography (CT) can be used as a laboratory method for investigation of cored specimens of shotcrete (sprayed concrete) from tunnels. The method is well suited to describe the distribution and orientation of steel fibres in the shotcrete, and also how interfaces between rock-shotcrete and between layers of different spray stages can be detected. Examples show how distributions of voids, cracks and aggregates can be described. It proved relatively difficult to clearly distinguish between cement and small aggregate fractions and therefore these are here combined and presented as cement paste.

**Key words:** Aggregate, Cracking, Corrosion, Fibres, Sustainability, Testing.

### 1. INTRODUCTION

With knowledge of the internal material structure, shotcrete (sprayed concrete) materials can be optimized for use in rock engineering, to produce cost-effective, sustainable and safe tunnels and subspace structures. The investigation methods used today for in situ test specimens are usually destructive methods, such as slicing/sawing followed by microscopy. This is time consuming and also leads to that the studied specimen is destroyed, preventing further investigations. New possibilities now exist in using computed tomography (CT), an advanced

method using integrated equipment for X-ray scanning and image detection with a computerized visualization system that can reproduce a three-dimensional virtual, transparent model of the studied object. Using the CT scan equipment at the KTH Civil and Architectural Engineering laboratory, a pilot study has now been carried out to describe the possibilities and limitations of the technique [1], with a focus on finding practical routines for obtaining quantitative and qualitative data. The work presented here is focuses on investigation of in situ samples from shotcrete of the type used in civil engineering rock work and tunnel construction.

## 2. INVESTIGATION METHOD

X-ray computed tomography (CT) is a non-destructive technique used for visualizing the interior of solid objects using digital information of the objects down to microscopic detail level. Medical CT systems are used for acquiring image of soft tissues and bones while high-resolution industrial X-ray CT utilize higher energy X-rays with more penetrative power and is used for materials within disciplines such as geo-sciences, engineering and manufacturing. A cylindrical volume can be described by sequential 2D CT images, corresponding to slices with an associated thickness that together defines the volume as composed by 3D elements, i.e. voxels. The quality of these scanned images depends on the X-ray source, the detectors used and the scanning configuration. More details on the sequential procedure of sample preparation, calibration, data acquisition and reconstruction are given by e.g. [2]. Other interesting studies on concrete using CT technique are e.g. summarized in [3]. The X-ray CT system used in this study is of the type NSI X5000 [4]. Within a radiation shielded enclosure there are 225 kV and 450 kV X-ray tubes with focal spot sizes of 5  $\mu\text{m}$  and 400  $\mu\text{m}$ , respectively, with a high resolution digital detector with 200  $\mu\text{m}$  pixel pitch. Depending on specimen size, degree of geometrical magnification and the tube used, tomography data with voxel sizes down to 5  $\mu\text{m}$  can be obtained. The system also contains a workstation with software for CT calibration, cone-beam reconstruction, 3D real time visualization and numerical analysis tools. There is also an integrated MTS Model 370 Uniaxial Test System for up to 100 kN force and 150 mm displacement and a chamber that can produce testing temperatures within  $-20^{\circ}\text{C}$  to  $+80^{\circ}\text{C}$ .

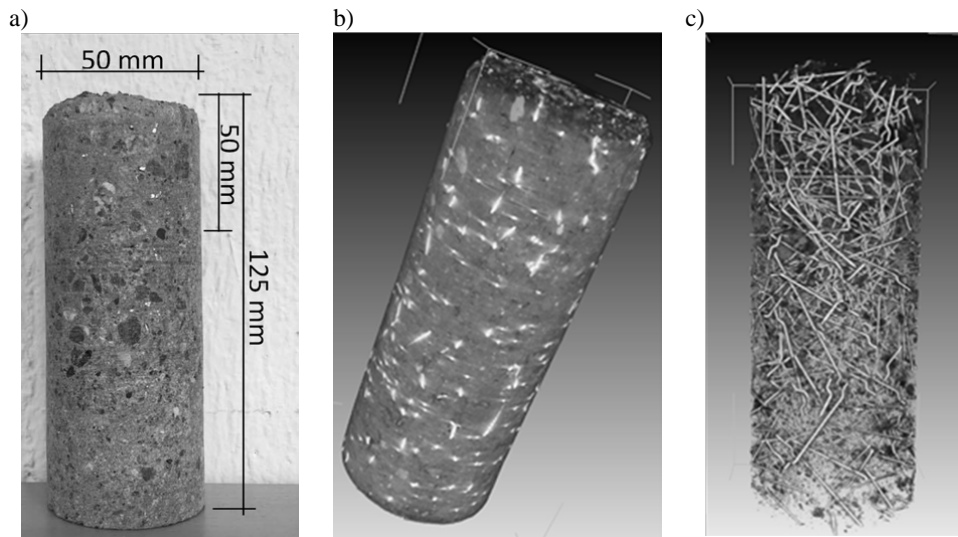


Figure 1 – Shotcrete core drilled out from a laboratory test beam (a), CT image of its outer cylinder surface (b) and of the steel fibre configuration only (c). From [1].

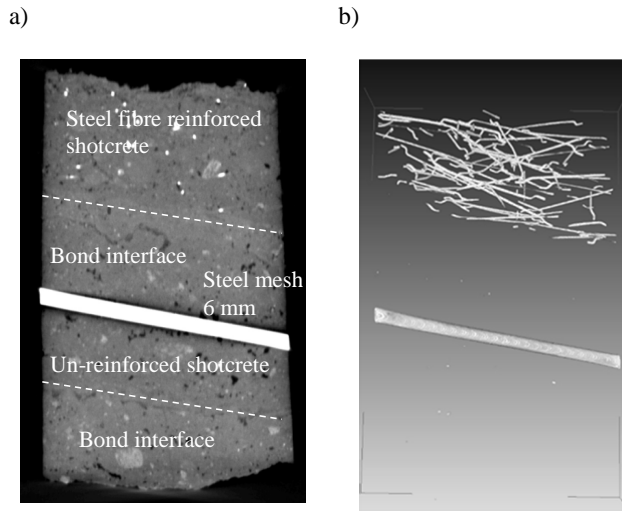


Figure 2 – CT image of an in situ core with three layers of shotcrete, one un-reinforced, one with steel mesh and one with steel fibres (a). Steel fibre and mesh configuration (b) and two cross-sectional views through a core with steel fibres (c). From [1].

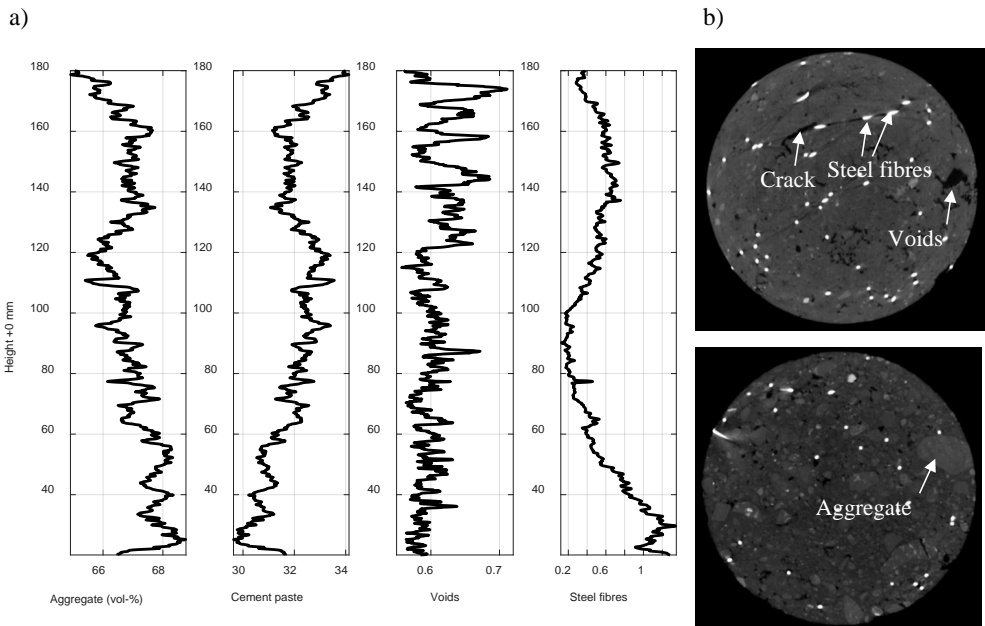


Figure 3 – Example of distribution of aggregates, cement paste, voids and steel fibres along 160 mm of a CT-scanned concrete cylinder. From [\*].

### 3. TEST RESULTS

An example of a drilled out core from a laboratory tested shotcreted beam is shown in Fig. 1. The specimen of steel-fibre reinforced shotcrete come from a long-term observation project and was exposed to flowing freshwater [5], after which the cylinders were cored for examination in the laboratory. The cylinder diameter is 50 mm and its length 125 mm, of which the bottom 50 mm has been immersed in water. The figure shows a photo and a three-dimensional CT image of the specimen exterior and a 3D image showing the steel fibre configuration only, which shows that the fibre orientation is highly variable. The second example shown in Fig. 2 describes a core drilled from a shotcrete lining consisting of three layers. It is here possible to distinguish two bond interfaces, between a lower unreinforced layer, a layer with steel mesh reinforcement and a thinner layer with steel fibre reinforced shotcrete. Probably, the lower layer was first sprayed, on top of which the steel mesh was mounted. This was later over-sprayed and then covered by a layer of steel fibre reinforced shotcrete. The cylindrical sample show no bond fracture surface towards rock and it can thus be assumed that there was tensile shotcrete failure during pulling out of the core. In the three-dimensional picture Fig. 2 (b), only the steel material is shown with the sections of the reinforcing mesh and fibres. The fibre orientation here coincides with the tunnel surface direction and the shotcrete is thus anisotropic with a significant reinforcing effect in the surface plane, but not in the thickness direction. Two-dimensional sections in the form of CT images are also shown in Fig. 3 (b), where cracks, voids, fibres and aggregates can be clearly distinguished. An example of calculated distributions of steel fibres, aggregates, cement paste and voids over the height of a test core is shown in Fig. 3 (a).

### 4. CONCLUSIONS

The summarized pilot study [1] shows that the method is suitable for practical analysis of in situ shotcrete specimens. The results from the CT investigations can be further analyzed and presented in the form of quantitative data, as distributions of cement paste, aggregates, steel fibers and voids, and as qualitative data that shows 3D distributions of steel fibers, aggregates, etc. It is recommended that the method should be established as a standardized method for non-destructive testing when developing new, optimized shotcrete types and for investigations of damaged and degraded concrete structures in tunnels and subspace structures.

### ACKNOWLEDGEMENT

The presented project was supported by BeFo, The Rock Engineering Research Foundation, which is hereby gratefully acknowledged!

### REFERENCES

- [1] Ansell, A., Ahmed, L., Guarin, A.: "Computed tomography as investigation method for young and old, sprayed and cast concrete for tunnels", BeFo report 165, Stockholm, 65 pp. (2017)
- [2] Ketcham, R.A., Carlson, W.D.: "Acquisition, optimization and interpretation of X-ray computed tomographic imagery: applications to the geosciences", *Computers & Geosciences*, 27, pp. 381-400 (2001)
- [3] Fuentes, R., Geiker, M.R., Stang, H.: "Characterisation of fibre content, distribution and orientation to predict Fibre Reinforced Concrete behaviour", *Nordic Concrete Research* no. 52, pp. 1-22 (2015)
- [4] X5000 system, North Star Imaging Inc., <http://4nsi.com/systems/x5000/> (2016)
- [5] Nordström, E.: "Evaluation after 17 years with field exposures of cracked steel fibre reinforced shotcrete", BeFo report 153, Stockholm, 35 pp. (2016).

## Dynamic measurements for determination of Poisson's ratio of young concrete



Lamis Ahmed  
Ph.D., Assistant Professor  
KTH Royal Institute of Technology  
Division of Concrete Structures  
SE-100 44 STOCKHOLM, Sweden  
e-mail: lamis.ahmed@byv.kth.se



Anders Ansell  
Ph.D., Professor  
KTH Royal Institute of Technology  
Division of Concrete Structures  
SE-100 44 STOCKHOLM, Sweden  
e-mail: anders.ansell@byv.kth.se

### ABSTRACT

Knowledge of the elastic properties of concrete at early age is often a prerequisite for numerical calculations. This paper discusses the use of a laboratory technique for determination of Poisson's ratio at early concrete age. A non-destructive test set-up using the impact resonance method have been tested and evaluated. With the method it has been possible to obtain results already at 7 hours of concrete age. The Poisson's ratio is found to decrease sharply during the first 24 hours to reach a value of 0.06 and then increased to approximately 0.13 after seven days.

**Keywords:** Modelling, Testing, Poisson's Ratio, Young Concrete.

### 1. INTRODUCTION

Young concrete is studied, with special focus on the period from the first contact between cement and water and up to 12 hours of age, which often is regarded as the most critical period with respect to e.g. vibration damage [1]. In some structural applications, for example in tunnelling, mining, bridge deck maintenance, construction of hydropower and nuclear power facilities, there is a need to control the response of young concrete that can be subjected to different types of dynamic loads, for example from impact vibration. Due to difficulties in performing experiments on young concrete due to for example early formwork removal problems, simulation models the finite element method are needed as a complement. These models require insertion of material data for concrete, such as the development of compressive strength, tensile strength, modulus of elasticity and Poisson's ratio. In numerical tests [1] it was found that Poisson's ratio has a significant effect on the numerical results for young concrete.

Of the studies that measured Poisson's ratio at early age, most concluded that this parameter is insensitive to age, i.e. the measured Poisson's ratio show practically the same value for all ages and curing conditions, see [2]. However, two important studies, by Byfors [4] and Mesbah [5], describe a significant decrease in Poisson's ratio at very early ages. Decreasing trends for Poisson's ratio are presented, from approximately 0.4 to 0.1 during the first 10-15 hours, at a compressive strength of about 1 MPa [4]. After this, Poisson's ratio increases with strength growth. The results from an investigation on high-performance concrete using the pulse velocity method [5] showed similar results, with Poisson's ratio decreasing during a short period of about 9 to 18 hours, reaching a value of 0.14, then increasing to its final value after seven days. To date, there is no information given in the Eurocode 2 [3] about how to specify Poisson's ratio at early ages. Although some experimental results [2] show increasing values of Poisson's ratio with age during the first 12 hours, for example up to about 25%, is this often considered as a close to constant value. It is thus likely that this parameter has a significant effect on numerical results for early age concrete. Therefore, a small-scale laboratory test is performed to find a technique to measure Poisson's ratio at early concrete age, which is here briefly summarized. For more details, see [1].

## 2. EXPERIMENTAL WORK

### 2.2 Materials

In this study, two concrete beams of  $180 \times 150 \times 800 \text{ mm}^3$  are cast. The concrete composition is presented in Tab. 1, chosen on the basis of laboratory investigations performed by Bryne [6]. A series of 150 mm cubes were cast to determine the development of compressive strength which was possible from 10 hours. The equation, where  $t$  is curing age in days, is derived from tested cubes, giving the relation between compressive strength ( $f_c$ ) and the age of concrete [6] as:

$$f_c = 28.4 e^{-0.661/t^{1.653}} \text{ (MPa)} \quad (1)$$

*Table 1 – Compositions of the concrete used in the tests.*

Composition	Content
Cement, $\text{kg/m}^3$	495
Water, $\text{kg/m}^3$	220
Aggregate 0-8 mm, $\text{kg/m}^3$	1540
Silika U/D, $\text{kg/m}^3$	20
Glenium, $\text{kg/m}^3$	4

### 2.3 Test Method

A non-destructive test is carried out using the impact resonance method where a freely supported (hanging) test beam is struck with a small impactor. The test is carried out at room temperature. The specimen response is measured using an accelerometer on the specimen; see Fig. 1(a). In this test, the longitudinal, transverse and torsional frequencies of the concrete beam at various times after casting were measured so that Poisson's ratio could be calculated, according to the testing standard [7]. To enable recording of particle acceleration for the three fundamental transverses, longitudinal and torsional resonance frequencies, three accelerometers were positioned on the specimen, as shown in Fig. 1 (b). According to [7], the fundamental frequencies of the three modes of vibration are obtained by proper location of the impact point and the accelerometers. The recording time was approximately 0.03 s with a sampling frequency of 9600 Hz, the highest possible.



Figure 1 – The suspended beam and the position of the accelerometers.

### 3. RESULTS

The obtained longitudinal and torsional frequencies are given in Tab. 2. The longitudinal and torsional modulus of elasticity and Poisson's ratio are calculated in accordance with [7], see Tab. 2. The growth of the Poisson's ratio during the seven days is shown in Fig. 2 (a). This demonstrates the evolution of Poisson's ratio as function of time for two test prisms. It can be seen that during the first 12 hours, a significant variation of Poisson's ratio occurs, which after that stabilises. By using Eq. (1), the corresponding curve for the compressive strength after 10 hours can also be presented in Fig. 2 (b).

Table 2 – Measured frequencies and calculated longitudinal and torsional modulus of elasticity and Poisson's ratios

Curing age (hours)	Longitudinal frequency (Hz)	Torsional frequency (Hz)	Longitudinal modulus of elasticity (GPa)	Torsional modulus of elasticity (GPa)	Estimated Poisson's ratio
7.0	(526)	(271)	1.48	0.58	0.276
7.5	951	277	4.82	2.02	0.192
8.0	(693)	(374)	2.56	1.10	0.163
8.5	(749)	(412)	2.99	1.34	0.120
9.5	(824)	(454)	3.62	1.62	0.116
9.0	(880)	(447)	4.13	1.87	0.106
10.0	(941), 1369	(520), 314	4.72, 10.00	2.13, 4.70	0.086*
11.0	(1049), 1460	(590), 341	5.87, 11.36	2.74, 5.40	0.061*
12.0	1547	874	12.76	6.01	0.062
14.0	1730	975	15.96	7.48	0.067
15.0	1787	1003	17.03	7.92	0.076
18.0	1927	1076	19.80	9.11	0.087
24.0	2041	1140	22.22	10.23	0.086
30.0	2110	1175	23.74	10.86	0.093
72.0	2295	1255	28.09	12.39	0.133
144.0	2375	1300	30.08	13.30	0.131
168.0	2385	1304	30.34	13.38	0.134

- The values within parentheses refer to beam No.2., - \* average value

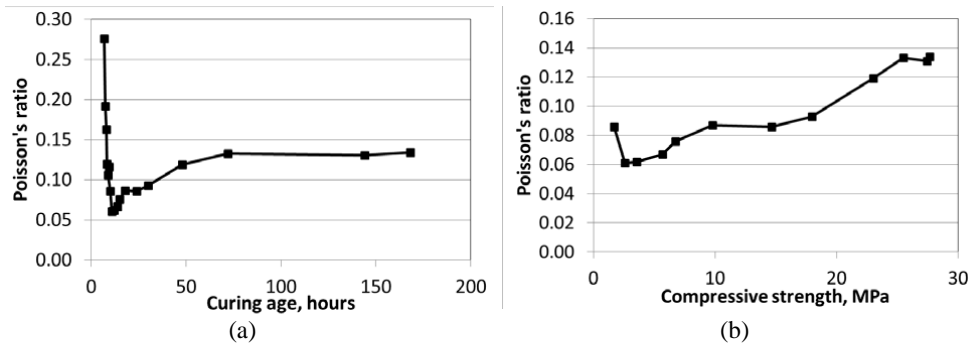


Figure 2 – Poisson's ratio versus (a) curing age and (b) compressive strength.

#### 4. CONCLUSION

The purpose of this study was to test and evaluate an experimental technique for estimation of the development of Poisson's ratio, an important material property needed in numerical calculations involving young concrete. From the results, it can be observed that the Poisson's ratio to a great extent depend on concrete age during the first few hours after casting. The measurement results show similar decreasing trends as previously suggested for other concrete types in [4,5].

#### REFERENCES

- [1] Ahmed, L., Ansell, A., Malm, R.: "Numerical modelling and evaluation of laboratory tests with impact loaded young concrete prisms", *Materials and Structures* ,49(11), 4691-4704, 2016.
- [2] Oluokun, F.A., Burdette, E,G, Deatherage, J.H.: "Elastic modulus, Poisson's ratio and compressive strength relationship at early ages", *ACI Journal*. 88(1), 3-10, 1991.
- [3] EN 1992-1-1. "Eurocode 2 Design of concrete structures- Part 1-1: General rules and rules for buildings", European Committee for Standardisation (CEN), Brussels, 2004.
- [4] Byfors, J.: "Plain concrete at early ages", Swedish Cement and Concrete Institute, Stockholm, 1980.
- [5] Mesbah, H.A., Lachemi, M., Aitcin, P.-C.: "Determination of elastic properties of high-performance concrete at early ages", *ACI Material Journal*, 99(1), 37-41, 2002.
- [6] Bryne, L.E.: "Time dependent material properties of shotcrete", Doctoral thesis, KTH Royal Institute of Technology, Stockholm, 2014.
- [7] ASTM C215-08. "Standard test method for fundamental transverse, longitudinal, and torsional frequencies of concrete specimens", ASTM International; West Conshohocken, PA, 2008.

## NPP containment wall mock-up for long-term NDE and monitoring



Miguel Ferreira  
M.Sc, Ph.D.  
VTT Technical Research Institute of Finland Ltd.  
Kemistintie 3, P.O. Box 1000  
FIN-02044, Espoo, Finland  
miguel.ferreira@vtt.fi



Edgar Bohner  
M.Sc, Dr. -Ing.  
VTT Technical Research Institute of Finland Ltd.  
Kemistintie 3, P.O. Box 1000  
FIN-02044, Espoo, Finland  
edgar.bohner@vtt.fi



Fahim Al-Neshawy  
D.Sc. (Tech.), Staff Scientist  
Aalto University School of Engineering  
Department of Civil Engineering  
P.O.Box 12100,  
FIN-00076, Espoo, Finland  
fahim.al-neshawy@aalto.fi

### ABSTRACT

Non-destructive examination (NDE) plays an important role in the support of ageing management programs, where the renewal of an operating licence requires that nuclear power plant (NPP) demonstrate that their facilities are ageing under controlled conditions. The inspection of NPPs concrete structures present challenges different from those of conventional civil engineering structures. The project WANDA (Non-Destructive Examination of Nuclear Power Plant Primary Circuit Components and Concrete Infrastructure) focuses on the development and understanding of NDE methods in two important NPP environments: primary circuit component materials and concrete infrastructure. This paper addresses the latter.

The NDE research on NPP concrete infrastructure focuses on the evaluation and calibration of the available NDE methods and monitoring systems for concrete structures. This is achieved through the design and construction of a real-scale mock-up (reinforced concrete containment wall) for NDE, monitoring, R&D and education purposes.

**Key words:** NDE, NDT, NPP, non-destructive examination, concrete, nuclear power plant, infrastructure, performance, testing, mock-up.

### 1. INTRODUCTION

The Finnish Research Programme on Nuclear Power Plant Safety (SAFIR2018) is guiding research towards NPP safety. In this research programme, the project WANDA (Non-Destructive Examination of NPP Primary Circuit Components and Concrete Infrastructure) is focusing on

the development and understanding of NDE methods, with special focus on reactor internals and more recently concrete infrastructure. This paper addresses the latter.

The inspection of NPPs concrete structures present challenges different from those of conventional civil engineering structures, such as infrastructure wall thicknesses (typically >1.0 m); dense and complex reinforcement detailing; penetrations or cast-in-place items; limited accessibility (i.e. liners or other components); severe environments; inaccessible structures; limited experience with NDE methods for NPP and lack of specific equipment or knowledge for NDE of NPP RCS [1].

There is a clear need for means of ensuring that concrete structures meet their design criteria, during and immediately following construction. Here, NDE methods can provide quality control and verification. However, with time, NPP reinforced concrete structures (RCS) are subject to ageing, resulting in their degradation and consequently deterioration in their performance. NDE methods can be used to characterize material properties, measure performance, and provide valuable input for the assessment of the RCS performance.

Research has shown the need for realistic specimens to be developed to allow for the assessment of various techniques, with consideration given to ensuring a broad range of faults/defects, and to ensure the limit of detection for a method can be properly understood and quantified [2]. This is achieved through the design and construction of a real-scale mock-up of a reinforced concrete containment wall [3].

## **2. DESIGN OF A NPP CONTAINMENT WALL MOCK-UP**

Adequately designed test mock-ups are important since they provide defined conditions under which different NDE methods can be evaluated. Material properties as well as the location of reinforcement, tendon ducts, and defects/flaws must be well documented.

To understand the design requirements for a NPP mock-up concrete specimen, discussions were held with the Finnish utilities, regulator (STUK) and Finnish Transport Agency, to understand their needs and focus on defining research actions to address specific NDE and monitoring interests and knowledge gaps that can improve the reliability, sustain the safety, and extend the life of operating reactors. Several aspects were highlighted [4]: i) NDE of concrete (defects, cracks, quality control issues, material and structural properties, complicated geometries, lack of access, etc.); ii) NDE of steel (reinforcement (concrete cover detection, corrosion of reinforcement, definition of layout), prestressed reinforcement (corrosion, grouting defects, prestress loss), and liner (corrosion, detachment, concrete NDE behind liner)); iii) monitoring (automation systems, data analysis, alerts, use of data); others aspects covering inclusions, piping, joints, leaking containments, etc.); and, iv) new NDE technologies. The following issues and limitations were identified:

- Every NDE method has some limitations, generally perform well on relatively thin concrete structures, however better understanding is required to see how these methods perform on thick and heavily RCS;
- Based on NPP structural typology, there is a need for testing concrete specimens much larger and more heavily reinforced than typically tested due to representativeness, thick-walled challenges, boundary conditions, etc.;
- Deterioration of RCS of NPP are typically in the form of cracking, spalling, general deterioration, delamination cracks/gaps near layers of reinforcement;
- Examination of NDE test specimens with intentional defects has shown current NDE method limitations. These NDE test specimens also tested the creation of realistic flaws to simulate defects created by construction methods;
- Examination of volumetric imaging techniques (beamforming and multi-transducer array) have shown it possible to detect structures at greater depths that may be obstructed by reinforcement closer to the surface.

An important aspect of this project is that the mock-up will allow for continuous long term testing, i.e., more than 20 years, which will allow future equipment to be assessed in a well-documented situation, and to assess in real-time the effects of ageing of RCS. Furthermore, the mock-up will be available for users of NDE equipment to test and calibrate performance accordingly. The mock-up will allow for the training of young engineers in the use of different NDE equipment and in the development of expertise with RCS similar to that of NPPs.

## **2.1 Defects for NDE detection**

A list of structural flaws for inclusion in the mock-up has been compiled based on examinations of previous NPP structure failures and the processes that lead to the deterioration of these structures [5]. For the construction of the mock-up, various types of artificial defects and materials/methods used should be considered, for example [5, 6]:

- Delaminations simulated with plastic sheets (0.05 mm) and cloths squares (0.25 mm);
- Air-filled voids simulated by inserting foam squares 13 mm thick in vacuum-sealed plastic bags;
- Water-filled voids simulated by water-filled plastic bags;
- Cracks simulated with laminar sheets of different material densities;
- Honeycombing simulated by glueing large aggregates carefully;
- Steel reinforcement corrosion simulated with section reduction prior to casting;
- Voids in grouted ducts simulated by polyurethane foam;
- Insufficient (inadequate) concrete cover depth.
- Liner corrosion simulated with cross section reduction prior to casting;
- Concrete-liner debonding simulated by low-density material sheet.

The mock-up will enable the assessment of current NDE methods concerning their capability to detect various defects/faults and forms of degradation. Clayton et al. [5] referred to a critical trade-offs within the space constraints of the mock-up: how realistic defects are versus how controlled each defect should be. Simulated defects/faults used in the mock-up should carefully represent activities that may (or have) occurred during the construction process and/or because of concrete deterioration with time. Furthermore, the design of the mock-up should include defects that challenge the capabilities of detection of the most advanced NDE methods, and yet include some basic defects that the majority of the NDE methods can detect. This will ensure that NDE methods incapable of detecting basic defects can be excluded, while the base-line level of achievement of the methods performing well can be identified.

## **2.2 Assessment of NDE and monitoring methods**

An integral part of the project is the evaluation and calibration of NDE methods, sensors and monitoring methods. This includes the determination of the NDE methods capabilities of detection and accuracy, calibration of NDE methods, correlation between NDE methods, and the effect of time dependency and testing conditions on test methods. The focus will be on existing test methods and promising new test methods.

Although access to both sides would allow for test methods using two-sided access measurements, the testing should focus on one-side per measurement to simulate realistic access to the containment wall.

The purpose of the monitoring program is to address calibration and validation of sensors, correlation between different NDE methods and sensors, effect of time dependency and testing conditions on sensors results, resolution and accuracy of sensors. The focus will be on the available and new sensors and wireless monitoring systems.

Sensor-based monitoring systems can be used to continuously follow the performance of the structures in real-time, mostly over long periods starting with the manufacturing of the

structures. The application of both, NDE methods and monitoring systems, allows for the best performance assessment by generating partly redundant data and using synergetic effects [7].

### 2.3 Probability of Detection methodology applied to concrete NDE

For the in-service condition assessment of reinforced concrete structures, it is necessary to qualify and quantify the extent of the defects using a range of NDE methods. The analysis and reliability check of the data produced by these tools and methods gives a large amount of information over a long period. The assessment of the capability of NDE methods is based on the determination of the “probability of detection”. The capability is defined as the probability of detecting a defect with a particular size under specified inspection conditions and a defined procedure. This approach, while commonly used in other fields of NDE is only taking its first steps for concrete NDE. Research will focus on studying the use of the probability of detection curve in the field of reinforced concrete structures NDE

### 3. FINAL CONSIDERATIONS

A study of NDE for detection of defects and faults in NPP reinforced concrete mock-ups is an essential component in defining the most promising techniques and directing the R&D efforts in this field. For the success of such an approach, a realistic containment mock-up is to be built. This mock-up contains realistically simulated defects to be evaluated by existing NDE methods. It is also critical that the evaluation mock-up and embedded defects be representative of in situ NPP concrete infrastructure.

A preliminary assessment of the basic restrictions and potential complexities involved with construction of large reinforced concrete mock-up has been conducted with a focus on defining the general requirements for the design and construction of the mock-up.

### REFERENCES

- [1] Wigggenhauser, H., Helmerich, R., Karuse, M., Mielentz, F., Niederleithinger, E., Taffe, A., Wilsch, G. Non-destructive testing of NPP concrete structures. State of the art report. BAM - Bundesanstalt für Materialforschung und –prüfung. 2013. 119p.
- [2] OECD/NEA. Final Report of Assessment of Structures subjected to Concrete pathologies (ASCET) phase 1. OECD, Nuclear Safety, NEA/CSNI/R(2016)13 .
- [3] Jäppinen, T., Ferreira, M., NDE Research of Nuclear Power Plant Primary Circuit Components and Concrete Infrastructure in Finland. 19th World Conference on Non-Destructive Testing (WCNDT 2016). 13-17.6.2016, Munich, Germany (2016), 7 p.
- [4] Al-Neshawy, F., Ferreira, M. & Bohner, E. 2016c. Pre-design considerations for large-scale NDE mock-up. Espoo. VTT Research Report. VTT-R-00645-17. 30p.
- [5] Clayton, D., Khazanovich, L., Hoegh, K., Hileman, M., (2014) Preliminary Conceptual Design of a Thick Concrete Non-destructive Evaluation Specimen. ORNL/TM-2014/146. Oak Ridge National Laboratory.
- [6] Wimsatt, A., White, J., Leung, C., Scullion, T., Hurlebaus, S., Zollinger, D., et al. (2012) Mapping voids, debonding, delaminations, moisture, and Other Defects Behind or Within Tunnel Linings SHRP 2 Renewal Project R06G. Transportation Research Board. 555 p.
- [7] Bohner, E., Kuosa, H., Al-Neshawy, F., Ferreira, M., 2016. NDE of thick-walled reinforced concrete structures – Technologies and systems for performance monitoring. VTT Research Report. VTT-R-00449-16. 63p.

## Development of a laboratory method for assessing the cement content of an arbitrary sample of mortar or concrete



Oskar Linderöth  
M.S.c, Ph.D-student  
Lund University  
John Ericssons väg 1, 223 63 Lund, Sweden  
e-mail: oskar.linderöth@byggtex.lth.se



Peter Johansson  
M.S.c, Ph.D., associate professor  
Lund University  
John Ericssons väg 1, 223 63 Lund, Sweden  
e-mail: peter.johansson@byggtex.lth.se

### ABSTRACT

This paper describes a method that allows the assessment of the cement content in small samples of concrete or mortar. The samples have been picked out of a larger mix and the aggregate content is therefore unknown. The method is key in the analysis of samples that have, for example, been measured by thermogravimetric analysis (TGA) and isothermal calorimetry. The result of such analysis need to be presented as: “per gram of cement” in order to compare results from different specimens. By dissolving the samples in hydrochloric acid and filtering the residue the aggregate content is determined. Assuming the weight prior to dissolution (dry samples) or the water-cement ratio (sealed samples) is known, the cement content can then be calculated.

**Key words:** Aggregate, Cement, Supplementary Cementitious Materials (SCM)

### 1. INTRODUCTION

Concrete is one of the most used building materials and as expected there is a lot of research into its behaviour and development [1]. The future of concrete is greatly influenced by the environmental challenges that arise from the fact that the production of cement accounts for 5-8 % of the worlds CO<sub>2</sub> emissions [2, 3]. From such environmental challenges spawns this study.

The study is part of a project that aims to investigate how fly ash affects the microstructural development of concrete and also how the curing temperature, at early ages, influences the hydration of fly ash blended cements. This is important to understand in order to predict the moisture properties and in turn the drying of concrete with fly ash blended cements. To answer these questions measurements using, among others, thermogravimetry (TGA), isothermal calorimetry and X-ray diffraction (XRD) are conducted. The samples are mortar or concrete

samples that have been mixed in batches of 20-70 litres. Isothermal calorimetry measurements are conducted on 1-1.5 grams of sample picked out of the fresh mortar or concrete batch. TGA and XRD samples are sawn out at different ages and hydration is stopped before measurements are conducted. In all cases the amount of aggregates within the sample is unknown. This is problematic in the cases of isothermal calorimetry and TGA as the results need to be presented as “per gram of cement” in order to compare the results of different samples.

One could argue that it is better to use well-defined samples that have been mixed in the desired volume with a correct distribution of the constituents. However, earlier studies by Linderoth and Wadsö [4] indicate that the mixing method and the presence of aggregates influence the rate of reaction. Other, similar, studies agree with this and conclude that the shear force put in to the mix is an important factor for the hydration process [5, 6]. Both the mixer and the roughness of the aggregates is a source of shearing. Geiker [7] and Farrington [6] also found that these differences are enhanced in the presence of super-plasticizing additives (SP) and when mixing large volumes of mortar or concrete at low water-cement ratios such additives are key to getting a good rheology. However, downscaling the SP is not trivial and therefore mimicking their effect on hydration in small volume mixes is hard. This has been studied by the author and will be published in a future paper.

Changes in the rate of reaction will affect the evolution of the microstructure [8]. The microstructure will determine the pore structure which in turn is closely related to the moisture properties. Yang and Jennings [9] studied the connection between mixing, rheology and microstructure on cement paste. They stress the importance of choosing a proper mixing method, especially when comparing measurements on cement paste to actual concrete. These reasons led to the conclusion that conducting measurements on pure cement paste samples was not the best option in this project.

The method declared in this paper uses hydrochloric acid to dissolve the cement paste phase of small mortar or concrete samples. After dissolving, the residue is filtered and the mass of aggregate is determined. Assuming the w/c-ratio is known it is possible to calculate the cement content of a sealed sample. For completely dry samples, only the weight prior to dissolution is needed. Similar methods have been published before, for example in [10-12]. However, their purpose and required level of detail vary from that of the method presented here.

## **2 MATERIALS AND METHODS**

The method was developed to determine the cement content of small samples (1-2 grams) of mortar or concrete. The cement used here is an OPC blended with 15 % siliceous fly ash (class F) the aggregate is sand (Normensand GmbH, Beckum, Germany). The sample size was chosen in accordance with samples typically used in isothermal calorimetry and TGA measurements. In order to get a good result the solubility of the constituents need to be individually determined to make proper corrections of the results. For similar reasons the water-cement ratio need to be known.

Prior to analysis, circular cellulose filter papers (Munktell 185 mm, 1-2  $\mu\text{m}$  retention) are dried at 105°C to determine their dry-weight. Hydrochloric acid (HCl) is mixed in a large tank using 1 part HCl (25%) and 5 parts de-ionised water. For each analysis, 180 ml HCl (25% 1:5) is poured into a beaker. The sample is coarsely crushed using a small hammer then finely grinded using a pestle. The samples along with a stirring magnet is then put into the beaker with acid which is placed on a magnetic stirring device (Variomag multipoint HP15, Variomag, USA) (Fig 1-L). It is left on the stirring device for 45( $\pm$ 15) minutes.

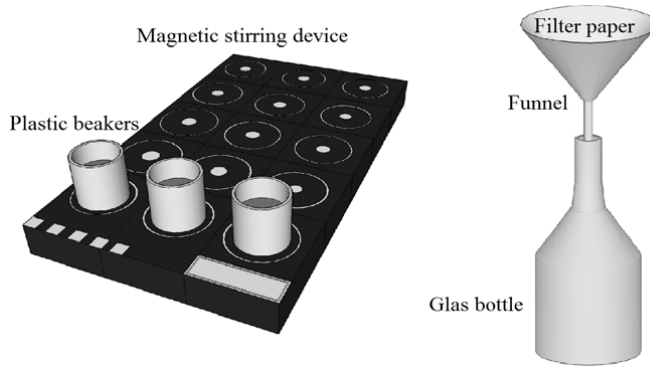


Figure 1- Left: the beaker while placed on the magnetic stirring device. Right: The liquid is filtered through a filter paper placed in a funnel connected to a glass bottle.

The residue is filtered (fig 1-R) in two steps. 1) Acid and residue is poured into the funnel. 2) When most of the liquid has run through the filter, de-ionized water is used to stir up the residue into suspension. The latter is done in order to prevent fine material from clogging the filter thus inhibiting proper filtering. After this step the filter and residue is folded, placed on a petri dish and dried at 105°C for 24h.

### 3 RESULTS

In table 1, dissolution conducted on the raw materials are listed. In addition to this, dissolution was also conducted on mortar samples with a known content of constituents.

Table 1 – The dissolution ( $D$ ) and the corrected ( $D_{corr}$ ) with respect to the raw materials solubility.

	Binder (C) [g]	Sand (S) [g]	Water [g]	D [%]	$D_{corr}$ [%]
FA	-	0.647	-	38.6	-
Sand	-	0.750	-	5.7	-
OPC-FA	1.000	-	-	89.8	-
Mortar	0.606	0.603	0.317	97.1	99.7

The residue ( $w_R$ ) is corrected with respect to the soluble part of the sand and the insoluble part of the OPC-FA binder (1), i.e. these factors are material specific. For sealed samples the weight of cement (C) is then calculated by assuming that the water-cement ratio (wcr) of the analysed sample is the same as that of the original recipe (2). In (2)  $w$  is the sample weight prior to dissolution. For dry samples the cement content is obtained directly from the corrected weight of the residue ( $w_{Rcorr}$ ) by subtracting that weight from the weight of the sample prior to dissolution ( $w$ ).

$$w_{Rcorr} = w_R \cdot (1.057 - 0.102) \quad (1)$$

$$C = \frac{w - w_{Rcorr}}{1 + wcr} \quad (2)$$

#### 4 DISCUSSION

For our application the current method give a sufficient approximation of the cement content. The method is only applicable for samples that have been completely dried (1000°C) or sealed since the time of mixing. For partially dried samples one has to know the degree of hydration as well as the water-cement ratio in order to make an accurate calculation of the cement content. A possible source of error not mentioned above is the pore openings of the filter paper. The finest cement particles ( $<2\mu\text{m}$ ) represent an average of 5.3 % of the total cement content. Since the typical retention of the filter papers are 1-2  $\mu\text{m}$ , some un- or partly dissolved cement particles may pass through the filter, thus affecting the result. The volume and concentration of the acid was found empirically by trial and error. It is possible that this can be further optimised in relation to the weight and chemistry of the samples the method is, however, still a work in progress.

#### REFERENCES

- [1] B. C. Lippiatt and S. Ahmad, "Measuring the life-cycle environmental and economic performance of concrete: the bees approach," presented at the International workshop on sustainable development and concrete technology, Ames, Iowa State University, 2004.
- [2] J. S. Damtoft, J. Lukasik, D. Herfort, D. Sorrentino, and E. M. Gartner, "Sustainable development and climate change initiatives," *Cement and concrete research*, vol. 38, pp. 115-127, 2008.
- [3] K. L. Scrivener and R. J. Kirkpatrick, "Innovation in use and research on cementitious material," *Cement and concrete research*, vol. 38, pp. 128-136, 2007.
- [4] O. Linderoth and L. Wadsö, "Examining hydration kinetics obtained from different mixing procedures using isothermal calorimetry," in *International RILEM Conference Materials, Systems and Structures in Civil Engineering*, Lyngby, Denmark, 2016, pp. 95-104.
- [5] D. Han and R. D. Ferron, "Influence of high mixing intensity on rheology, hydration, and microstructure of fresh state cement paste," *Cement and Concrete Research*, vol. 84, pp. 95-106, 6// 2016.
- [6] S. A. Farrington, "Evaluating the Effect of Mixing Method on Cement Hydration in the Presence of a Polycarboxylate High-Range Water Reducing Admixture by Isothermal Conduction Calorimetry," presented at the 12th International Congress on the Chemistry of Cement (ICCC 2007), Montreal, Canada, 2007.
- [7] M. R. Geiker, J. P. Ekstrand, and R. Hansen, "Effect of mixing on properties of SCC," presented at the 5th International RILEM Symposium on Self-Compacting Concrete, Ghent, Belgium, 2007.
- [8] P. Juilland, A. Kumar, E. Gallucci, R. J. Flatt, and K. L. Scrivener, "Effect of mixing on the early hydration of alite and OPC systems," *Cement and Concrete Research*, vol. 42, pp. 1175-1188, 9// 2012.
- [9] M. Yang and H. M. Jennings, "Influences of mixing methods on the microstructure and rheological behavior of cement paste," *Advanced Cement Based Materials*, vol. 2, pp. 70-78, 1995/03/01 1995.
- [10] J. I. Alvarez, A. Martín, P. G. a. Casado, I. Navarro, and A. Zornoza, "Methodology and validation of a hot hydrochloric acid attack for the characterization of ancient mortars," *Cement and Concrete Research*, vol. 29, pp. 1061-1065, 1999.
- [11] X. X. Gao et al., "A three-step method for the recovery of aggregates from concrete," *Construction and Building Materials*, vol. 45, pp. 262-269, 2013.
- [12] V. A. Quarcioni and M. A. Cincotto, "Optimization of calculation method for determination of composition of hardened mortars of Portland cement and hydrated lime made in laboratory," *Construction and Building Materials*, vol. 20, pp. 1069-1078, 2006.

## Concrete-ice abrasion: Laboratory studies using a sawn concrete surface



Guzel Shamsutdinova  
M.Sc., Ph.D. candidate,  
Norwegian University of Science and Technology  
Richard Birkelands vei 1a, NO-7034 Trondheim  
e-mail: guzel.shamsutdinova@ntnu.no



Max A.N. Hendriks  
M.Sc., Ph.D., professor  
Norw. Univ. of Sc. and Tech./Delft University of Technology  
Richard Birkelands vei 1a, NO-7034 Trondheim  
e-mail: max.hendriks@ntnu.no



Stefan Jacobsen  
M.Sc., Ph.D., professor  
Norwegian University of Science and Technology,  
Richard Birkelands vei 1a, NO-7034 Trondheim  
e-mail: stefan.jacobsen@ntnu.no

### ABSTRACT

Concrete-ice abrasion is a surface degradation mechanism due to ice-structure interaction especially relevant for concrete gravity-based structures in the Arctic offshore.

Experiment is the main evaluation method for concrete durability against ice abrasion. The paper presents NTNUs lab facilities and a 4 km concrete-ice abrasion test between a sawn concrete surface with  $f_{c \text{ cube}} = 110$  MPa and unidirectionally grown fresh water ice. Results demonstrate the load cells response, coefficient of friction and a 0.03 mm/km abrasion rate measured with laser scanner. Further research is discussed.

**Key words:** Surfaces; Concrete; Ice; Abrasion; Experiment; Testing.

### 1. INTRODUCTION

The concrete-ice abrasion process has been defined as the surface degradation of concrete structures due to interaction with drifting ice floes. Several research groups have studied this topic through laboratory experiments [1,2,3,4,5,6] and field observations [1,7]. Hara et al. [8] recommended the concrete-ice sliding abrasion test, during evaluation of various test methods of concrete-ice abrasion resistance. Most experimental work the last 30 years has been based on the sliding interaction between ice and concrete, whether ice on concrete [4,5,9,10] or concrete on ice [2,5,11,12].

Our experimental method is based on the sliding of an ice sample along a fixed concrete sample. It controls exposure and measures relevant response parameters during concrete-ice interaction, including concrete-ice abrasion with a laser scanner. We used a concrete sample with a sawn surface, same as [5]. The wear rate of a surface with exposed aggregates is of great importance for the durability against concrete ice abrasion [12] and sawing also ensures a standard type of test surface.

## 2. EXPERIMENT

The experiments presented here include the simulation of concrete-ice abrasion with an abrasion rig, and laser scanner measurements of abrasion. The tests were performed in the abrasion laboratory at air temperature  $-10^{\circ}\text{C}$ . The ice pressure was 1 MPa. The average sliding velocity was 0.16 m/s.

### 2.1. Abrasion machine

The abrasion machine simulated concrete-ice abrasion according to the principle in Fig. 1(a), with a sliding ice specimen along a fixed concrete sample. The machine makes the ice sample holder move in repeated sliding movements in a horizontal direction, with the average velocity 0.16 m/s. The piston continuously pushes the ice sample against the concrete surface with a 1 MPa load. A feedback system keeps the loading as constant as possible during the test while moving back and forth. The temperature in the concrete-ice abrasion lab is kept at  $-10^{\circ}\text{C}$ . The concrete sample temperature control goes through an aluminium heating plate below the concrete sample. The plate is connected to a controlled temperature liquid (alcohol) circulator. This means that the temperature of the concrete surface in the concrete-ice abrasion zone can be adjusted. The temperature of the concrete surface in the contact zone was measured with an infrared scanner.

### 2.2. Laser scanner

Recently, we developed a non-contact Laser Scanning measuring method (Fig. 1(b)) to measure concrete-ice abrasion. It allows scanning of the concrete surface with accuracy  $10\ \mu\text{m}$  in reasonable time. The laser moves continuously along the sample according to a predefined “snaking” path. The measuring point distance is approximately  $50\ \mu\text{m}$  in the Y direction, and the step size in the X direction, the sliding direction, is 1 mm (Fig. 1(b)). The measured data is transformed to a matrix of surface heights, with  $1900 \times 300$  points.

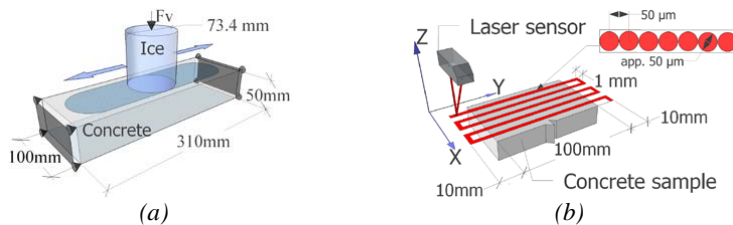


Figure 1 – (a) The principal scheme of an abrasion test, (b) simplified schematic of measurement process (not to scale)

### 2.3. Ice

Our abrasion machine is designed for fresh-water cylindrical ice samples. We used unidirectionally grown ice made from tap water. An ice mould made of Polyoxymethylene (POM) 13.3 mm thick and 370 mm high and covered with thermal insulation on the sides and the bottom is filled with tap water and put in a freezer at  $-20^{\circ}\text{C}$  for 48-72 hours. The freezing of the water starts at the top of the mould, but later it also takes place from the bottom. The upper part of the ice sample is transparent (unidirectionally grown ice) with very few air voids. The lower part of the ice sample contains a lot of air voids and unfrozen water. The ice sample is cut in two, and only the upper part is used for the test.

### 2.4. Concrete

The tested concrete sample was made of Norcem Anlegg (CEM I) cement and 2% Elkem silica fume substitution, fine aggregate (Årdal sand, 0-8 mm grain size) and coarse aggregate (Årdal,

8-16 mm grain size). The mix was made with the following proportions:  $W/(C+2S)=0.42$ , where  $W$ ,  $C$  and  $S$  are the weight of water, cement and silica fume powder, respectively. The cement paste volume was 29.5%. Superplasticizing additive Dynamon SX-23 from Mapei was used to achieve flowing workability. The 28-day cube compressive strength of the concrete was 90 MPa, increasing to 110 MPa after curing in water at  $+20^{\circ}\text{C}$  for 11 months, as the test started.

### 3. RESULTS

The data acquisition system logged horizontal and vertical load cells responses during the test at 500 Hz frequency. The coefficient of friction (COF) is plotted in Fig. 2(a). The highest COF corresponds to the turning points of the ice specimen where the ice sample makes a full stop. We distinguished the coefficient of kinetic friction (0-0.2) during sliding interaction, and the coefficient of static friction (0.05 – 0.10) at the turning points.

Laser scanning gave abrasion as the difference between the unabraded rim of the concrete sample and an abraded central band of 10 mm width as done with mechanical measurements in [5]. However, a much higher number of data points was collected with the laser scanner, so the calculation here was done for each millimeter of concrete sample length and each 50 microns across the 10 mm wide central band. Figure 2(b) shows the abrasion of sawn concrete sample.

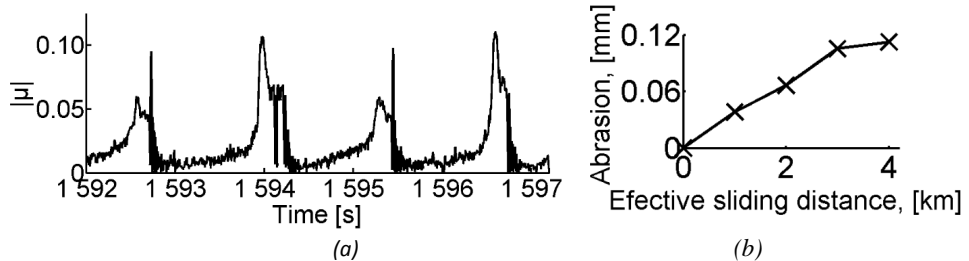


Figure 2 – (a) Coefficient of friction, (b) abrasion of sawn concrete surface.

Figure 3 shows the average profiles of the abraded central band (10 mm wide) along the sample width (Fig. 3(a)) and length (Fig. 3(b)), before and after 4 km abrasion test. The difference between two lines shows the abrasion.

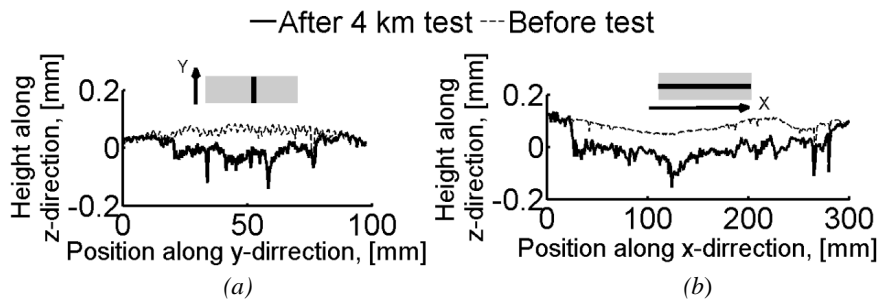


Figure 3 – Average profiles, of the central band (10 mm wide), of the sawn concrete surface before and after 4 km abrasion test: (a) along y-direction, (b) along x-direction (see inserts).

### 4. DISCUSSION AND CONCLUSION

The measured coefficient of kinetic friction is of the same magnitude as test results of other concrete-ice abrasion tests with the same sliding speed (0.16 m/s): 0.00 – 0.01 and 0.06

respectively [5,12]. The results of the abrasion depth were found similar to the previous study by Møen et al., where concrete samples with cylindrical compressive strength from 72.8 to 147.8 MPa under similar experimental conditions had a maximum abrasion rate 0.025 mm/km of effective sliding distance. Beside coefficient of friction and wear rate, the ice failure mode, concrete surface roughness and wear particle characteristics are in the focus of our interest and being investigated in further works.

## 5. ACKNOWLEDGMENT

This research forms part of the DACS (Durable Advanced Concrete Solutions) project. The financial contribution of the Norwegian Research Council is gratefully acknowledged. The DACS project partners are: Kværner AS (project owner), Axion AS (Stalite), AF Gruppen Norge AS, Concrete Structures AS, Mapei AS, Multiconsult AS, NorBetong AS, Norcem AS, NPRA (Statens Vegvesen), Norges Teknisk-Naturvitenskapelige Universitet (NTNU), SINTEF Byggeforsk, Skanska Norge AS, Unicon AS and Veidekke Entreprenør AS.

## 6. REFERENCES

- [1] Huovinen, S.: "Abrasion of concrete structures by ice" *Cement and Concrete Research* 23(1): p. 69-82 (1993)
- [2] Bekker, A.T., Uvarova, T.E., Pomnikov, E.E., Farafonov, A.E., Prytkov, I.G., Tyutrin, R.S.: "Experimental study of concrete resistance to ice abrasion" *Proceedings of the International Offshore and Polar Engineering Conference* (2011)
- [3] Hanada, M., Ujihira, M., Hara, F., Saeki, H.: "Abrasion rate of various materials due to the movement of ice sheets" *Proceedings of the International Offshore and Polar Engineering Conference* (1996)
- [4] Fiorio, B.: "Wear characterisation and degradation mechanisms of a concrete surface under ice friction" *Construction and Building Materials* 19(5): p. 366-375 (2005)
- [5] Møen, E., Høiseith, K.V., Leira, B., Høyland, K.V.: "Experimental study of concrete abrasion due to ice friction - Part I: Set-up, ice abrasion vs. material properties and exposure conditions" *Cold Regions Science and Technology* 110: p. 183-201 (2015)
- [6] Tijssen, J., S. Bruneau, and B. Colbourne: "Laboratory examination of ice loads and effects on concrete surfaces from bi-axial collision and adhesion events" *Proceedings of the International Conference on Port and Ocean Engineering under Arctic Conditions, POAC* (2015)
- [7] Itoh, Y., Tanaka, Y., Delgado, A., Saeki, H.: "Abrasion depth distribution of a cylindrical concrete structure due to sea ice movement". *International Journal of Offshore and Polar Engineering*, 6(2): p. 144-151 (1996)
- [8] Hara, F., Y. Takahashi, and H. Saeki: "Evaluation of test methods of abrasion by ice movements on the surface of reinforced concrete structures" *Concrete Under Severe Conditions Environment and Loading* p. 475-484 (1995)
- [9] Saeki, H., Ono, T., Nakazawa, N., Sakai, M., Tanaka, S.: "Coefficient of friction between sea ice and various materials used in offshore structures" *Journal of Energy Resources Technology, Transactions of the ASME* 108(1): p. 65-71 (1986)
- [10] Jacobsen, S.: "A Norwegian concrete-ice abrasion laboratory" *Nordic Concrete Research Publ.No.50 ISSN 0800-6377*, pp. 119-122 (2014)
- [11] Hoff, G.C.: "Evaluation of ice abrasion of high-strength lightweight concretes for arctic applications" *Proceedings of the International Offshore Mechanics and Arctic Engineering Symposium* (1989)
- [12] Itoh, Y., Yoshida, A., Tsuchiya, M., Katoh, K., Sasaki, K., Saeki, H.: "An experimental study on abrasion of concrete due to sea ice" *Twentieth Annual Offshore Technol. Conf.* pp. 61-68 (1988)